Characterization of PARL-Mediated Intramembrane Proteolysis

by

Laine Riki Lysyk

A thesis submitted in partial fulfillment of the requirements for the degree of

Master of Science

Department of Biochemistry
University of Alberta

ABSTRACT

Intramembrane proteolysis is the process by which membrane-embedded proteases cleave substrates that are also embedded within the lipid bilayer or lie near to the bilayer. Rhomboid intramembrane proteases are a ubiquitous superfamily of serine intramembrane proteases that play a role in a wide variety of cellular processes. The mammalian mitochondrial rhomboid protease, Presenilin-Associated Rhomboid Like (PARL), is a critical regulator of mitochondrial homeostasis through its cleavage of substrates such as PINK1 (Phosphatase and tensin (PTEN)-induced putative kinase 1), PGAM5 (phosphoglycerate mutase family member 5), and Smac (Second mitochondrial-derived activator of caspases), which have roles in mitochondrial quality control and apoptosis.

This thesis aims to assess PARL-mediated cleavage of several different substrates using an *in vitro* FRET-based kinetic assay with recombinantly expressed and purified human PARL (HsPARL). We hypothesize that truncations of PARL identified *in vivo* will have a regulatory effect on PARL-mediated cleavage and that there will be significant differences in the catalytic parameters obtained for cleavage of each unique substrate by HsPARL. Furthermore, we hypothesize that the lipid cardiolipin, which is specific to the inner mitochondrial membrane where PARL resides, will have an effect on the proteolytic activity of HsPARL. Finally, we aim to assess PARL-mediated cleavage of several Parkinson's disease-associated variants of PINK1 that harbour a mutation within or near the PARL cleavage site. We hypothesize that these mutations in PINK1 will impair PARL-mediated cleavage and this may provide rationale for the molecular etiology of these mutations in Parkinson's disease pathogenesis.

ACKNOWLEDGMENTS

First and foremost, I would like to extend tremendous thanks to my supervisor Dr. Joanne Lemieux for her unwavering support, enthusiasm, and mentorship over these past two and a half years. I was first inspired to pursue science after I completed a summer research project in your lab through the W.I.S.E.S.T. program when I was yet in high school and your excitement and passion for science was contagious. I feel like my scientific journey thus far has truly come full circle now that I am completing my master's and I could not be more grateful for my time spent in your lab. I will be forever thankful for the opportunities you have given me through the course of this degree and the countless ways you have supported, encouraged, and challenged me as a scientist.

I am also truly grateful for being part of such a wonderful lab environment. Thank you to Dr. Elena Arutyunova, Dr. Yurong Wen, and Dr. Rashmi Panigrahi for sharing your expertise and for always being willing to give advice and scientific insights. A special thank you to Elena for all your help in the lab and for taking the time to teach me the majority of the methods I used throughout this degree; taking on this project would have been impossible without your practical scientific knowledge. Thank you to Raelynn Brassard for bringing new energy to the lab and for the conversations and fun both in and out of the lab. Also, thank you to the many undergraduate students who have come to the lab and who I have had the privilege to work closely with and share my knowledge.

Thank you to my committee members Dr. Joe Casey and Dr. Ing Swie Goping. Your support, advice, and scientific thoughts have been most appreciated. Thank you for pushing me to produce high quality scientific work and to articulate myself in a precise and insightful manner; our committee meetings have been immensely helpful in my growth as a scientist. I would also like to extend a thank you to Dr. Richard Schulz for participating in my thesis defense.

Finally, I would like to thank all my friends and family who have supported me through this stage of my life. In particular, I would like to thank Emmanuella Takyi. I don't know what I would have done without you through the course of this degree. It is an amazing coincidence that we started our master's degrees at the same time in Joanne's lab and that we became such close friends. I would never have expected that I'd come out of this program with not only a master's degree, but a best friend as well. I cannot express how thankful I am for your friendship and all the memories we have made over the past two years. I know that just because the course of our degrees has come to an end, our friendship has not.

TABLE OF CONTENTS

LIST OF FIGURES

LIST OF TABLES

LIST OF ABBREVIATIONS

ANOVA	analysis of variance
BMGY	buffered complex glycerol medium
BMMY	buffered complex methanol medium
CL	cardiolipin
CyPet	cyan fluorescent protein for energy transfer
DABCYL	4-(4-dimethylaminophenylazo)benzoyl
ddH$_2$O	double distilled water
DDM	n-dodecyl β-D-maltoside
DMSO	dimethyl sulfoxide
Dnp	2,4-dinitrophenyl
EDANS	5-[(2-aminoethyl) amino] naphthalene-1-sulfonic acid
EDTA	Ethylenediaminetetraacetic acid
Ec	*Escherichia coli*
EtOH	ethanol
FRET	Förster resonance energy transfer
GFP	green fluorescent protein
Hi	*Haemophilus influenzae*
Hs	*Homo sapiens*
IMM	inner mitochondrial membrane
IQ	internally quenched
k_{cat}	catalytic rate constant (turnover)
k_{cat}/K_M	catalytic efficiency
K_M	Michaelis-Menten constant
LB	Lysogeny broth
LC-MS/MS	liquid chromatography mass spectrometry
Mca	7-methoxycoumarin-4-acetic acid

mPEMT	mouse phosphatidylethanolamine methyl transferase
MPP	matrix processing peptidase
MS	mass spectrometry
MTS	mitochondrial targeting sequence
OMM	outer mitochondrial membrane
PARL	Presenilin-associated rhomboid-like
PD	Parkinson's disease
PGAM5	phosphoglycerate mutase family member 5
PINK1	phosphatase tensin homolog (PTEN)-induced putative kinase 1
PMSF	phenylmethylsulfonyl fluoride
RFU	relative fluorescence unit
ROS	reactive oxygen species
SDS-PAGE	sodium dodecyl sulfate polyacrylamide gel electrophoresis
Smac	second mitochondrial-derived activator of caspases
SEM	standard error of the mean
TBS	tris buffered saline
TCEP	tris(2-carboxyethyl)phosphine
TEMED	tetramethylethylenediamine
TEV	tobacco etch virus
TIM	translocase of the inner membrane
TM	transmembrane
TMD	transmembrane domain
TOM	translocase of the outer membrane
WT	wild-type
YNB	yeast nutrient broth
YPD	yeast extract peptone dextrose media
YPDS	yeast extract peptone dextrose sorbitol media
YPet	yellow fluorescent protein for energy transfer

CHAPTER 1: INTRODUCTION

1.1 Intramembrane proteolysis and the rhomboid protease family

Proteases are a class of enzymes that function to hydrolyze peptide bonds. They have been widely studied since their initial discovery over 150 years ago and are considered master regulators of cellular processes with extensive physiological roles ranging from regulation of cell division and differentiation to apoptosis[1]. Proteases are categorized based on the reactive residue that acts as the nucleophile in the hydrolysis reaction. A protease will typically fall into one of four categories: serine, cysteine, aspartyl, or metallo, though other mechanisms of proteolysis have been identified with some proteases using nucleophilic threonine or glutamic acid resides[2-4]. The serine protease mechanism is well understood and employs a catalytic triad consisting of the nucleophilic serine, general base histidine, and an aspartate residue. Upon binding of the protease to its substrate and formation of the enzyme-substrate complex, nucleophilic attack by the catalytic serine residue at the carbonyl group of the substrate's scissile bond to be hydrolyzed results in the formation of the tetrahedral intermediate. During the formation of this tetrahedral intermediate, a proton is transferred to the histidine residue and stabilized by hydrogen bonding between the histidine and aspartate residues. The tetrahedral intermediate decomposes to the acyl-enzyme intermediate upon proton donation from the histidine. The newly formed N-terminus of the cleaved substrate is then replaced by a water molecule and a second tetrahedral intermediate is formed upon nucleophilic attack by the water molecule. The final step in the serine protease mechanism is decomposition of the tetrahedral intermediate and results in the enzyme returning to its active form (Figure 1.1)[5].

In the late 1990s, intramembrane proteolysis was discovered[6]. Intramembrane proteolysis is a process by which proteases embedded within a lipid bilayer cleave transmembrane substrates, often to release signalling molecules. The idea that proteins can be cleaved within the plane of a cellular membrane was proposed in the early 1990s. However, the requirement of a nucleophilic water molecule in the hydrolysis mechanism rendered the idea that this reaction could occur in a water-excluding environment, such as a lipid bilayer, controversial.
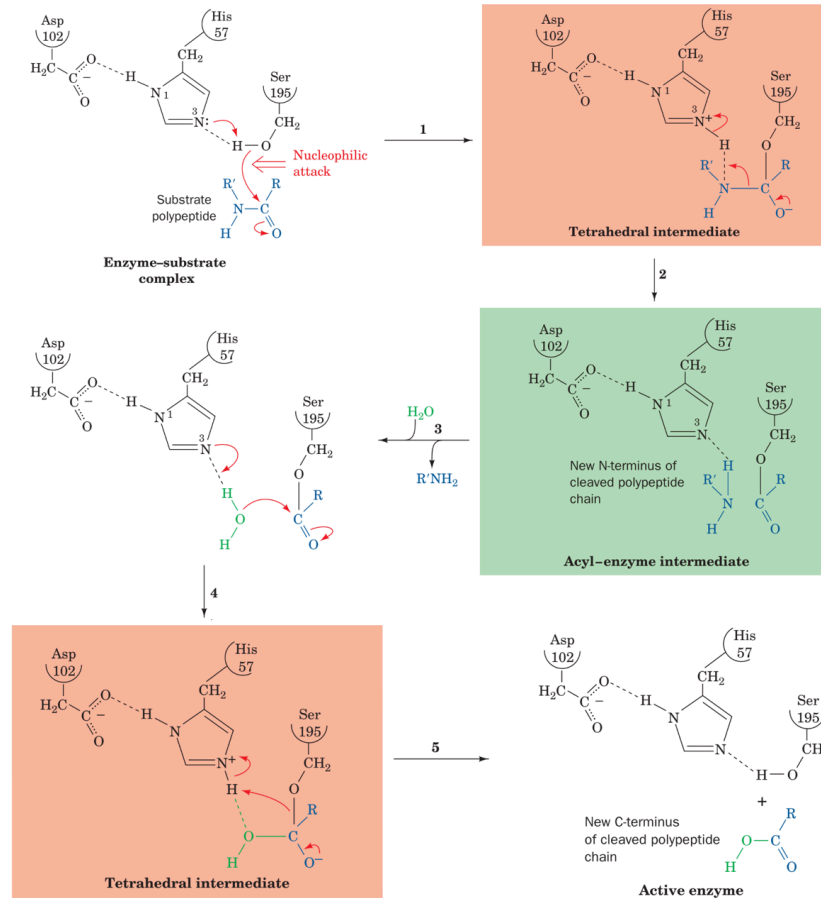
Figure 1.1: Serine protease mechanism of peptide bond hydrolysis by chymotrypsin. A proton is transferred to the general-base histidine and the catalytic serine residue carries out a nucleophilic attack on the scissile bond resulting in the formation of a tetrahedral intermediate. Hydrogen bonding between the histidine and aspartate residues of the catalytic triad stabilize this intermediate (1). Proton donation from the histidine results in decomposition of the tetrahedral intermediate and subsequent formation of the acyl-enzyme intermediate (2). The newly formed N-terminus of the cleaved substrate leaves and is replaced by a water molecule (3). Proton transfer to the histidine occurs again and the water molecule carries out a nucleophilic attack to produce a second tetrahedral intermediate (4). Histidine then donates a proton, the tetrahedral intermediate decomposes, and the enzyme returns to its active form while the C-terminus of the cleaved substrate is released (5)[7]. From Voet, D., *et al*. (2008). *Fundamentals of Biochemistry: Life at the Molecular Level 3rd Edition.* Hoboken, NJ: Wiley.

Particularly when taken into consideration that the active site of intramembrane proteases was predicted to be buried within the hydrophobic bilayer[8]. Since their initial discovery, four classes of intramembrane proteases have been identified: site 2 protease-type metalloproteases, intramembrane aspartyl proteases, rhomboid serine proteases, and a glutamyl protease[6,9-11]. Many of the intramembrane proteases that have been identified participate in regulated intramembrane proteolysis (RIP), the specific term used to describe proteolysis within the membrane that results in the release of a signalling molecule[12]. An example of RIP is proteolysis that mediates the release of transcription factors, thus facilitating organelle-nucleus communication[13]. The knowledge gathered on these intramembrane proteases remains minimal when compared to that of soluble proteases, however advances in research have begun to minimize this gap in knowledge.

Rhomboid proteases are a superfamily of ubiquitously expressed intramembrane proteases that, since their discovery, have become the best studied intramembrane protease family. The rhomboid gene was first identified in *Drosophila* in 1984 while researchers were screening for embryonic lethal mutations[14]. They observed that mutation of this gene resulted in larvae having a rhombus-shaped head, thus giving name to the *rhomboid* gene. Mutation of a second gene resulted in the same phenotype seen with *rhomboid* and was given the name *spitz*. Sequence analysis of these genes predicted that *rhomboid* encoded for an integral membrane protein composed of seven transmembrane (TM) segments, while *spitz* encoded for an epidermal growth factor-like protein[15,16]. This sequence analysis provided no indication of protease motifs within *rhomboid*. Four main lines of evidence that the *rhomboid* gene encoded for a protease came from cell culture studies that showed that: (i) expression of rhomboid induced the cleavage of Spitz, (ii) cleavage of Spitz could be prevented by mutation of four rhomboid residues that were consistent with catalytic residues of serine proteases or (iii) by using a serine protease inhibitor, and that (iv) the cleavage site of Spitz resided at a similar depth in the membrane to the proposed catalytic serine of the rhomboid[10]. Taken together, this evidence suggested that rhomboid acted as a serine intramembrane protease, which was then

confirmed by *in vitro* analysis of cleavage with purified proteins[17-19]. After the discovery of the first rhomboid gene, a further six rhomboid genes were identified in *Drosophila* (*rhomboid-1* to 7)[20]. Genome sequencing has identified rhomboid homologs in all branches of life, indicating these are evolutionarily conserved proteins; of these identified rhomboids, many are catalytically inactive yet highly conserved. The existence of these catalytically inactive rhomboid pseudoproteases suggests that there may be undefined cellular roles of the rhomboid family that are not mediated through their proteolytic activity[21]. There are currently 14 identified mammalian rhomboid family members. Of these 14, only five are catalytically active, RHBDL-1 to 4 and PARL. The remaining nine are classified as iRhoms, or inactive rhomboid homologs, and are considered pseudoproteases as they retain rhomboid characteristics however lack the catalytic residues[22].

Rhomboid proteases belong to the serine protease family, in which a serine residue acts as the nucleophile in the hydrolysis reaction. Unlike the majority of soluble serine proteases, rhomboid intramembrane proteases carry out the hydrolysis reaction by employing a catalytic dyad composed of a serine and histidine residue as opposed to the canonical catalytic triad[23-26]. It is proposed that other residues near the catalytic core of rhomboid proteases take on the role of the aspartate residue in the catalytic triad to stabilize the transition states formed during proteolysis[25,27].

Structural studies of rhomboid proteases, from sequence-based topology predictions to X-ray crystallography methods have provided a wealth of information regarding the function of these enzymes. Sequence-based analysis has identified that rhomboids present themselves in three topological variations[28] (Figure 1.2) The first consists of six TM segments (6TM), mainly found in bacterial rhomboids. The second form has a 6+1TM topology, with a seventh TM segment predicted at the C-terminus of the 6TM core; this is the most commonly occurring eukaryotic rhomboid topology. The final topological variation is the 1+6TM form in which a seventh TM segment is appended at the N-terminus, preceding the 6TM rhomboid core. This form is found
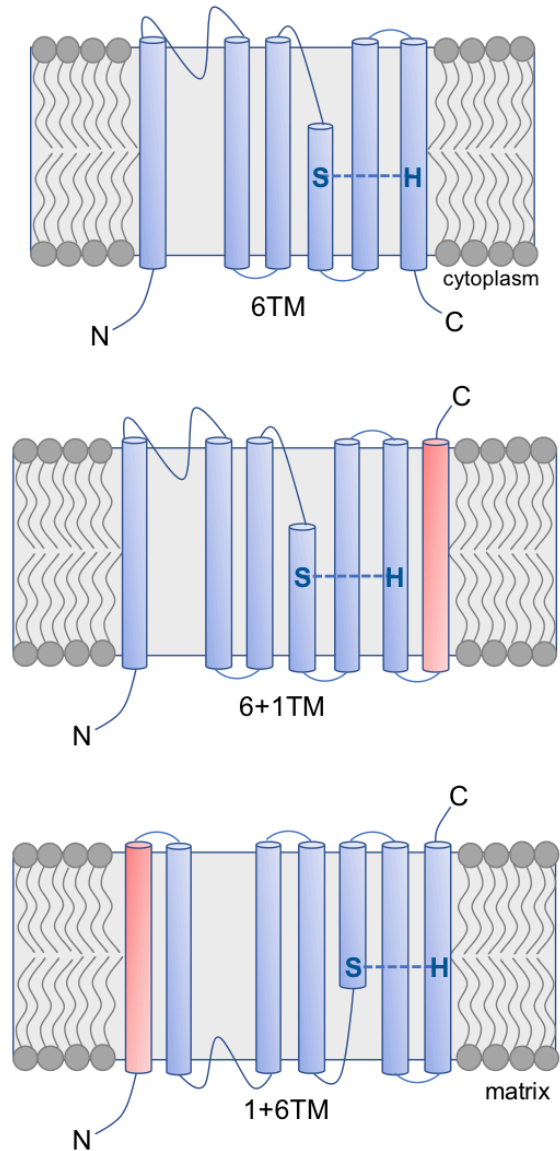
Figure 1.2: Topologies of rhomboid intramembrane proteases. Rhomboid proteases have been categorized in three topologies. Bacterial rhomboids are characterized by the 6TM core rhomboid domain (top). Most eukaryotic rhomboids have a 6+1TM topology, composed of the core 6TM rhomboid domain with an extra TM segment appended at the C-terminus (middle). Mitochondrial rhomboids are characterized by a 1+6TM architecture, in which a seventh TM segment at the N-terminus precedes the 6TM rhomboid core (bottom). The catalytic dyad is composed of a serine and histidine residue on TM segment 4 and 6, respectively. Structures have been determined only for the 6TM rhomboid topology.

with rhomboids that localize to endosymbiotic organelles such as the mitochondria or plastid of plant cells. Aside from varying membrane topologies, there is also much diversity in the cytosolic N-terminal region of the proteins, though the effect of these topological modifications is unclear.

High resolution crystal structures of the bacterial rhomboid GlpG from *E. coli* and *H. influenzae*, solved to 2.1 Å and 2.2 Å respectively, provided a breakthrough in our understanding of intramembrane proteolysis as these were the first high-resolution structures of intramembrane proteases[23,26]. The GlpG crystal structure revealed a 6TM helical bundle with several interesting features, most notably an overall asymmetry of the protein (Figure 1.3). The crystal structure also confirmed that, while the active site of the enzyme is buried within the plane of the hydrophobic bilayer, the active site cavity is solvent accessible, thus being able to facilitate entrance of a water molecule during the hydrolysis reaction. Though sequence identity between rhomboids is low, homology models based on the GlpG structure display high structural similarity with the HiGlpG crystal structure, the rhomboid protease from *H. influenzae*. High resolution structures of EcGlpG with inhibitors and peptides revealed the catalytic mechanism of rhomboid-mediated proteolysis, which is predicted to be similar to soluble serine proteases[23,26,27,29-32].

The main feature of the crystal structure is the organization of the 6TM rhomboid core. In the structure, TM1, 2, 3, 5, and 6 encircle TM4. From this core helical bundle, the L1 loop that connects TM1 and TM2 protrudes into the lipid bilayer as a helical hairpin; this L1 loop contains a conserved WR motif and is proposed to have a key role in substrate binding and participates in hydrogen bonding to stabilize the protein[31,33]. Further stabilizing the helical bundle are GxxxG motifs between TM4 and TM6, the TM segments which contain the catalytic dyad. Flexibility is observed for TM5 and the L5 loop which do not participate in any stabilization interactions; these structural elements are proposed to be responsible for substrate gating with TM5 acting as a gate for lateral substrate entry within the plane of the bilayer and the L5 loop
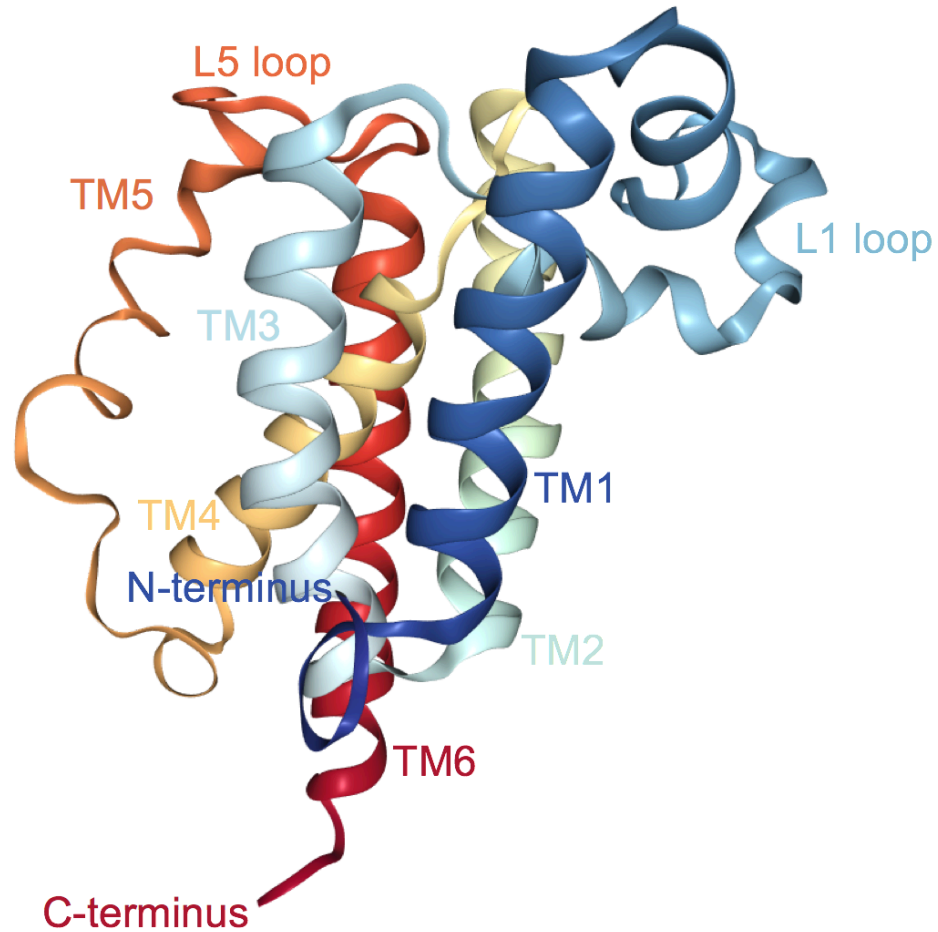
Figure 1.3: Crystal structure of the rhomboid protease GlpG from _Haemophilus influenzae_ (RCSB PDB 2NR9[34]). The crystal structure of the bacterial rhomboid protease HiGlpG was solved in 2007 to a resolution of 2.2 Å. The crystal structure displays a tight helical bundle composed of six transmembrane segments. From the helical bundle, the L1 loop extends into the plane of the bilayer, while TM4 that contains the catalytic serine is located in the middle of the helical bundle.

covering the active site cavity on the extracellular face, though the exact gating mechanism required for substrate access to the active site remains controversial[24,35]. Rhomboid proteases are proposed to recognize substrates based on the helical TM domain of the substrate as well as a substrate recognition motif that surrounds the cleavage site. This has led to the development of two models for substrate cleavage. The first model suggests that TM5 and the L5 loop become displaced, granting lateral substrate access to the catalytic core. Once the substrate enters the active site, unwinding of the TM segment occurs to facilitate positioning of the catalytic serine and histidine along the recognition motif of the substrate and hydrolysis of the peptide bond occurs[35]. This model is supported by the fact that mutations that weaken the interaction between TM5 and TM2 enhance proteolytic activity by up to ten-fold[36]. The second proposed model involves a two-step substrate recognition mechanism in which there is only movement of the L5 loop. The first step involves the TM segment of the substrate binding to an exosite, a secondary binding site away from the active site, on the protease. Upon substrate docking at this exosite, a minor displacement of the L5 loop occurs which facilitates entrance of the unwound helix containing the substrate recognition motif into the active site and hydrolysis occurs. Further structural analysis is required to confirm the mechanism of substrate binding and cleavage as there is inconsistency in regards to TM5 acting as a mobile substrate gate or merely facilitating substrate binding to an exosite[37].

While there have been major advancements in our understanding of rhomboid proteases, one key factor has impeded further knowledge. There is a lack of known physiological substrates for rhomboid proteases, particularly for the bacterial rhomboid proteases that serve as models for this protease family. It is ironic that despite the wealth of structural and functional studies that have been performed with GlpG, its physiological substrates, and therefore functions, remain unknown. There is currently only one endogenous bacterial rhomboid substrate that has been identified; the TatA protein in *Providencia stuartii* is cleaved by the rhomboid AarA[38]. Advancements in proteomics methods have become a powerful tool to identify novel substrates and interacting partners of the rhomboid family. Single-pass transmembrane

substrates are most often identified as rhomboid substrates, though evidence has shown the ability of rhomboid to cleave soluble substrates as well[19,39]. Whether the cleavage of soluble substrates is physiologically relevant remains to be determined as these assays have only been performed with model substrates, not verified *in vivo* substrates. The range of identified rhomboid substrates reveal their diverse array of cellular functions. The original rhomboid protease identified in *Drosophila* is essential in epidermal growth factor signalling during development, while other roles of rhomboid proteases include protein translocation and intercellular signalling for bacterial rhomboids, mitochondrial dynamics in yeast, and parasitic cell growth and host invasion[40]. In respect to mammalian rhomboid proteases, RHBDL-2 localizes to the plasma membrane and has a role in cell migration and proliferation, while RHBDL-4 resides in the ER membrane and assists in ER-associated degradation[41,42]. The substrates, and therefore function, of RHBDL-1 and RHBDL-3 have yet to be identified, though their high expression in brain tissue, and the severe phenotype of their KO mice (lethality), indicates that they likely have an important function in the central nervous system[43,44]. The mammalian mitochondrial rhomboid, PARL, has been the focus of extensive research and plays an important role in mitochondrial homeostasis which will be discussed in section *1.2*[45].

With the diverse physiological roles of proteases, it is not surprising that proteolytic impairment or dysregulation is implicated in numerous diseases. Rhomboid proteases have been implicated in cancer, diabetes, and neurodegenerative diseases, as well as parasitic host invasion[46-50]. Many proteases have been identified as potential drug targets due to their role in disease pathology; protease inhibitors are currently approved for the treatment of hypertension, cancer, diabetes, and HIV[51]. While the discovery of small molecule inhibitors and drug design targeted to proteases is a rapidly progressing area of research, small molecule inhibitors that are both specific and potent towards intramembrane proteases remain elusive. The development of inhibitors for the rhomboid protease family has been particularly challenging, though recent advances have produced novel bacterial rhomboid inhibitors that are effective at low-micromolar concentrations[51,52]. Thus far, no inhibitors have been identified

for the mitochondrial rhomboid PARL. Much effort has been invested in developing inhibitors for the γ-secretase intramembrane proteolytic complex due to its direct link to Alzheimer's disease. γ-secretase is responsible for cleaving the amyloid precursor protein; specific cleavages of amyloid precursor protein result in the formation of Aβ-peptides which accumulate and form amyloid plaques in the brains of those diagnosed with Alzheimer's[53]. High potency inhibitors were able to be generated for γ-secretase, however, they had severe side effects, likely due to the fact that γ-secretase cleaves over 80 substrates[54]. The research focus has now shifted to designing modulators of γ-secretase activity, however, none of these compounds have passed the clinical trial stage yet[51,55].   A recent structure of γ-secretase with amyloid precursor protein bound is likely to assist in specific inhibitor development[56]. For successful inhibitor design and validation of rhomboid proteases as therapeutic targets, a greater understanding of the structural and mechanistic features of this exciting class of proteases is needed. Currently, rhomboid protease structures are limited to the 6TM bacterial form of the enzymes. Because eukaryotic rhomboids contain a seventh TM segment at the N- or C-terminus along with cytoplasmic domains that may have regulatory functions in regards to activity or substrate recognition, our understanding of their mechanism remains limited. It would be highly beneficial to both our understanding of eukaryotic rhomboid regulation and therapeutic development to have a high resolution structure of a eukaryotic rhomboid.

Since their initial discovery, intramembrane proteases have remained an exciting field of research due to constant advancements in our understanding of their cellular roles in health and disease. Rhomboid proteases are the most widely studied family of intramembrane proteases and demonstrate the importance of intramembrane proteolysis in regulating a diverse array of cellular processes. Research to further develop our understanding of the structural, functional, and mechanistic aspects of these intramembrane proteases is likely to remain a field of great interest and relevance.

1.2 PARL: The mammalian mitochondrial rhomboid protease

The mitochondrial form of rhomboid was first identified in yeast in 2002, though the extent of the importance of rhomboid in mitochondrial biology was not yet realized[57]. Following the initial discovery of a mitochondrial rhomboid in yeast, conserved mitochondrial rhomboids were identified in *Drosophila* and mammalian cells, the Rho-7 and PARL proteins respectively[58,59].

In 2001, through a yeast-two hybrid screen that was identifying presenilin-associated proteins, the mammalian orthologue of the mitochondrial rhomboid, PARL (Presenilin-associated rhomboid-like), was identified[60]. At the time of this screen, the first mitochondrial rhomboid had yet to be identified and PARL was speculated to be a protease that interacted with the presenilins, leading to its misnomer as a presenilin-associated protein. We now know that PARL is an intramembrane serine protease, belonging to the rhomboid superfamily, and is localized to the inner mitochondrial membrane (IMM) of mammalian cells, with its N-terminus in the mitochondrial matrix and C-terminus extending into the inter-membrane space (IMS) (Figure 1.4)[61]. As a member of the rhomboid superfamily of intramembrane proteases, PARL is characterized by having a catalytic dyad composed of a serine and histidine residue buried within a helical bundle of six transmembrane segments; serine 277 and histidine 335 make up the catalytic dyad of PARL and this active site faces the mitochondrial matrix. Like the other mitochondrial rhomboids, PARL is predicted to have a seventh transmembrane segment appended at its N-terminus, giving it a 1+6TM architecture, however without a crystal structure available, this is only a prediction supported by current modelling software and sequence alignments[60].

PARL is 379 amino acid protein; several truncated forms of PARL have been identified *in vivo* (Figure 1.4)*. Upon removal of the N-terminal mitochondrial targeting sequence (MTS), the resulting PARLΔ53 truncation is considered the mature form of the protease and is the predominant species present in lung, brain, heart, and muscle tissues[62]. A second processing

event occurs at Ser77, termed β-cleavage, resulting in the PARLΔ77 truncation of the enzyme which is observed in spleen, lung, brain, and kidney tissues[62]. This β-cleavage event is proposed to be autocatalytic as mutation of Ser277, the catalytic serine, results in reduced formation of PARLΔ77[61-63]. Expression of PARLΔ77 in HeLa cells results in mitochondrial fragmentation, suggesting that this truncation alters the function of PARL[61].

There is contradictory evidence in the literature about the importance of these truncations. β-cleavage was proposed to be required for an active form of the enzyme, however new evidence suggests that PARLΔ53 may be the more active form of the enzyme[64,65]. Perhaps these truncation events are not activating or inhibiting the protease, but rather influencing other mitochondrial processes that rely on PARL-mediated cleavage events. In addition, these truncations may be regulated by physiological conditions that favour cleavage of one particular substrate over another. For example, in times of mitochondrial stress, β-cleavage was increased resulting in higher levels PARLΔ77[65]. While we could think of this as resulting in decreased activity of PARL, it results specifically in decreased cleavage of PINK1, therefore allowing for higher mitophagy levels in this mitochondrial stress condition, which is ultimately favourable[65]. Upon mutation of Ser77 to a residue that prevented β-cleavage, impaired PARL activity was noted towards several substrates[49,61,63]. These findings suggested that β-cleavage was necessary to activate the enzyme, however it may be that these substrates are preferentially cleaved when β-cleavage is enhanced, such as mitochondrial stress conditions. Decreased β-cleavage is observed upon phosphorylation of PARL at Ser70[61]. With decreased β-cleavage and more mature PARLΔ53 present, cleavage of PINK1 was enhanced, thus β-cleavage was speculated as a positive regulator of mitophagy[65].

A further truncated form of the enzyme that results in removal of the N-terminal TMS, leaving just the 6TM core rhomboid domain, has been found predominantly in kidney tissue, however there is little knowledge on the physiological relevance of this truncation or the processing event that results in it[62]. Taken together, these results suggest distinct regulation and roles of
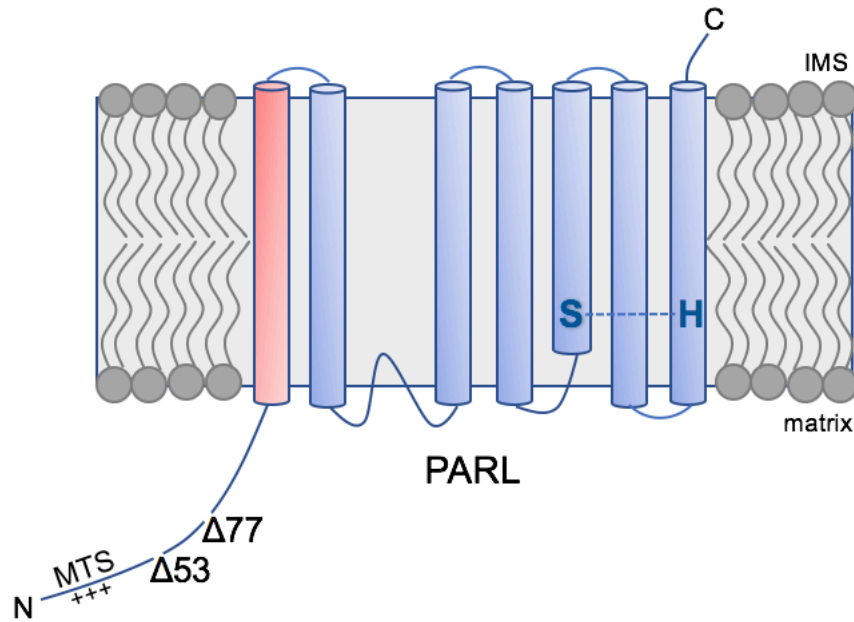
Figure 1.4: Topology diagram of HsPARL. Presenilin-associated rhomboid like (PARL) protease is an intramembrane serine protease belonging to the rhomboid family. It has a 1+6TM rhomboid topology and localizes to the inner mitochondrial membrane due to its mitochondrial targeting sequence (MTS) that features a motif of positively charged residues (+++). The N-terminus extends into the mitochondrial matrix and C-terminus into the intermembrane space (IMS). It undergoes processing events *in vivo*, resulting in the Δ53 and Δ77 truncations of the protein. The catalytic dyad is composed of Ser277 (S) and His335 (H).

the various PARL truncations depending on the physiological condition of the mitochondria, however, the direct influence of PARL truncations on substrate cleavage has not been examined *in vitro*.

Phosphorylation is also proposed to play a key role in the regulation of PARL activity. As mentioned above, phosphorylation of Ser70 results in decreased β-cleavage and thus alters the activity of PARL. Ser65, Thr69, and Ser70 of PARL have all been identified as phosphorylation sites; phosphomimetic mutations at any of these residues drastically reduces β-cleavage and the production of PARLΔ77[61]. The three phosphorylation sites are in relatively close proximity to Ser77, the residue at which β-cleavage occurs, indicating that perhaps steric hindrance or local conformational changes resulting from the addition of the phosphate group impair this cleavage event. PARL truncations appear to be a main way that PARL activity is regulated depending on cellular conditions and the propensity for one substrate to be cleaved over another. When PARL is phosphorylated, increased levels of PARLΔ53 are present because β-cleavage is inhibited. This enhances PARL activity and promotes cleavage of substrates such as PINK1. Phosphorylation is suggested to be a main regulator of PARL's response to cellular conditions in relation to enhancing or inhibiting the formation of specific PARL species that then results in altered activity of the protease depending on physiological need.

In addition to the truncations and phosphorylation of PARL being regulatory mechanisms for the protein, it has recently been proposed that PARL may reside in a larger proteolytic hub in the IMM consisting of PARL, the *i*-AAA protease YME1L, and the scaffold stromatin-like protein 2 (SLP2)[66]. Large multi-protein complexes are quite common in the IMM, with the respiratory chain supercomplexes being the best characterized. These large protein complexes are proposed to serve as a functional compartmentalization of the membrane, in which localized protein-lipid arrangements and protein-protein interactions facilitate regulatory mechanisms. This proteolytic hub may have profound effects on the regulation and activity of PARL and

presents numerous questions that require further study. Does PARL require these interacting partners for maximal activity? If one of these partners is missing do the other two still associate? Can these two proteases compensate for each other if loss of activity happens to one? Can these proteases act on the same substrates? Understanding the activity and regulation of PARL in the context of a larger proteolytic hub within the IMM is an interesting development in the study of this protease.

PARL is known as a critical regulator of mitochondrial function and heath as its identified substrates are implicated in maintaining mitochondrial homeostasis (Table 1.1 and Figure 1.5). Interestingly, the PARL-KO mouse does not display any drastic mitochondrial dysfunction or morphology abnormalities despite experiencing multisystem atrophy due to massive apoptosis, ultimately resulting in post-natal death[59]. While the PARL-KO mouse displays no obvious mitochondrial defects in regards to function or morphology, there are subtle phenotypes associated with apoptosis susceptibility. Cristae remodelling and cytochrome c release occur more quickly upon stimulation of apoptosis in mitochondria isolated from the liver of PARL-KO mice in comparison to wild type mice, suggesting that an increased rate of apoptosis is a large factor in the multisystem atrophy observed[59]. There are currently speculative roles of PARL in apoptosis, mitochondrial morphology, mitochondrial biogenesis, and mitochondrial degradation through the process of mitophagy[45].

The most studied substrate of PARL is the Phosphatase and tensin homolog (PTEN)-induced putative kinase 1 (PINK1). In healthy mitochondria, the PARL protease cleaves PINK1, which serves as a sensor of mitochondrial health[64]. Upon import of PINK1 to the IMM through the TOM and TIM translocation machinery, the mitochondrial processing protease (MPP) cleaves PINK1 to remove the MTS and sequentially PINK1 is cleaved at Ala103 by PARL[67]. Several studies performed in various cell lines provide evidence that PARL is the primary protease responsible for PINK1 cleavage at this site, though cleavage of PINK1 by PARL has yet to be demonstrated using a system with purified proteins *in vitro*. In the presence of the inactive

Table 1.1: Mitochondrial rhomboid proteases and their identified substrates. A list of the current substrates known for mitochondrial rhomboid proteases across species.

Species	Rhomboid	Substrate	Cellular role
S. cerevisiae	Rbd1/Pcp1	Ccp1[57,68] Mgm1[57,69,70]	Cytochrome c peroxidase maturation Mitochondrial membrane dynamics
D. melanogaster	Rho-7	Opa1-like[71] Pink1[72] Omi[72]	Mitochondrial fusion and apoptosis Mitophagy Apoptosis
Mammals	PARL	PINK1[49,64,67,73] PGAM5[74] Smac/DIABLO[75] STARD7[75] TTC19[75] CLPB[75]	Mitophagy Necroptosis/apoptosis Apoptosis Lipid transfer Cellular respiration Protein quality control

mutant of PARL, PARL-S277A/G, PINK1 is primarily localized to the mitochondria and there are minimal levels of the cleaved PINK1 fragment detected[67]. In the mitochondrial fraction of PARL-KO mouse embryonic fibroblasts (MEFs) that had been treated with the proteasomal inhibitor MG132, very minimal levels of the PARL-cleaved fragment of PINK1 are detected[73]. And, when PARL is knocked down by siRNA in HEK293 cells, there is an accumulation of both full-length PINK1 and the MPP-cleaved fragment; knockdown of two other IMM proteases also results in an accumulation of PINK1, suggesting there may be redundancy in the processing of PINK1 or compensatory mechanisms in place for a loss of PARL-mediated cleavage in specific situations[76]. After PINK1 processing, this 52 kDa cleaved fragment is then released back into the cytosol where it undergoes rapid proteasome-dependent degradation following the N-end rule pathway[77]. PARL-mediated cleavage of PINK1 is necessary to rapidly turn over PINK1 in the cell and signals that the mitochondrial pool is healthy[78]. When mitochondria are damaged, PINK1 accumulates on the OMM, thus preventing PARL-mediated cleavage. This accumulation then initiates a signal cascade that results in mitophagy, the pathway by which damaged mitochondria are selectively degraded to minimize cellular stress; the role of PINK1 in mitophagy will be discussed in greater detail in section *1.4*.

Phosphoglycerate mutase family member 5 (PGAM5), a Ser/Thr phosphatase implicated in apoptosis and necroptosis pathways, was identified as a substrate of PARL when it was observed that processing of PGAM5 was impaired when cells were treated with a coumarin-based protease inhibitor that is effective on rhomboids[17,74]. This was further validated by a decrease in PGAM5 processing upon PARL downregulation and an ability of wtPARL overexpression to restore processing, but not an overexpression of catalytically inactive PARL[74]. The PARL-mediated cleavage of PGAM5 is thought to be a pro-apoptotic signal; cells treated with staurosporine, a depolarizing agent, accumulate cleaved PGAM5 in the cytosol which is a substrate of the inhibitor of apoptosis proteins (IAPs) and this parallels an increase in active caspase 3, signalling apoptosis[79]. Interestingly, PGAM5 cleavage by PARL is mediated in the opposite manner to that of PINK1. Upon CCCP-induced mitochondrial

depolarization (decrease in $\Delta\psi$), an increase in PGAM5 processing is observed, contrasting to the decrease of PINK1 cleavage[74]. There is much speculation that PINK1 and PGAM5 may act on shared substrates, eliciting opposing responses depending on physiological conditions, however there is no current evidence that supports this. This inverse regulation of PARL-mediated cleavage of PINK1 and PGAM5 suggests that PGAM5 likely plays some role in the cellular response to mitochondrial stress, however because many of the target proteins of PINK1 and PGAM5 kinase and phosphatase activities respectively remain unknown, the physiological significance of PARL-mediated cleavage of PGAM5 remains to be elucidated.

In a recent study, several novel substrates of PARL were identified through two complementary proteomic mass spectrometry methods. Charge-based fractional diagonal chromatography was used to identity N-terminal peptides that accumulated in PARL^{+/+} and PARL^{-/-} HEK293 cells, while an affinity-enrichment proteomics approach looked at mitochondrial proteins that immunoprecipitated with either PARL[FLAG] or PARL[S277A-FLAG] expressed in PARL^{-/-} HEK293 cells[75]. Using these complementary methods, six unique proteins were identified. Identification of PINK1 and PGAM5 validated that the method was able to identify substrates of PARL, while new substrates identified included tetratricopeptide repeat domain 19 (TTC19), a subunit of the mitochondrial respiratory chain complex III, second mitochondrial-derived activator of caspases (Smac), a pro-apoptotic protein, STARD7, a lipid transferase, and CLPB, a proposed mitochondrial chaperone. The identification of these substrates further supports the role of PARL in mitochondrial homeostasis. Of particular interest was Smac as it is a pro-apoptotic protein and provides a more direct link for PARL and its long-speculated role in apoptosis (Figure 1.6). PARL cleaves Smac within its TM domain at Cys55, releasing the cleaved Smac fragment into the cytosol containing an AVPIA motif at its N-terminus[75]. This motif binds to IAPs, thus exerting a pro-apoptotic signal. The cleaved form of Smac binds to XIAP, a caspase inhibitor. Upon this binding, a caspase cascade is initiated in which caspase 9 is activated and further activates caspase 3 and caspase 7, triggering apoptosis. There is however some controversy in regards to PARL's role in apoptosis as it

was first speculated that PARL had an inhibitory role in apoptosis as opposed to the pro-apoptotic role seen with the Smac substrate and speculated with PGAM5. Early reports suggested that PARL had an anti-apoptotic role as PARL-deficient cells and the PARL-KO mouse display an increase in cytochrome c release and subsequent apoptosis[59]. These conflicting reports imply that PARL may have several distinct roles in apoptosis pathways that are regulated by specific cellular conditions.

With PARL's clear importance in mitochondrial homeostasis, it has been implicated in several disease pathologies. The first disease-relevance for PARL came from a study examining candidate genes for type 2 diabetes in rats[80]. The expression of PARL mRNA was decreased in diabetic rats, but restored when the disease was treated. This study also found that a common polymorphism of PARL resulting in the L262V amino acid substitution was associated with increased plasma insulin levels, an indication of insulin resistance. Further studies on insulin-resistant rats and diabetic human patients confirmed the observation of decreased PARL mRNA levels. The decreased mRNA levels were associated with reduced mitochondrial mass and activity, as well as impaired insulin signalling; a growing body of evidence suggests a link between mitochondrial dysfunction and diabetes[47,81-85]. The mechanism by which PARL could mediate insulin resistance in diabetes is not established, though it is proposed that decreased PARL levels result in an altered balance between mitochondrial biogenesis and mitophagy that impairs mitochondrial homeostasis. A skeletal muscle-specific PARL-KO in mice resulted in decreased mtDNA levels and altered mitochondrial morphology, which both point towards defects in mitochondrial biogenesis[47].

PARL is most commonly associated with Parkinson's disease (PD), though its role in disease pathology remains unclear. Mitochondrial dysfunction, and mitophagy dysfunction in particular, have been implicated in PD. Because PINK1 is a substrate of PARL and plays such a critical role in initiating mitophagy, dysregulation of PARL-mediated cleavage of PINK1, and therefore mitophagy initiation, has been purported as a possible underlying molecular mechanism of

disease. Further supporting this role of PARL in PD is the cleavage of PGAM5; this substrate is also implicated in the mitophagy pathway and therefore could contribute to mitochondrial dysfunction. The role of PARL in apoptosis as a potential contributing factor to PD also remains unclear. Several studies imply that PARL has anti-apoptotic activities while recent studies with PGAM5 and Smac show the contrary[59,75,79]. In brain tissue samples from PD patients, reduced PARL mRNA levels are detected providing some support to the idea of PARL inhibiting apoptosis and thus in its absence there is an increased rate of cell death[86]. However, if PARL exerts pro-apoptotic signalling and this is impaired, many cellular consequences can arise as well. Furthermore, a PD-associated mutation has been identified in PARL itself. The PARL-S77N mutation was identified in two PD patients and prevents β-cleavage and the formation of PARLΔ77. The identification of this mutation further complicates our understanding of how PARL may be contributing to the pathogenesis of PD, but it does support the idea that the dysregulation of PARL-mediated cleavage events can lead to overall defects in mitochondrial homeostasis which in turn is a risk factor for the development of PD. Our understanding of PARL and its role in PD will be further discussed in section *1.5* and Chapter 5.

With the recent identification of the three novel substrates of PARL, new disease-implications have arisen. TTC19 is a subunit of complex III of the respiratory chain and is associated with complex III deficiency, resulting in respiration defects which manifest as major neurological impairments[87]. Several mutations found in CLPB have been associated with brain atrophy, neutropenia, cataracts, and movement disorders, while STARD7 is implicated in acute asthma[75]. Further studies on these substrates and their PARL-mediated cleavages are required before any speculations can be made about the potential role of PARL in their associated diseases.

The current knowledge in the field highlights PARL as an essential mediator of mitochondrial homeostasis and quality control and as a regulator of cellular signalling. While many unanswered questions remain regarding its regulation, mechanisms of substrate recognition
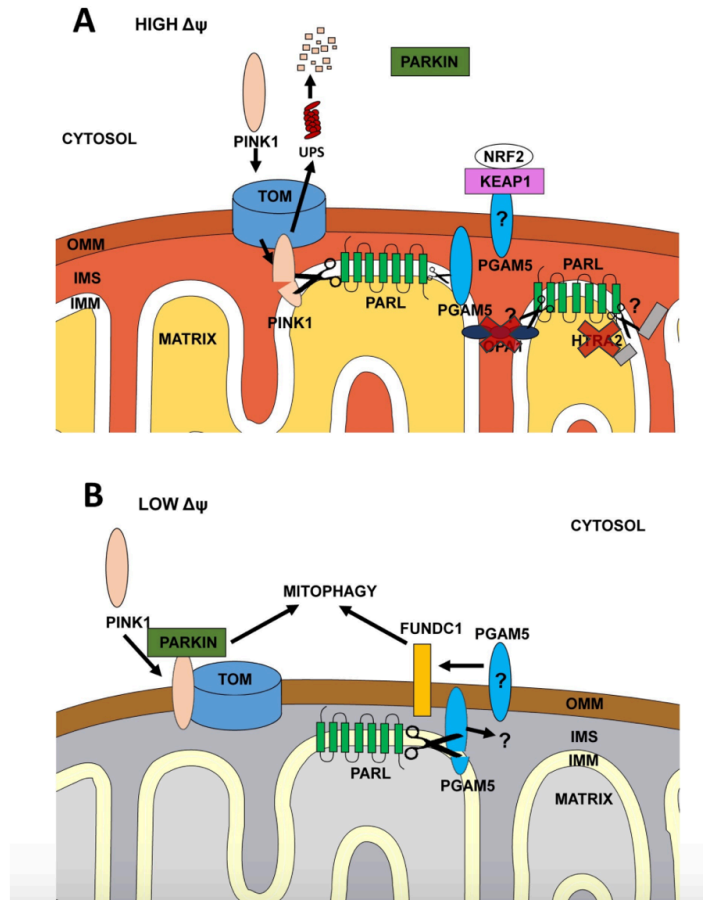
Figure 1.5: Cartoon schematic illustrating PARL and its proposed substrates. PARL resides in the inner mitochondrial membrane (IMM). **A)** When mitochondrial membrane potential ($\Delta\psi$) is maintained, PARL cleaves PINK1 in the IMM. Cleavage of PGAM5 is reduced in polarized mitochondria, as PINK1 is the preferred substrate. OPA1 and HTRA2 are no longer considered substrates of PARL, though new substrates such as Smac (not depicted in this schematic) have been identified. **B)** Upon membrane depolarization, PINK1 import to the IMM is inhibited and it accumulates on the OMM to initiate mitophagy. PARL now preferentially cleaves PGAM5 which also contributes to the process of mitophagy[45]. Adapted from Spinazzi, M. and de Strooper, B. (2016). PARL: The mitochondrial rhomboid protease. *Semin Cell Dev Biol 60*, 19-28.
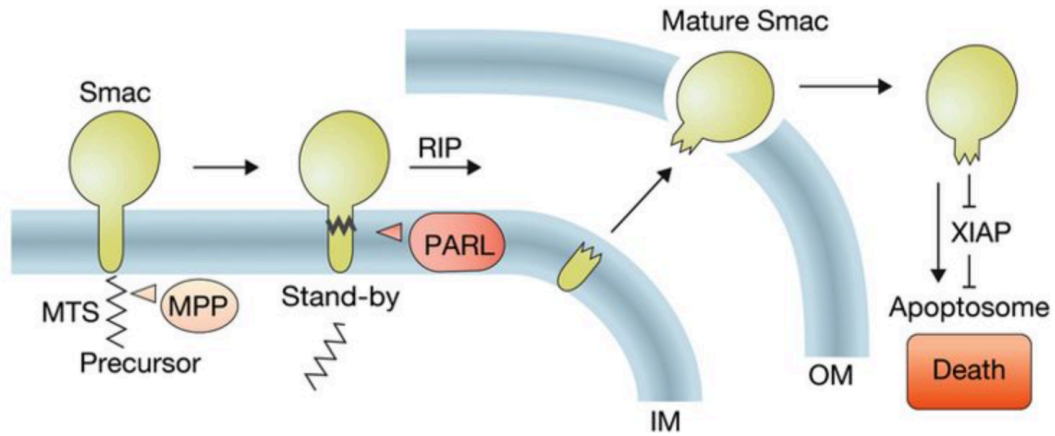
Figure 1.6: The role of PARL in apoptosis. PARL cleaves Smac within its TM domain in the IMM resulting in the release of mature Smac. Mature Smac binds to XIAP, a caspase inhibitor. Upon this binding, a caspase cascade is initiated in which caspases are activated and apoptosis is triggered[88]. Adapted from Ishihara, N. and Mihara, K. (2017). PARL paves the way to apoptosis. *Nat Cell Biol 19*, 263-265.

and cleavage, and physiological functions, advances in proteomic, biochemical, and cellular methodologies are poised to address key questions related to PARL and its role in mitochondrial and cellular pathways.

1.3 Mitochondrial homeostasis

Mitochondrial homeostasis is maintained through ongoing dynamic processes; biogenesis and mitophagy maintain the overall cellular mitochondrial pool while dynamic fission and fusion events maintain the integrity of an individual mitochondrion[89]. Signalling effects resulting from maintaining this mitochondrial homeostasis can determine the heath of the cell and influence decisions regarding cell fate such as apoptosis (Figure 1.7).

Mitochondrial biogenesis requires the tight regulation of numerous nuclear and mitochondrial factors in order to be successfully carried out. While the majority of mitochondrial proteins are encoded by nuclear DNA, proteins encoded by mitochondrial DNA, like those of the respiratory complexes, are necessary for mitochondrial function. In order for respiratory complexes to form, tight coordination between transcription and translation of both nuclear and mitochondrial genes is required. Cells have developed sophisticated methods for ensuring the synchronization of these processes. Several nuclear transcription factors orchestrate the specific expression of nuclear genes that encode for mitochondrial proteins such as components of the respiratory complexes (cytochrome C oxidase subunits and cytochrome C for example) or mitochondrial import machinery (TOMM34 of the TOM complex)[90,91]. These nuclear encoded gene transcripts are then stabilized by a subunit of the TOM complex which allows them to be translated on ribosomes in close proximity to the mitochondrion, facilitating their subsequent mitochondrial import[92]. Replication of mtDNA, along with its transcription and translation is the second aspect of mitochondrial biogenesis that requires tight regulation. Mitochondrial transcription requires the mtRNA polymerase as well as several transcription factors[93,94]. Translation of these mitochondrial transcripts occurs in the mitochondrial matrix
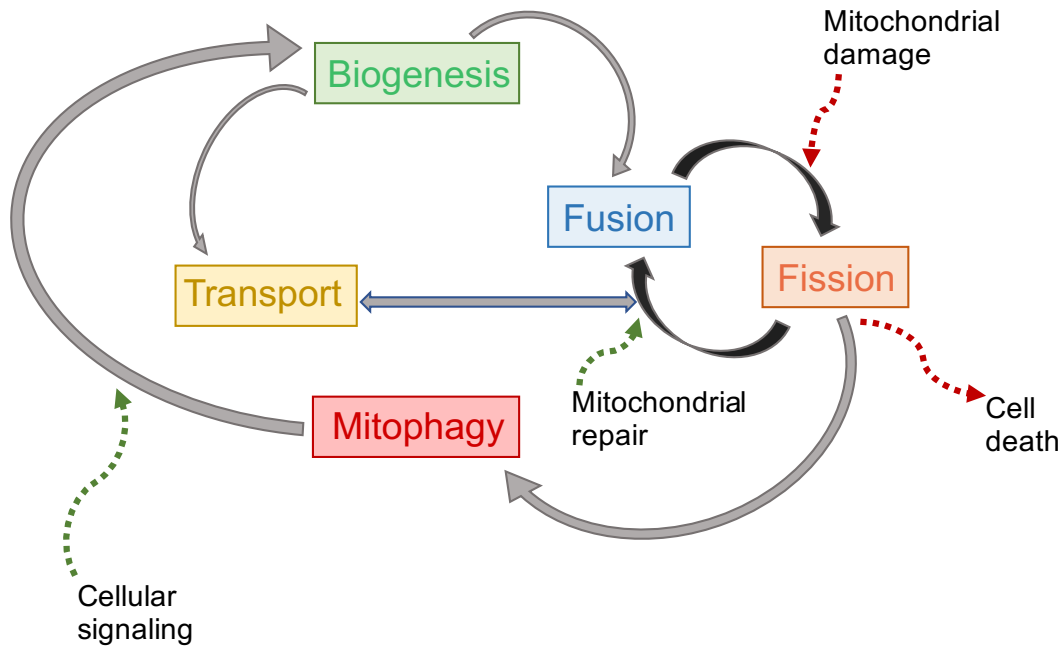
Figure 1.7: Mitochondrial homeostasis. Ongoing dynamic processes maintain mitochondrial homeostasis. Mitochondrial biogenesis and mitophagy, the selective autophagy of mitochondria, maintain the mitochondrial pool. The processes of fusion and fission maintain the health of an individual mitochondrion. Healthy mitochondria, whether after biogenesis or mitochondrial repair, are constantly coming together in the process of fusion to maintain mitochondrial fidelity. Upon mitochondrial damage, fission will occur; this will promote mitophagy of the damaged mitochondrial species or lead to cell death if damage is too extensive. The degradation of damaged mitochondria through mitophagy results in cellular signalling to initiate biogenesis, thus continuing the mitochondrial lifecycle and maintaining homeostasis[95]. Adapted from Chu, C. T. (2010). Tickled PINK1: Mitochondrial homeostasis and autophagy in recessive Parkinsonism. *Biochim Biophys Acta 1802*, 20-28.

on ribosomes that interact with the IMM and requires the assistance of both mitochondrial and cytoplasmic factors that add further layers of regulation to the process[96-98].

To maintain the fidelity of an individual mitochondrion, the highly dynamic organelles are constantly in a flux of fission and fusion events in response to cellular and organellar conditions. The processes of fission and fusion are mediated by proteins within the dynamin family, including Drp1, Mfn1, Mfn2, and OPA1[99]. The dynamin family proteins are a class of GTPases involved in fission and fusion of vesicular and organellar membranes. During mitochondrial fission, damaged pieces of mitochondria are essentially isolated and segregated from the otherwise healthy organelle, thus maintaining the heath of the individual mitochondrion. Mitochondrial fission is mediated primarily by dynamin-related protein 1 (Drp1) through a mechanism in which Drp1 is recruited to fission sites marked by mitochondrial fission protein 1. At these fission sites, Drp1 polymerizes and constricts the damaged area of the mitochondrion, resulting in separation of the OMM and IMM and a division of the healthy and damaged regions of the mitochondrion. These released fragments of damaged mitochondria will then be degraded in an autophagic manner. Mitochondrial fusion is the reverse of the fission process and involves the fusing together of mitochondrial fragments to produce a healthy mitochondrion. Mitochondrial fusion is mediated by mitofusin 1 and 2 (Mfn1 and Mfn2), as well as optic atrophy type 1 protein (OPA1). Mfn1 and Mfn2 are dynamin family proteins that are anchored to the OMM where they facilitate fusion of the outer membrane of mitochondrial fragments that are joining together[100]. Fusion of the IMM is mediated through OPA1, a protein anchored to the IMM and residing in the IMS[101].

While fission is an ongoing process used to mediate mitochondrial damage, there are other, more specialized, forms of damage control that the organelle employs as well. If a mitochondrion experiences an increase in unfolded proteins or proteins that have been damaged by oxidative stress, specific ATP-dependent proteases, such as the Lon protease or *m-* and *i*-AAA proteases, in various subcompartments of the mitochondrion will recognize the

compromised proteins and initiate their degradation by proteolysis. If such damaged proteins are localized to the OMM, they can be recognized and subsequently degraded by the ubiquitin proteasome system[102]. Accumulation of unfolded proteins can also trigger the mitochondrial unfolded protein response (mtUPR); a system in which the expression of mitochondrial chaperones is upregulated in an attempt to minimize the buildup of unfolded proteins[103]. More recently, a new mitochondrial damage control mechanism was identified that is similar to fission. Mitochondrial-derived vesicles (MDVs) form around regions of damage in a mitochondrial membrane and are then cleaved and released to the cytosol to undergo lysosomal degradation. While this process seems very similar to fission, the release of the MDVs to the cytosol occurs in a fission-independent manner[104].

If fission and fusion dynamics or other mitochondrial quality control mechanisms are unable to mitigate mitochondrial damage, pathways are activated to remove the damaged organelle in its entirety before it can cause further cellular stress. The pathway of mitophagy, the selective autophagy of damaged mitochondria, implicates both PARL and PINK1 in maintaining mitochondrial homeostasis and will be covered in detail in section *1.4*.

Mitochondria are essential organelles as they function in cellular pathways such as oxidative phosphorylation, calcium homeostasis, lipid metabolism, and apoptosis[89]. The importance of maintaining mitochondrial homeostasis and health is evident by the extensive disease states associated with mitochondrial dysfunction. Any impairment of the balance between mitochondrial biogenesis and mitophagy or fission and fusion can result in great consequences to the cell.

1.4 PINK1 and mitophagy

The PTEN-induced kinase, PINK1, is a sensor of mitochondrial health and is responsible for initiating mitophagy of damaged mitochondria under stress conditions. PINK1 is a cytosolic

Ser/Thr kinase composed of 581 amino acids and organized into three main domains, an N-terminal MTS, a small TM domain spanning residues 89-111, and a large kinase domain spanning residues 156-511 (Figure 1.8). Under healthy mitochondrial conditions, PINK1 is directed from the cytosol to the mitochondria due its MTS where it is then translocated through the TOM and TIM complexes, allowing it to be integrated into the IMM; this translocation process requires the IMM to have an intact electrochemical gradient[73]. Once situated in the IMM, the N-terminal MTS that extends into the mitochondrial matrix is cleaved by MPP and a 60 kDa PINK1 fragment is produced. Subsequently, PARL cleaves PINK1 at Ala103 resulting in a 52 kDa cleaved product[67]. Knockdown of both MPP and PARL results in an accumulation of full-length PINK1, indicating that these proteolytic events are constitutive and that removal of the MTS is required before further processing can occur[76]. This second cleavage event releases the cleaved 52 kDa PINK1 fragment containing the kinase domain back into the cytosol where it undergoes rapid proteasome-dependent degradation following the N-end rule pathway (Figure 1.9)[77]. This rapid turnover of PINK1 is necessary to maintain the fidelity of the mitochondrial pool and results in minimal levels of the wild-type protein being able to be detected in cellular studies[77]. It has been demonstrated that mutations in the PINK1 TM region lead to aberrant cleavage by PARL which could have detrimental effects to the cell due to a dysregulation of mitophagy[73]. Helix-stabilizing mutations appear to have the greatest effect on altering PINK1 cleavage. For example, the PINK1-R98F mutation is hydrolysed much more poorly than PINK1-WT. It has been proposed that for cleavage of TM substrates by rhomboid proteases, local helix unwinding around the cleavage site is required for the protease to cleave efficiently; the WT Arg residue at position 98 would be destabilizing to the helix, thus promoting helical unwinding and promoting cleavage[105]. A mutation to Phe at this site would make the helical propensity go from destabilized to stabilized, thus reducing the ability of PARL to cleave within that region and dysregulating PINK1 turnover. In addition, some evidence suggests that Arg residues that are present in transmembrane helices can be thermodynamically stable and may influence the dynamic stability of a protein in the bilayer, essentially making the TM segment less static[106].

Figure 1.8: Domain organization of PINK1. An outline of the three domains of PINK1 (UniProtKB Q9BXM7)[107]. Highlighted in orange is the N-terminal mitochondrial targeting sequence (MTS) spanning residues 1-77, in red is the putative transmembrane domain (TMD) from residues 89-111, and in pink is the large C-terminal PTEN-kinase domain spanning residues 156-511.

Mitophagy is a cellular process by which damaged mitochondria are selectively targeted for autophagic degradation. Damage to mitochondria can arise from perturbations such as an increase in reactive oxygen species (ROS), a dissipation of the mitochondrial electrochemical gradient, an accumulation of misfolded proteins, mutations in mitochondrial DNA, or simply a loss of mitochondrial viability due to age[108]. The process of mitophagy is critical for clearing the cell of the impaired organelles to prevent further cellular stress and mitigating the initiation of cell death.

When mitochondria are damaged, PINK1 will accumulate on the OMM due to a loss of electrochemical potential to drive the translocation of PINK1 to the IMM (Figure 1.9). In the OMM, PINK1 dimerizes and autophosphorylates itself at Ser228 and Ser402 within the kinase domain[109,110]. This accumulation of PINK1 results in the recruitment of the E3 ubiquitin ligase Parkin. PINK1 phosphorylates Parkin at Ser65 and ubiquitin at Ser65, thus activating Parkin and allowing its E3 ubiquitin ligase activity to proceed[111-114]. Parkin then ubiquitinates target proteins on the OMM, producing K6-, K11-, K48-, and K63-linked ubiquitin chains which signals extraction and proteasomal degradation of OMM proteins along with the recruitment of autophagy machinery[115-118]. To date, there have been 36 OMM proteins identified as substrates of Parkin-dependent ubiquitination. This suggests that it is not the ubiquitination of a specific protein that triggers mitophagy, but rather the type of ubiquitin chain linkage and the density of ubiquitinated proteins on the OMM[108]. Following ubiquitination of target OMM proteins and their subsequent degradation by the proteasome, autophagy machinery is recruited to the damaged mitochondrion that has been tagged for degradation. Autophagosomal membranes are generated and surround the damaged mitochondrion, facilitating the removal of the dysfunctional organelle and its degradation by lysosomal hydrolases[119] (Figure 1.10). Data suggests that mitochondrial fragmentation enhances autophagic engulfment of the damaged organelle. There is strong evidence that mitochondrial fission machinery is required for the process of mitophagy in yeast. Studies in PINK1 and Parkin-mutant *Drosophila* have observed that promoting mitochondrial fission reverses their
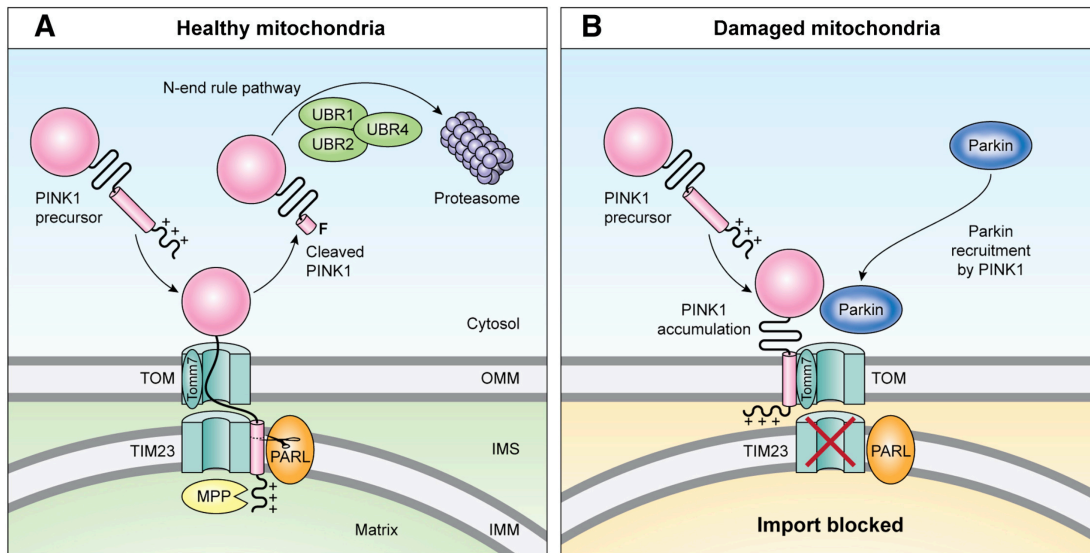
Figure 1.9 Model for mitochondrial import and processing of PINK1. Cytosolic PINK1 is directed to the mitochondria by its N-terminal mitochondrial targeting sequence (MTS). When mitochondrial membrane potential is intact, signalling healthy a mitochondrion, PINK1 is translocated through the TOM and TIM complexes into the inner mitochondrial membrane (IMM). Upon insertion of the transmembrane domain (TMD) into the IMM, the N-terminal MTS is cleaved by the mitochondrial processing peptidase (MPP), a metalloprotease that resides in the mitochondrial matrix. Subsequently, PINK1 meets PARL, the mitochondrial rhomboid protease, and is cleaved within its TMD at Ala103. Upon this processing event, the soluble kinase domain of PINK1 is released back to the cytosol, with a Phe residue at the N-terminus, where it undergoes rapid proteasome-dependent degradation following the N-end rule pathway. If the membrane potential of the IMM is dissipated, PINK1 will accumulate on the OMM due to the energetics of translocation being unfavourable. Here on the OMM, PINK1 will recruit Parkin to initiate mitophagy[108] (outlined in Figure 1.9). From Pickrell, A. M. and Youle, R. J. (2015). The roles of PINK1, parkin, and mitochondrial fidelity in Parkinson's disease. *Neuron 85*, 257-73.
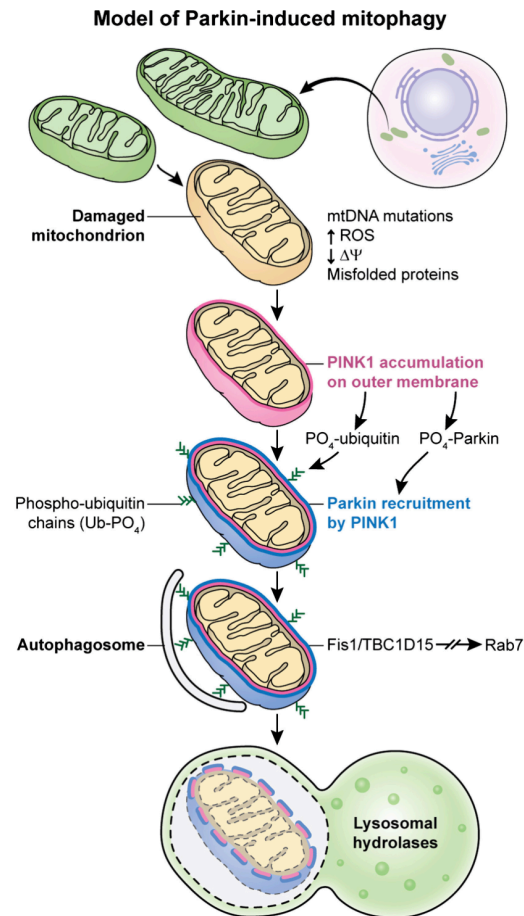
Figure 1.10: Mitophagy schematic. Upon damage to the mitochondria, PINK1 is unable to translocate to the IMM and thus accumulates on the OMM. This accumulation results in the recruitment of the E3 ubiquitin ligase Parkin. PINK1 phosphorylates both Parkin and ubiquitin, activating the ubiquitin ligase activity of Parkin. Parkin ubiquitinates target proteins on the OMM, triggering the extraction and degradation of OMM proteins and subsequently recruiting autophagy machinery to the damaged organelle. The mitochondrion that has been tagged for degradation is then engulfed by autophagosomes and degraded by lysosomal hydrolases[108]. From Pickrell, A. M. and Youle, R. J. (2015). The roles of PINK1, parkin, and mitochondrial fidelity in Parkinson's disease. *Neuron 85*, 257-73.

phenotype[120-128].

The PINK1 protein is most commonly studied in the context of Parkin recruitment and mitophagy initiation, though other potential functions in the cell have been identified. PINK1 has been proposed to phosphorylate proteins involved in mitochondrial dynamics, quality control, and bioenergetics though these targets have not been validated *in vitro*[111,112,129,130].

PINK1 is a main regulator of mitochondrial homeostasis, though with phosphorylation targets only validated in the mitophagy pathway, the full extent of PINK1-mediated regulation of mitochondrial homeostasis is not yet clear. Impaired mitophagy can result in an accumulation of damaged mitochondria in the cell; this increased cellular stress can lead to the initiation of apoptosis or other cell death mechanisms. It has been proposed that mitochondrial dysfunction and mitophagy impairment are underlying factors in the etiology of neurodegenerative diseases, particularly Parkinson's disease, thus implicating PINK1 as a potential disease target. This highlights the importance of its study and the mechanism by which it is cleaved by the PARL protease.

1.5 Parkinson's disease

Parkinson's disease (PD) is the most common movement disorder and the second most common neurodegenerative disorder, following Alzheimer's disease[131]. It is estimated that 1-2 in 1000 are diagnosed with the disease and that 1% of the population over the age of 60 is affected by PD[132,133]. Neurodegenerative diseases are characterized by a loss in structure or function of neurons, including neuronal death. Parkinson's disease is characterized by progressive dopaminergic neuronal loss, with the pathological hallmark being the presence of Lewy bodies, protein aggregates composed primarily of α-synuclein. Neuronal loss is observed predominantly in the substantia nigra pars compacta region of the brain[134] As dopamine signalling is required for motor function, those affected with PD present symptoms of impaired voluntary motor function. There are four cardinal motor symptoms associated with

PD: tremor, rigidity, bradykinesia/akinesia, and postural instability[134,135]. In recent years, focus has also been placed on non-motor symptoms associated with the disease such as sleep and autonomic dysfucntion[136]. While the pathology and physiology of PD have been extensively characterized, a concrete understanding of the etiology of the disease has proved elusive[137,138].

A substantial body of evidence supports the concept of mitochondrial dysfunction playing a central role in disease etiology. The first direct evidence that mitochondrial dysfunction could play a role in PD was that accidental exposure of patients to a selective inhibitor of complex I resulted in parkinsonism and dopaminergic neuron degeneration[139]. Further studies identified reduced complex I activity in tissue samples from PD patients and found that exposure to other complex I inhibitors can induce dopaminergic neuron loss and parkinsonism phenotypes[140,141].

Most commonly presented as a sporadic disease in an aged population, considered the idiopathic form of the disease, mutations in several genes have been implicated in inherited familial forms of the disease (Table 1.2). The first genetic links to PD were identified in 1997 in the gene encoding for α-synuclein and in an unidentified gene that was later sequenced and identified as *PARK2* encoding for the Parkin protein[142,143]. Interestingly, mutations in the *PARK2, PARK6* and *PARL* loci, encoding for the Parkin, PINK1, and PARL proteins respectively, have been identified in PD patients. These proteins all play important roles in mitochondrial homeostasis and further support the notion of mitochondrial dysfunction as a contributing factor to PD pathogenesis. As neurons have high energy requirements, it is not surprising that mitochondrial dysfunction is often implicated in neurodegenerative diseases. Dopaminergic neurons in particular, like those affected in PD, have distinct physiological features that may increase their susceptibility to mitochondrial dysfunction[144]. It is commonly thought that because dopaminergic neurons have high metabolic activities, there is increased production of reactive oxygen species which leads to extensive mitochondrial damage[145]. With high metabolic activities and the presence of a mutation within a gene essential in maintaining

Table 1.2: Genetic forms of Parkinson's disease. A compiled list of all currently identified genes implicated in inherited forms of PD[146]. Inheritance is classified as autosomal dominant (AD) or autosomal recessive (AR). Onset is classified as idiopathic-onset (IO) or early-onset (EO).

LOCUS	GENE	GENE PRODUCT	INHERITANCE	ONSET
PARK1/PARK4	SNCA	α-synuclein	AD	EO / IO
PARK2	PRKN	Parkin	AR	EO
PARK5	UCHL1	UCHL1	AD	IO
PARK6	PINK1	PINK1	AR	EO
PARK7	DJ-1	DJ1	AR	EO
PARK8	LRRK2	LRRK2	AD	IO
PARK9	ATP13A2	AT13A2	AR	EO
PARK11	GIGYF2	GIGYF2	AD	IO
PARK13	HTRA2	HTRA2	AR	IO
PARK14	PLA2G6	Cal-PLA2	AR	EO
PARK15	FBXO7	FBXO7	AR	EO
PARK17	VPS35	VPS35	AD	IO
PARK18	EIF4G1	eIF-4G1	AD	IO
PARK19	DNAJC6	DNAJC6	AR	EO
PARK20	SYNJ1	SYNJ-1	AR	IO
PARK21	DNAJC13	DNAJC13	AD	IO
PARK23	VPS13C	VPS13C	AR	EO

mitochondrial homeostasis, it is likely that these dopaminergic neurons would be highly sensitive to any mitochondrial perturbations and would not be able to mediate large amounts of mitochondrial damage, leading to neuronal death.

The phenotype of inherited forms of PD associated with recessive mutations in PINK1 or Parkin are indistinguishable from sporadic cases, however they tend to be of early-onset[138,147,148]. The PARK2 and PARK6 forms of PD, in which mutations in either Parkin or PINK1 are observed, are the two most common forms of inherited PD[149]. Extensive studies have been performed in animal models to decipher the specific role these two proteins play and how they may contribute to a disease phenotype. Unexpectedly, both Parkin-KO and PINK1-KO mice failed to model the pathophysiology of PD seen in humans, specifically the loss of dopaminergic neurons. Parkin-KO mice have mild phenotypes, including a disruption to fine motor skills and slight impairment of dopamine metabolism, while PINK1-KO mice have no dopaminergic neurodegeneration or altered dopamine metablism[150-152]. While no clear phenotype is seen with the KO mouse models, there are mitochondrial impairments such as altered mitochondrial protein expression levels, impaired respiration, altered calcium homeostasis, increased ROS production, and impaired ATP synthesis[153-157].

The lack of an adequate mammalian model led to the generation of *Drosophila* models that provided a much greater understanding of the roles of Parkin and PINK1. Both Parkin-null and PINK1-null flies have severe phenotypes characterized by flight muscle degeneration, locomotive issues, abnormal mitochondrial morphology, male sterility, and, most importantly, abnormalities in dopaminergic neurons and neuronal loss[158-161]. It is now well established that Parkin and PINK1 have central roles in the mitophagy pathway (section 1.4), thus why we see such a dramatic phenotype in relation to mitochondrial health. It is speculated that the milder phenotype is observed in the mouse models due to compensatory mechanisms in place to mitigate the loss of PINK1 or Parkin. The identification of inherited PD mutations in Parkin and PINK1 greatly implicates the process of mitophagy and mitochondrial health in the

pathogenesis in PD as these two proteins play a central role in sensing and maintaining mitochondrial homeostasis.

Recently, other proteins have been identified that may influence the PINK1/Parkin mitophagy pathway. In *Drosophila*, deficiencies in the mitochondrial protein PGAM5 have been shown to result in a PD-like movement disorder[162]. Interestingly, PGAM5-KO mice display dopaminergic neuron degeneration, thus resulting in the PD-like movement disorder. This is unlike the PINK1-KO mice, in which only a slight phenotype is displayed and no abnormalities in dopaminergic neurons are observed. This study identified PGAM5 as a potential new regulator of the PINK1/Parkin mitophagy pathway in its ability to stabilize PINK1 and protect against dopaminergic neuron degeneration, a hallmark of the PD phenotype. While there have been no PD-associated mutations identified in PGAM5, it does show that there may be numerous unidentified interacting proteins in converging mitochondrial homeostasis pathways that contribute to overall mitochondrial health and impairments in the function of any of these factors could present risk factors for developing PD.

Currently, therapies for PD are limited to symptomatic treatments and relief, such as deep-brain stimulation or supplements of levodopa (L-DOPA), a dopamine precursor. The autosomal recessive forms of the disease associated with mutations in PINK1 and Parkin respond well to levodopa treatments, perhaps due the slower disease progression noted for these forms compared to idiopathic PD[163]. A more thorough knowledge of the molecular etiology of the disease is required for the development of therapies that target the molecular mechanism of the disease, perhaps even before observable symptoms, such as the cardinal motor defects, present themselves.

Parkinson's disease is the most common movement disorder, however there remains a vast lack of knowledge on the underlying molecular etiology of the disease due to complexities and heterogeneity in the pathology of the disease. The misfolding and subsequent aggregation of

α-synuclein into the pathological hallmark Lewy bodies are a primary suspect for disease etiology and progression, however multiple other cellular processes are thought to be involved that either contribute to protein aggregation and Lewy body formation or impair other cellular processes that enhance disease progression. Mitochondrial dysfunction appears to be at the forefront for a plausible etiology of PD, with numerous mitochondrial proteins having a genetic link to the disease and resulting in impaired mitochondrial homeostasis. Defective protein clearance and neuroinflammation also have speculative roles in the development of PD[146]. As research into the numerous pathways implicated in PD continues, we will likely have a greater understanding of the molecular landscape that contributes to disease pathogenesis and how the dysfunction of multiple regulatory pathways converges to result in the PD phenotype.

1.6 Thesis objective

This thesis aims to address questions regarding molecular determinants and regulators of PARL-mediated intramembrane proteolysis. PARL is clearly a very important enzyme in mitochondrial homeostasis, however, key questions regarding its proteolytic activity have remained unanswered due to the lack of established *in vitro* assays using purified protein. *In vitro* studies of recombinantly expressed and purified bacterial rhomboid proteases were essential in validating the findings observed in initial cellar studies. To date, there is no published literature on recombinantly expressed HsPARL. Cellular studies have provided great insights into identified substrates and regulatory mechanisms of the PARL protease, though elucidating physiological relevance from these studies has remained a challenge. Many of these cellular studies utilize whole cell lysates which contain a plethora of proteases in addition to the use of harsh treatments, such as CCCP to dissipate the mitochondrial electrochemical gradient, or full protein knockouts in order to observe changes in substrate processing. While this provides valuable insights, such harsh methods may be exacerbating the results we see.

Using a highly sensitive and robust kinetic assay with HsPARL, we aim to assess the cleavage

of several PARL substrates *in vitro* to address key questions related to the activity of PARL. Chapter 3 and 4 focus on validating and characterizing the proteolytic activity of recombinant HsPARL. We will first look at cleavage of a model internally quenched (IQ) peptide to assess the activity of the recombinant PARL we expressed and purified. Upon validation of sufficient activity, we will assess cleavage of several PARL substrates; substrates tested will include small IQ peptides of the identified PARL substrates PINK1, PGAM5, and Smac, as well as a longer, more physiological substrate composed of residues 70-134 of HsPINK1 flanked by a FRET pair. An examination of PARL-mediated cleavage with different substrates using an *in vitro* assay will allow us to obtain specific catalytic parameters that can provide new insights into PARL-mediated cleavage events. We hypothesize that the truncations of PARL identified *in vivo* as well as the lipid cardiolipin (CL), which is unique to the IMM where PARL localizes, will have an observable effect on PARL proteolytic activity. Observing PARL proteolytic activity in the context of its different truncations and lipid environment will validate these factors as regulators of PARL activity. By observing the cleavage of several substrates, we can compare specific catalytic parameters obtained for each substrate to determine if a preferred substrate of PARL can be identified. Identifying a potentially preferred substrate of PARL can place cleavage of these different substrates in the context of the differential regulation of cleavage of different substrates, for example as seen for decreased PINK1 cleavage and increased PGAM5 cleavage upon mitochondrial stress.

In Chapter 5, we aim to begin elucidating a mechanism of PD pathogenesis that may implicate PARL in the etiology of the disease. We hypothesize that PD-associated variants of PINK1 that harbour mutations within the transmembrane region will display altered cleavage, and therefore altered catalytic parameters, compared to those observed for PINK1-WT cleavage by PARL. We will use the longer HsFRET-PINK1(70-134) substrate to address cleavage of the PD-associated PINK1 variants as mutations further from the PINK1 cleavage site may still affect substrate recognition and cleavage. We will assess cleavage of PINK1-WT and the PD-associated variants PINK1-C92F, R98W, I111S, and Q126P.

The aims of this thesis will address several unanswered questions related to PARL-mediated cleavage by utilizing a sensitive *in vitro* assay. Substrates of PARL identified in cellular studies will be validated with our *in vitro* proteolytic assay and insights into regulatory mechanisms of PARL will be clarified. Furthermore, a potential role of PARL in mitophagy dysfunction and PD will be presented.

CHAPTER 2: MATERIALS & METHODS

2.1 Materials

Standard reagents were ordered from BioBasic Inc., Becton, Dickinson & Company, Fisher Scientific, Roche, and Sigma Aldrich.

2.1.1 Protein expression solutions and media

Low-salt Lysogeny broth (LB), yeast peptone dextrose (YPD), and yeast peptone dextrose sorbitol (YPDS) media was prepared as outlined in Table 2.1 and autoclaved. If media were being prepared to make plates, 2% (w/v) agar was included. The pH of low-salt LB was adjusted to 7.5 using 5 M NaOH before autoclaving. Sterile 20% (w/v) dextrose prepared by filter sterilizing the solution into an autoclaved bottle using a 0.22 μm nitrocellulose membrane filter. Sterile dextrose was added to YPD and YPDS media after autoclaving to a final concentration of 2% (w/v). The required antibiotic was added once autoclaved media had cooled; ampicillin was added to low-salt LB and YPD media to a final concentration of 100 μg/mL and Zeocin was added to YPDS medium to a final concentration of 25 μg/mL. Plates and media containing Zeocin were stored in the dark as Zeocin is light sensitive.

Table 2.1: Autoclaved media for recombinant protein expression screening in *Pichia pastoris*.

SOLUTION	REAGENT(S)	AMOUNT (g/L)
Low-salt LB	Yeast extract	5 g
	Tryptone	10 g
	NaCl	5 g
YPD	Yeast extract	10 g
	Peptone	20 g
YPDS	Yeast extract	10 g
	Peptone	20 g
	Sorbitol	182.17 g (for 1 M)

Standard yeast media ingredients were prepared as outlined in Table 2.2 and Table 2.3. BMGY and BMMY broth to be autoclaved were prepared in 4 L baffled flasks as these allow

for greater aeration than standard 4 L culture flasks. All solutions that are heat-sensitive were filter sterilized into autoclaved bottles using a 0.22 μm filter before use and stored at 4°C. To autoclaved BMGY or BMMY broth, solutions were added to complete the growth or induction media (Table 2.4). Sterile technique was used in the preparation of the media.

Table 2.2: Non-autoclaved yeast media ingredients.

SOLUTION	REAGENT(S)	AMOUNT
0.02% (w/v) biotin	D-Biotin	0.02 g per 100 mL ddH$_2$O
10X KPO$_4$ buffer pH 6.0	K$_2$HPO$_4$ KH$_2$PO$_4$	23 g per 1 L 118.13 g per 1 L
10X YNB	Yeast Nitrogen Base w/o amino acids and w/o ammonium sulfate Ammonium sulfate	34 g per 1 L 100 g per 1 L
100 mg/mL ampicillin	Ampicillin salt	10 g per 100 mL

Table 2.3: Autoclaved yeast media ingredients

SOLUTION	REAGENT(S)	AMOUNT
BMGY or BMMY	Yeast extract Peptone	10 g 20 g in 780 mL ddH$_2$O
50% (v/v) glycerol	Glycerol	500 mL in 500 mL ddH$_2$O

Table 2.4: Recipe for 1 L BMGY or BMMY yeast media

	BMGY	BMMY
10X KPO$_4$ buffer pH 6.0	100 mL	100 mL
10X YNB	100 mL	100 mL
0.02% (w/v) biotin	4 mL	4 mL
100 mg/mL ampicillin	1 mL	1 mL
50% (v/v) glycerol	20 mL	--
100% methanol	--	20 mL

2.1.2 Protein purification solutions

Protein purification solutions were prepared as outlined in Table 2.5. All solutions were filter sterilized into autoclaved bottles using a 0.22 μm filter before use and stored at 4°C. Other

reagents used during protein purification included 100 mM PMSF (dissolved in anhydrous EtOH), 1 M TCEP, and cOmplete™ mini EDTA-free protease inhibitor cocktail tablets (Roche).

Table 2.5: Protein purification solutions. All buffer solutions used in the purification of HsPARL.

SOLUTION	REAGENT(S)	CONCENTRATION
Tris buffered saline (TBS)	Tris-HCl pH 8.0 NaCl	50 mM 150 mM
Solubilization buffer	Tris-HCl pH 8.0 NaCl Glycerol Imidazole pH 8.0	50 mM 200 mM 20% (v/v) 20 mM
Buffer A	Tris-HCl pH 7.0 NaCl Glycerol DDM	50 mM 300 mM 20% (v/v) 0.1% (w/v)
Buffer B	Tris-HCl pH 7.0 NaCl Glycerol DDM Imidazole	50 mM 300 mM 20% (v/v) 0.1% (w/v) 500 mM
Dialysis buffer	Tris-HCl pH 7.0 NaCl Glycerol	50 mM 300 mM 20% (w/v)

2.1.3 Kinetic assay buffers and substrates

Activity assay buffers were prepared as outlined in Table 2.6. All solutions were filter sterilized into autoclaved bottles using a 0.22 μm filter before use and stored at 4°C. Peptides for kinetic analysis were synthesized by Biomatik (Ontario, Canada) and received as trifluoroacetate salt. Lyophilized peptides were stored at -20°C until resuspended in DMSO for use; once resuspended, peptides were stored at 4°C. Peptide sequences are outlined in Table 2.7.

2.1.4 Reagent kits

Standard reagent kits were used for preparation of competent yeast cells (Pichia EasySelect Expression Kit, Invitrogen), DNA isolation (Geneadid Miniprep kit, QIAGEN Plasmid

Purification Midi and Maxi Kit, and QIAquick Gel Extraction Kit) and protein concentration determination (Pierce™ BCA Protein Assay Kit, ThermoFisher, USA).

Table 2.6: Protease activity assay buffers

SOLUTION	REAGENT(S)	CONCENTRATION
Assay buffer #1	Tris-HCl pH 7.0 NaCl Glycerol DDM	50 mM 150 mM 10% (v/v) 0.1% (w/v)
Assay buffer #2	Tris-HCl pH 7.0 NaCl Glycerol DDM	50 mM 150 mM 10% (v/v) 0.5% (w/v)

Table 2.7: Internally quenched peptides. Sequences of all internally quenched peptides used for kinetic assays. * denotes the proposed PARL cleavage site.

PEPTIDE NAME	PEPTIDE SEQUENCE
IQ-PINK1(99-108)	(DABCYL)-AVFLA*FGLGL-Glu(EDANS)
IQ-PGAM5(20-29)	(DABCYL)-AVFLS*AVAVG-Glu(EDANS)
IQ-Smac(51-60)	(DABCYL)-GVTLC*AVPIA-Glu(EDANS)
IQ-PINK1(97-107)-WT	Arg-Lys(DABCYL)-GRAVFLA*FGLG-Glu(EDANS)-Arg
IQ-PINK1(97-107)-R98W	Arg-Lys(DABCYL)-GWAVFLA*FGLG-Glu(EDANS)-Arg
IQ4	(Mca)-RPKPYA-Nva*WM-Lys(DNP)

2.2 Expression and purification of recombinant HsPARL

Human PARL (HsPARL) was cloned and expressed using the method established in the lab for rapid and efficient expression screening of eukaryotic membrane proteins[164]. This method utilizes *Pichia pastoris* as the expression system, which has become increasingly popular as it offers several advantages for heterologous protein expression. The media and inducing agent required for *P. pastoris* growth and protein expression are inexpensive, making large-scale expression more feasible; large-scale expression is also more fruitful as the yeast can grow to a high cell density, thus increasing the yield. Vectors used for protein expression in *P. pastoris* employ the *AOX1* promoter, which is tightly regulated and inducible with

methanol[165,166]. *P. pastoris* is an ideal yeast expression system for eukaryotic membrane proteins as it allows for co- and post-translational modifications, such as glycosylation, as well as membrane lipid requirements, which may be important in regards to synthesis, folding, and stability of recombinant membrane proteins[167-169]. Numerous eukaryotic membrane proteins have been successfully expressed and purified from *P. pastoris* for structural and functional analyses including ABC transporters, ion channels, and most recently an intramembrane methyltransferase[170-172]. *P. pastoris* facilitates genetic integration of the gene of interest into the *P. pastoris* host genome. This genetic integration allows for increased chances of highly expressing a eukaryotic membrane protein of interest as opposed to plasmid-based bacterial expression systems. By utilizing electroporation to transform competent yeast cells with a linearized vector containing our gene of interest under the control of the *AOX1* promoter, gene integration occurs directly into the 5' *AOX1* promoter. In non-transformed yeast cells, *AOX1* encodes for alcohol oxidase (AO), the protein responsible for the metabolism of methanol in yeast to generate carbon; *AOX1* is responsible for the production of most AO in the cell, though a second gene, *AOX2*, also encodes for AO[173]. In the presence of methanol, up to 35% of protein expression in *P. pastoris* can be that of AO[174]. Genetic integration of our gene of interest into the *AOX1* promoter, therefore results in direct expression of our protein of interest when the yeast cells are in the presence of methanol[175]. Because our protein of interest is now under the control of the *AOX1* promoter and not alcohol oxidase, the production of AO in the presence of methanol is dependent on the *AOX2* gene. This results in a Mut^s phenotype of the yeast, meaning methanol utilizing slow, in which yeast cells grow slowly in methanol-containing media. This slow growth phenotype is advantageous for protein expression as this can allow for proper folding, processing, and targeting of the recombinant protein of interest.

Another advantageous feature of this method is that our protein of interest, HsPARL, is expressed as a C-terminal GFP fusion protein. Having our protein of interested conjugated to GFP at its C-terminus allows us to visualize expression of our protein as induction is occurring. When transformant colonies are plated on induction plates that contain methanol, we can

visualize the plates under blue light and see fluorescence of the colonies. Because GFP is at the C-terminus of our protein, if we see fluorescence, it means that our protein of interest has also been translated. Colonies that have high fluorescence when compared to the positive control are considered to be high expressers of our protein of interest and will be preferentially chosen for large-scale expression, thus maximizing our protein yield.

Methods for the purification of HsPARL from *P. pastoris* were adopted from protocols for the purification of bacterial rhomboid proteases such as HiGlpG[176]. These protocols employ the use of the gentle non-ionic detergent n-dodecyl β-D-maltoside (DDM) which is commonly used in the purification of membrane proteins. DDM is one of the most popular detergents for both functional and structural studies of membrane proteins. It has a low critical micelle concentration that facilitates gentle extraction of membrane proteins from their native membrane environments. Because of its gentle nature, proteins solubilized using DDM are likely to retain their native confirmation and will often co-purify with some endogenous lipids that have not been stripped by the detergent, thus enhancing their stability. Purification parameters for HsPARL had previously been optimized in the lab, including detergent, salt, and glycerol concentrations in buffers, as well as the molarity of imidazole required to elute HsPARL from metal affinity chromatography columns. Immobilized metal affinity chromatography resulted in HsPARL of high yield and purity, thus further purification steps such as size exclusion chromatography were not necessary.

2.2.1 Cloning and expression screen of HsPARL-GFP.

HsPARL gene (PARLΔ55 or PARLΔ77) was cloned into the pPICZA-GFP vector with a C-terminal hexahistidine tag and contained a TEV protease cleavage site within the linker between HsPARL and GFP (Figure 2.1). The vector was transformed into TOP10 chemically competent *E. coli* cells and grown on low salt LB + Amp plates. Plasmids containing the HsPARL gene were purified by midi-prep kit (Qiagen). 10 µg of plasmid DNA was linearized

using the restriction enzyme Mss1. Electrocompetent *Pichia pastoris* GS115 were prepared according to the *Pichia* EasySelect[TM] Expression kit (Invitrogen, USA). In brief, one GS115 colony was grown overnight (28°C, 220 RPM) in 5 mL YPD media containing 100 μg/mL ampicillin in a 50 mL Falcon tube. From this overnight culture, 250 μL was used to sub-inoculate 50 mL YPD+Amp media and grown to an A_{600} of 1.5 (28°C, 220 RPM). Yeast cells were pelleted (5 000 x g, 5 min, 4°C), supernatant was discarded, and pellets were rinsed with 100 mL cold sterile ddH$_2$O two times. Following the rinses with cold sterile ddH$_2$O, cells were pelleted and resuspended in 20 mL cold sterile 1 M sorbitol. Cells were pelleted one final time, resuspended in 2 mL cold sterile 1 M sorbitol, and kept on ice until use.

For transformation, 5 μL of 1 mg/mL linearized HsPARL DNA was incubated with 100 μL electrocompetent GS115 on ice and electroporated at 1.25 kV, 25 μF, 100 Ω using a BioRad Gene Pulser. Cells were plated on YPDS + Zeocin (1% yeast extract, 2% peptone, 2% dextrose, 1 M sorbitol, 100 μg/mL zeocin) plates, and incubated at 28°C for 48h. Colonies on YPDS + Zeocin plates were transferred to new YPDS + Zeocin plates in grid pattern and then screened for expression on BMMY plates. BMMY plates were visualized every 24 h under blue light (ImageQuant LAS 4000) and high expressing colonies were identified. mPEMT was used a positive control for expression and non-transformed GS115 cells as a negative control (Figure 2.2)[164].

2.2.2 Large-scale expression of HsPARL

An identified high-expressing clone was grown overnight (28°C, 220 RPM) in 100 mL of BMGY media to an A_{600} of 4. A total of 6 L of BMGY media was sub-inoculated with the overnight culture to a starting A_{600} of 0.03 and grown for 20 h (28°C, 220 RPM). Cells were harvested by centrifugation in a Beckman JLA8.1000 rotor (800 x g, 20 min, 4°C) and cell pellets were resuspended in an equal volume of BMMY induction media (1 L BMMY media/pellet). Cultures were induced for 48 h (24°C, 220 RPM), with fresh methanol being added after 24 h (1%).
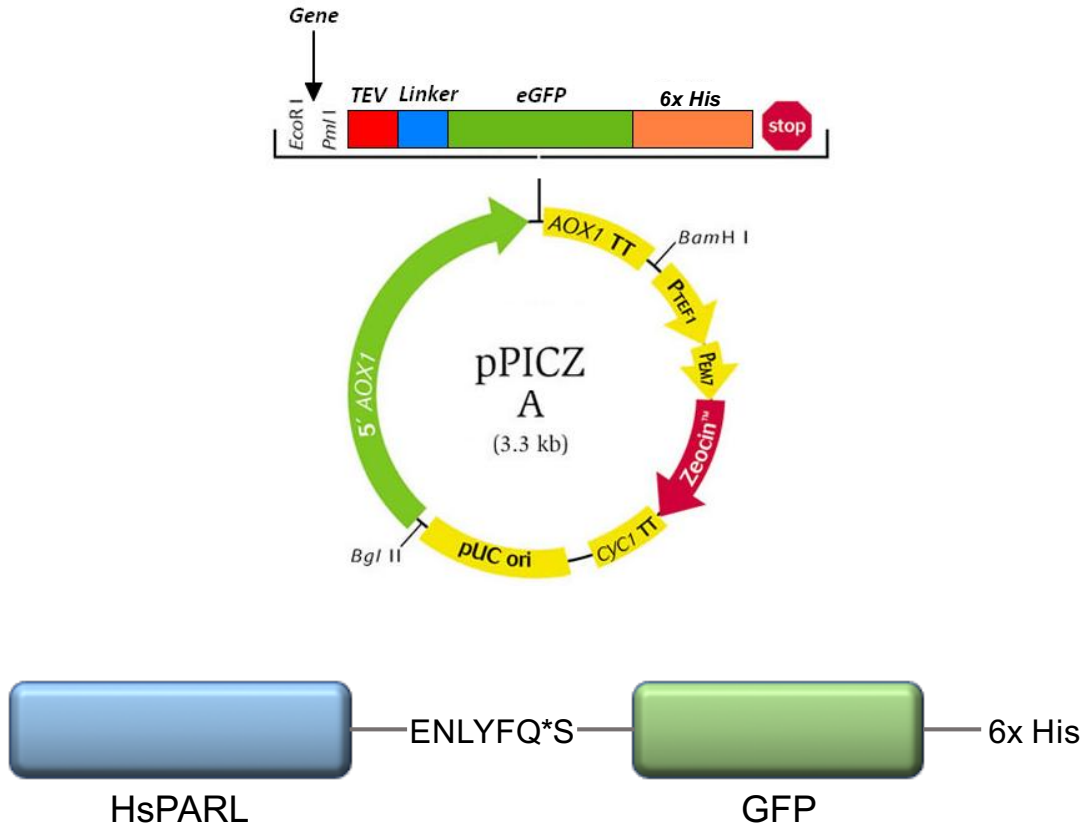
Figure 2.1: pPICZ plasmid map and HsPARL construct. The HsPARL gene was cloned into the pPICZA vector (top), which included a TEV protease cleavage site (ENLYFQ*S, where * denotes the cleavage site) and C-terminal GFP-fusion protein with a hexahistidine tag. The expressed HsPARL construct is outlined in the bottom panel.
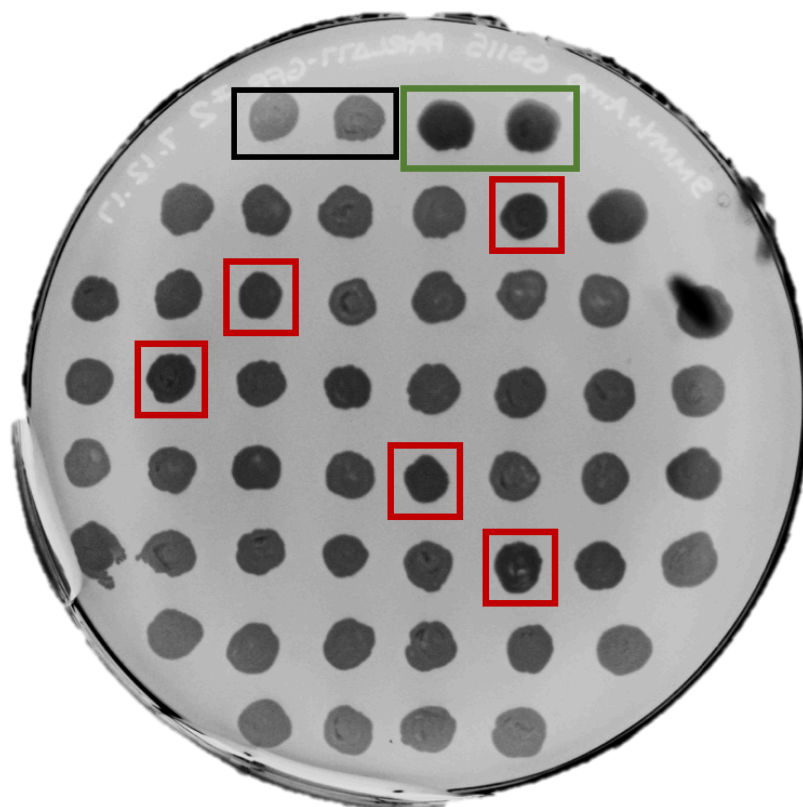
Figure 2.2: Induction plate expression screening of HsPARL-GFP. A sample BMMY plate from the expression screen for HsPARLΔ77-GFP after 48 h of induction. GS115 *P. pastoris* strain was transformed with DNA encoding for HsPARLΔ77-GFP and transformants were plated onto BMMY plates in a grid pattern and incubated at 28°C. Plates were visualized under blue light every 24 h (ImageQuant LAS 4000). Untransformed GS115 was used as a negative control in position one and two boxed in black. Positive control colonies are boxed in green, mPEMT was used as the positive control as it was known to express highly from previous expression screens. Examples of high expressing HsPARLΔ77-GFP colonies are boxed in red.

Fluorescence of the liquid culture was measured to indicate expression of HsPARL-GFP. To measure fluorescence, 1 mL culture was harvested in a desktop centrifuge at max speed (21 000 x g). Media was discarded and the cell pellet was resuspended in 200 μL 1X PBS; 100 μL of the resuspended cells were placed in a 94-well clear-bottomed plate. A ½ dilution of the remaining resuspended cells was prepared with 1X PBS and 100 μL of the ½ diluted cells were placed in the 94-well plate. Fluorescence was measured with λ_{ex} = 395 nm and λ_{em} = 509 nm in a multi-well plate reader (SynergyMx, BioTek). Representative fluorescence values obtained are shown in Table 2.8. Following induction, cells were harvested as above and cell pellets frozen at -20°C.

Table 2.8: HsPARL-GFP induction fluorescence values. Sample relative fluorescence units (RFU) obtained for expression of HsPARL-GFP after 24 h and 48 h of induction by addition of methanol.

		Flask #1	#2	#3	#4	#5	#6
HsPARLΔ55 -GFP	**24 h**	26120	25100	33500	28630	8750	15400
	48 h	56060	50850	58230	58300	42200	65000
HsPARLΔ77 -GFP	**24 h**	11570	14880	14000	21900	15870	10980
	48 h	32190	62640	34810	50010	34000	43610

2.2.3 Cell lysis and membrane isolation

Cells were thawed on ice and resuspended in TBS buffer (4:1 buffer volume to cell pellet weight). Resuspended cells were then lysed by passage through a Constant Systems cell disruptor at 38.2 kPSI two times. The chilling system of the cell disruptor was set to 4°C. After cell lysis, PMSF was added to a final concentration of 1 mM. Cell debris and unlysed cells were removed by two centrifugation steps in a Beckman JA-17 rotor (26 000 x g, 20 min, 4°C). Supernatant was then subjected to ultracentrifugation in a Beckman Ti45 rotor (95 800 x g, 2 h, 4°C) to isolate membranes. Supernatant was then discarded and the membranes were immediately stored at -20°C.

2.2.4 Immobilized metal affinity chromatography purification of HsPARL

Membranes were homogenized in solubilization buffer (10:1 buffer volume to pellet weight) using a Dounce homogenizer until fully resuspended. Homogenized membranes were then incubated with 1.8% (v/v) Triton X-100 at 4°C for 1 h with stirring to solubilize the membranes. Insoluble material was pelleted in a Beckman Ti45 rotor (95 800 x *g*, 30 min, 4°C) and the supernatant was passed through 2 mL settled HisPur™ cobalt resin (ThermoFisher, USA) by gravity flow two times to allow binding of HsPARL-GFP-His to the resin. The protein-bound resin was then washed with 20 mM imidazole in Buffer A to disrupt any non-specific binding. The protein of interest was eluted with imidazole (50 mM Tris-HCl pH 8.0, 300 mM NaCl, 20 % glycerol, 0.1% DDM, 0.5 M imidazole) in 1 mL fractions until eluted fractions were clear. Collected cobalt immobilized metal affinity chromatography elution fractions were then analyzed by SDS-PAGE and elution fractions containing PARL-GFP were pooled (Figure 2.3). The purified PARL-GFP fusion protein was digested by incubation with TEV protease and 1 mM TCEP overnight at 4°C.

Dialysis was performed for 2 h with stirring at 4°C to remove imidazole and TCEP (50 mM Tris-HCl pH 8.0, 300 mM NaCl, 20% glycerol). PARL was purified from GFP and TEV using HisPur™ Ni-NTA agarose resin (ThermoFisher, USA) and both GFP and TEV will bind to the resin due to their C-terminal His tags. The dialyzed protein sample was applied to the nickel resin and flow-through was collected in 1 mL fractions, then analyzed by SDS-PAGE to assess HsPARL purity (Figure 2.3). If many contaminants were still present in the protein sample, a second negative nickel column would be performed and again collected fractions analyzed by SDS-PAGE. Fractions containing the most pure HsPARL would be pooled and the protein concentrated using a 10 000 MWCO concentrator (Millipore, USA). Protein concentration was determined by BCA assay. Purified protein was incubated on ice with dried cardiolipin (Sigma-Aldrich, USA) to a final lipid concentration of 0.1 mg/mL. Protein-lipid sample was aliquoted, flash frozen in liquid nitrogen, and stored at -80°C.
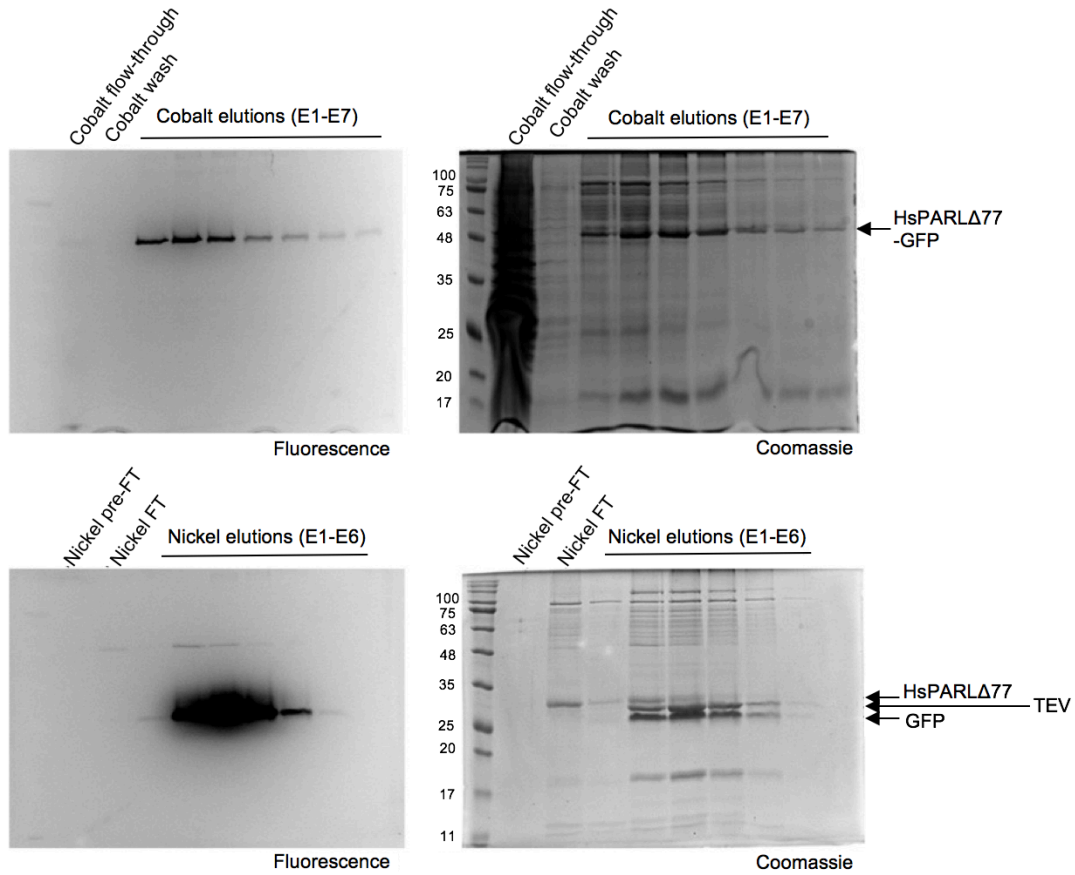
Figure 2.3: SDS-PAGE gels of HsPARL IMAC purification steps. Purification fractions from cobalt IMAC (top) and nickel IMAC (bottom) were run on 14% SDS-PAGE gels and run at 170 V for 45 min. Fluorescence of the gels was visualized under blue light to identify GFP and then gels were stained with Coomassie blue and destained in 15% acetic acid. Purified HsPARL is found in the nickel column flow-through (FT).
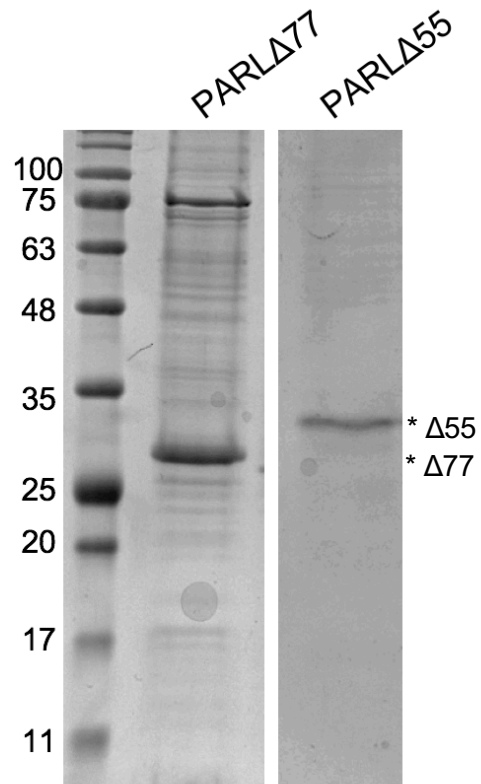
Figure 2.4: SDS-PAGE gel of purified HsPARL constructs. Purified HsPARL constructs were run on a 14% SDS-PAGE gel, stained with Coomassie blue, and destained in 15% acetic acid. The gel was imaged using the ImageQuant LAS4000.

2.3 Cloning, expression, and purification of HsFRET-PINK1(70-134)

.

The cloning, expression, and purification of all HsFRET-PINK1(70-134) constructs was completed by Emmanuella Takyi; the HsFRET-PINK1(70-134) constructs were expressed and purified based on the protocol established in our lab for PsTatA-FRET[177]. In brief, residues 70-134 of HsPINK1-WT were cloned into the pBad/HisB vector that already encoded for the CyPet/YPet FRET-pair (Figure 2.4). Site-directed mutagenesis was performed to introduce single point mutations; primers were designed to introduce the C92F, R98W, I111S, and Q126P mutations. Polymerase chain reaction (PCR) amplifications were carried out (T100 Thermal Cycler for PCR, BioRad) and 5 µL of the PCR product was used to transform 50 µL TOP10 chemically competent *E. coli* cells (ThermoFisher). Transformed cells were grown overnight at 37°C on LB agar plates containing 100 µg/mL ampicillin. Plasmids were isolated from resulting transformant colonies by miniprep (Geneaid) and sent for DNA sequencing to confirm success of the site-directed mutagenesis (The Applied Genomics Centre, University of Alberta).

Upon confirmation of mutagenesis, TOP10 chemically competent *E. coli* cells (ThermoFisher) were transformed with pBAD/HisB:FRET-PINK1 (WT, C92F, R98W, I111S, and Q126P). One transformant colony was selected and grown overnight (37°C, 220 RPM) in 120 mL of LB medium containing 100 µg/mL ampicillin. A total of 6 L LB media was sub-inoculated with 20 mL of overnight culture and grown to an OD_{600} of 0.7 (37°C, 220 RPM). Cultures were induced by addition of 0.02% (v/v) L-arabinose (8 h, 24°C, 220 RPM). After induction, cells were harvested by centrifugation in a Beckman JLA8.1000 rotor (6 900 x *g*, 20 min, 4°C), flash frozen in liquid nitrogen, and stored at -80°C.

Harvested cells were thawed on ice and resuspended in a 4:1 buffer volume to cell pellet weight ratio in resuspension buffer (50 mM Tris-HCl pH 8.0, 500 mM NaCl, 20% glycerol, 10 µg/mL DNase, 1 mM PMSF, two EDTA-free protease inhibitor cocktail tablets). Resuspended
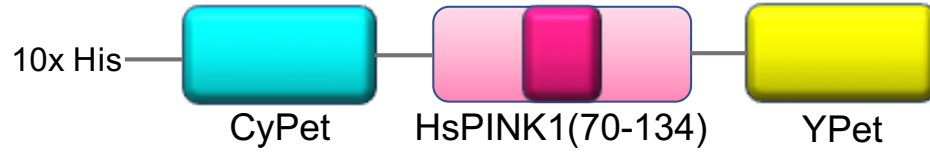
Figure 2.5: HsFRET-PINK1(70-134) construct. HsPINK1(70-134) was expressed as a FRET-substrate. The TM region of HsPINK1, from residues 89-111, is highlighted in dark pink. HsPINK1(70-134) is flanked by two fluorophores, CyPet at the N-terminus and YPet at the C-terminus. These fluorescent proteins are derivatives of GFP that are established as a FRET-pair. A decahistidine tag at the N-terminus was used for immobilized metal affinity chromatography purification.

cells were lysed using an Emulsiflex with a maximum pressure of 40 kPSI. Following cell lysis, the lysate was subjected to centrifugation using a Beckman TI45 rotor (31 300 x g, 20 min, 4°C) to pellet cell debris and unlysed cells. The supernatant was incubated with 1% (v/v) Triton X-100 at 4°C for 30 min with stirring. Supernatant was then passed through 1 mL settled HisPur™ cobalt resin (ThermoFisher, USA) by gravity flow to allow binding of Hs-FRET-PINK1-His to the resin. Protein was eluted (50 mM Tris-HCl pH 8.0, 500 mM NaCl, 20% glycerol, 250 mM imidazole), pooled, and concentrated for loading onto the Superdex 200 column for size exclusion chromatography. Size exclusion chromatography fractions were analyzed by SDS-PAGE and fractions containing FRET-PINK1 protein were pooled and concentrated. Concentrated sample was aliquoted, flash frozen with liquid nitrogen, and purified HsFRET-PINK1(70-134) was stored at -80 °C for subsequent use (Figure 2.5).

2.4 FRET-based protease kinetic assay.

Enzyme kinetics are an invaluable tool for understanding details and regulatory mechanisms of cellular reactions and have made it possible to identify physiological functions of numerous enzymes. Protease kinetics are a powerful means of increasing our knowledge on the mechanism and regulation of substrate cleavage. Kinetics allow us to quantify active proteases and cleavable substrates as well as characterize the protease-substrate or protease-inhibitor interaction. From kinetic assays, we can gain information on proteolytic mechanism, control, and regulation. This thesis focuses on the use of protease-substrate kinetics for functional characterization of HsPARL.

In order to assess the activity of our purified recombinant HsPARL and obtain individual catalytic parameters, an assay was needed in which we could monitor the cleavage of substrates in real-time. Continuous assays for protease kinetics often utilize chromogenic or fluorogenic substrates, or are coupled to other reactions. Detection of substrate depletion or product formation in a continuous assay can be recorded based on fluorescence intensity, time resolved fluorescence, fluorescence polarization, luminescence, or absorbance
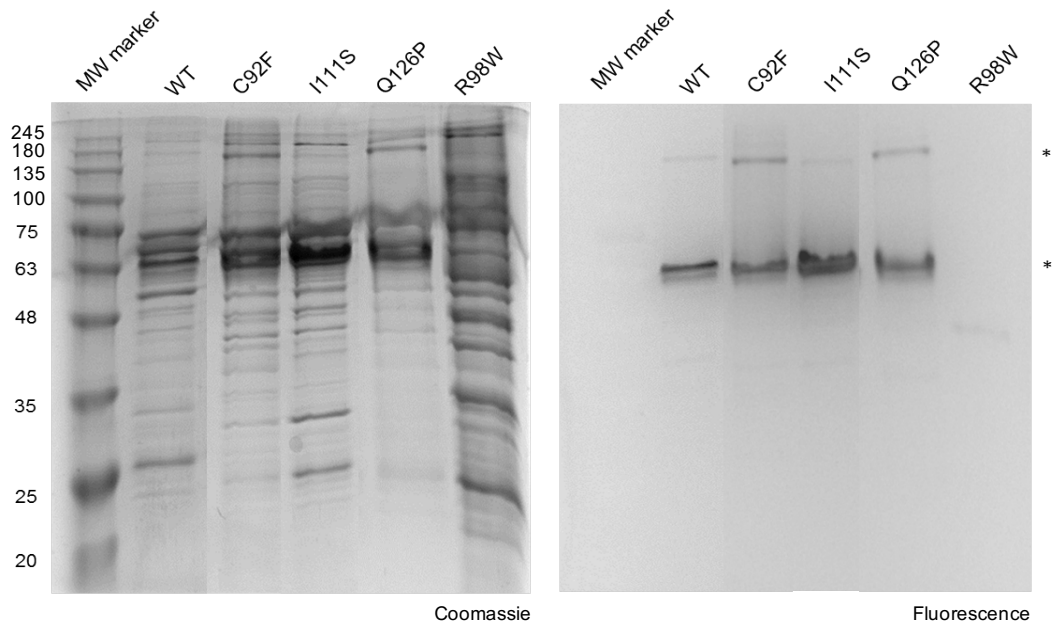
Figure 2.6: SDS-PAGE gel of purified HsFRET-PINK1(70-134) constructs. Purified

HsFRET-PINK1(70-134) constructs were run on a 14% SDS-PAGE gel. Fluorescence of the

gel was visualized under blue light using ImageQuant LAS4000, as we can observe the YPet

fluorophore. A predicted HsPINK1 dimer is observed in the fluorescence gel (denoted by *),

while the monomeric species runs at 63 kDa (denoted by **). All HsFRET-PINK1 constructs

co-purify with other proteins following size exclusion chromatography. The HsFRET-PINK1-

R98W construct was unable to be purified to a suitable quality or quantity for our needs as

observed by the multitude of co-purifying proteins on the Coomassie blue stained gel and the

lack of fluorescence. Data collected by Emmanuella Takyi, Lemieux lab, M. Sc. thesis, 2019.

depending on the substrate used or if the reaction is coupled. A FRET-based assay was employed as the means to assess proteolytic activity of HsPARL due to its high sensitivity and reproducibility. Very small changes in fluorescence intensity can be recorded that directly correspond to substrate cleavage and, therefore, enzymatic activity. FRET-based assays work based on the principal of energy transfer between a donor fluorophore and an acceptor (also known as a quencher). When the donor and acceptor are in close proximity, fluorescence will be quenched as the emission wavelength of the fluorophore will overlap with the excitation wavelength of the acceptor. Upon separation of the donor and acceptor, through cleavage of a substrate in our case, the full emission of the donor can be measured. Fluorescence based assays are well established for assessing protease activity and have been successfully used for the assessment of rhomboid activity[177-179].

We established the use of small internally quenched (IQ) peptide substrates to address the regulatory function of PARL truncations on cleavage of several substrates. These IQ peptide substrates contain a 10-residue span that encompasses the PARL cleavage site of the protein substrates PGAM5, PINK1, and Smac (Figure 2.7). We also used an already-established assay to assess a substrate with a full TM region. A FRET-based assay was developed in the lab to assess cleavage of a single-pass transmembrane substrate by bacterial rhomboid proteases[177]. The TM segment of the Twin arginine transport protein A (TatA) from *Providencia stuartii* was flanked by two fluorescent proteins, CyPet and YPet, and was able to be cleaved by the bacterial rhomboid PsAarA. CyPet and YPet are derivatives of cyan fluorescent protein and yellow fluorescent protein and their FRET-properties are well characterized. Upon cleavage within this TM region by the recombinant protease, the fluorophores are released, resulting in a measureable shift in fluorescence due to increased emission of the donor fluorophore. The uncleaved substrate shows partially quenched fluorescence of CyPet at 475 nm and full fluorescence of YPet at 530 nm. Upon cleavage, the emission of CyPet at 475 nm is increased while the emission of YPet at 530 nm is decreased due to a loss in FRET-based energy transfer. YPet and CyPet are well-characterized for their use in FRET-based assays;

they have been used to monitor reaction kinetics, protein-protein interactions, and have been adapted for proteolytic assays[180-182]. This FRET-based assay employing CyPet and YPet has been adapted for our use in assessing HsPARL activity; residues 70-134 of HsPINK1 have been cloned and recombinantly expressed between the FRET-pair (Figure 2.8). It is important to note that rhomboid-mediated cleavage does not appear to be affected by the use of a fusion protein for a substrate; rhomboids appear to recognize a specific sequence that surrounds the cleavage site[183].

Initial velocity (v_o) values obtained from a kinetic assay are used to plot a Michaelis-Menten kinetic curve which provides us with informative catalytic parameters for the proteolytic reaction. The Michaelis-Menten equation is outlined below. There are two assumptions of the Michaelis equation. The first is that all substrate production measured is due to enzymatic activity. The second assumption is that the enzyme is at "steady-state"; in steady-state kinetics, substrate production is linear with time. If the enzyme is not at steady-state, kinetic analysis can become convoluted due to the effects of reversible reactions, product inhibition, and progressive inactivation of the enzyme.

$$y = \frac{V_{max}x}{(K_M + x)}$$

In the Michaelis-Menten equation,

$$x = [substrate]$$

$$V_{max} = rate\ at\ substrate\ saturation$$

$$K_M = \frac{(k_{-1} + k_{cat})}{k_1} = Michaelis\ Menten\ constant$$

Catalytic parameters obtained directly from a Michaelis-Menten kinetic curve are the K_M (the Michaelis constant) and the V_{max}. The V_{max} is the maximal velocity of the enzymatic reaction and occurs when the enzyme is saturated. K_M is the substrate concentration at which half-

maximal activity is observed; K_M can also be considered a measure of the affinity of the enzyme for a particular substrate. From these two parameters, we can further calculate the k_{cat}, the catalytic turnover or number of substrate molecules cleaved per unit time, and the k_{cat}/K_M, a measure of the enzymatic efficiency. The k_{cat} catalytic parameter, as well as the standard error for the k_{cat} and k_{cat}/K_M parameters, are calculated according to the equations outlined below.

$$k_{cat} = \frac{V_{max}}{[enzyme]}$$

$$k_{cat}\ error = \frac{V_{max}\ error}{[enzyme]}$$

$$\frac{k_{cat}}{K_M}\ error = \left(\frac{k_{cat}}{K_M}\right)\left(\frac{k_{cat}\ error}{k_{cat}} + \frac{K_M\ error}{K_M}\right)$$

These catalytic parameters are unique for each enzyme-substrate pair and provide much information about reaction rates and enzyme specificity, however, they are unable to a determine a precise mechanism of reaction as there is no way to elucidate what intermediate states the enzyme-substrate complex undergoes. Luckily for protease kinetics, reaction mechanisms such as that for serine proteases described in Chapter 1 (Figure 1.1) have been elucidated through functional and structural studies that have confirmed the protease-substrate transition states that occur through the course of the reaction. Because the general reaction mechanism is characterized, the catalytic parameters obtained from a proteolytic kinetic assay can give direct evidence of regulation and modulation of the reaction.

2.4.1 10mer IQ peptide substrates

For internally quenched (IQ) EDANS/DABCYL 10mer peptides (PGAM5, PINK1, and Smac),

1 mg lyophilized peptide was dissolved in 1 mL DMSO to obtain a stock concentration. The IQ peptide substrate was incubated with activity assay buffer #1 and DMSO in a 364-well black-bottomed plate at 37°C for 30 min in a multi-well plate reader (SynergyMx, BioTek). For IQ peptide assays, the DMSO concentration was kept constant at 5% (v/v). Following pre-incubation, HsPARL was added to a final concentration of 0.8 µM to initiate the cleavage reaction, final reaction volume was 100 µL. The concentration of substrate ranged from 0.01 µM – 25 µM. Fluorescence readings were taken every 3 min over a 3 h time course, with fluorimeter sensitivity set to 60 for IQ-PGAM5, PINK1, and Smac. For IQ EDANS/DABCYL peptides, λ_{ex} = 336 nm and λ_{em} = 490 nm, corresponding to the excitation and emission wavelengths for the EDANS fluorophore. FRET-based kinetic cleavage assays were conducted for each PARL construct and substrate. The initial velocity was determined from the fluorescence readings over the time course; for each substrate concentration, a no-enzyme control was subtracted to eliminate background fluorescence changes not related to substrate cleavage.

Relative fluorescence units were converted to concentration (µM) by determining the maximum change in fluorescence observed for each substrate concentration when fully digested. The PeptideCutter online tool (ExPASy.org) was used to determine what common protease could be used to fully digest substrate for the RFU to µM conversion factor. Chymotrypsin was used for full digestion of IQ-PGAM5, IQ-PINK1, and IQ-Smac to correlate the fluorescence obtained with the amount of substrate peptide cleaved. In short, the IQ peptide substrate was incubated with activity assay buffer #1 and DMSO in a 364-well black-bottomed plate at 37°C for 30 min in a multi-well plate reader (SynergyMx, BioTek). For IQ peptide assays, the DMSO concentration was kept constant at 5% (v/v). Following pre-incubation, a baseline 0 h fluorescence measurement was taken. Chymotrypsin was added to a final concentration of 2 µM to initiate the cleavage reaction, final reaction volume was 100 µL. A fluorescence measurement was taken after 2 h of incubation at 37°C with chymotrypsin.
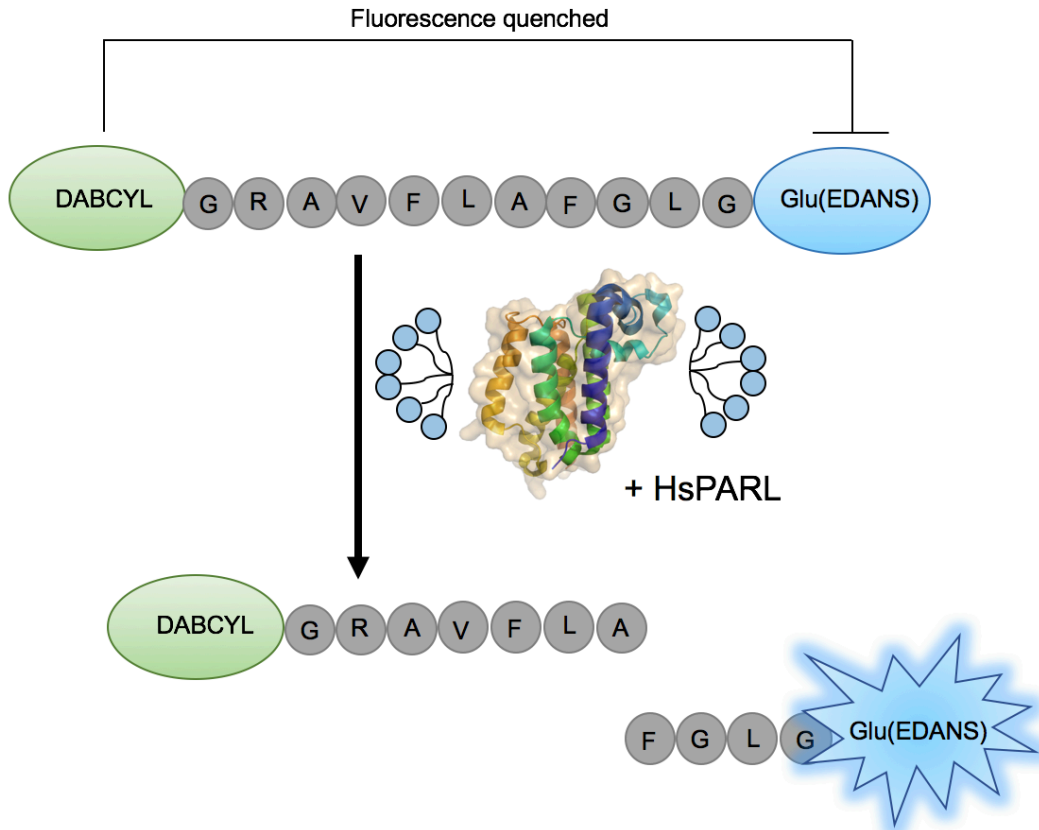
Figure 2.7: Proteolytic assay for IQ-peptides with HsPARL. A model schematic for the cleavage of IQ-peptides by HsPARL. Before addition of the protease, fluorescence of the EDANS fluorophore is quenched by the DABCYL acceptor. Upon incubation of the IQ-peptide with HsPARL, cleavage occurs resulting in an unquenched substrate and increasing fluorescence of the EDANS fluorophore is able to be monitored. In the above schematic, the sequence of the IQ-PINK1 peptide is outlined and HsPARL is depicted in a detergent micelle.

Following 24 h of incubation, additional chymotrypsin was added to a concentration of 4 µM. Fluorescence was recorded after 2 h of incubation following this chymotrypsin addition and if no fluorescence change was observed from the previous measurement, digestion of the substrate was complete. The maximum change in fluorescence for each substrate concentration was determined by first subtracting the no-enzyme control and then by subtracting the 0 h baseline. Values obtained for maximum change in fluorescence were plotted as a function of substrate concentration and the linear slope calculated as the conversion factor.

GraphPad Prism software was used for Michaelis-Menten analysis of kinetic curves. Values for V_{max} and K_M were obtained. This allowed for calculation of the k_{cat} and k_{cat}/K_M catalytic parameters. Unpaired t-tests or two-way analysis of variance (ANOVA) with a $p < 0.05$ cutoff were performed to determine significant differences between data sets. The Tukey method was used to correct for multiple comparisons in the two-way ANOVA. A minimum of three experimental replicates performed in duplicate were used for data analysis ($n \geq 3$).

2.4.2 HsFRET-PINK1 substrate

Assays with HsFRET-PINK1 variants were conducted as previously described[177]. In brief, HsFRET-PINK1(70-134) substrate was incubated with activity assay buffer #1 in a 364-well black-bottomed plate at 37°C for 30 min in a multi-well plate reader (SynergyMx, BioTek). Following pre-incubation, HsPARL was added to a final concentration of 1.25 µM to initiate the cleavage reaction, final reaction volume was 60 µL. The concentration of substrate ranged from 0.1 µM – 12.5 µM. For concentrations of the HsFRET-PINK1(70-134) substrate lower than 0.1 µM, initial velocity was not able to be determined. Concentrations greater than 12.5 µM were unable to be attained due to the stock concentrations of HsFRET-PINK1(70-134) not being high enough. Fluorescence readings were taken every 3 min over a 3 h time course.
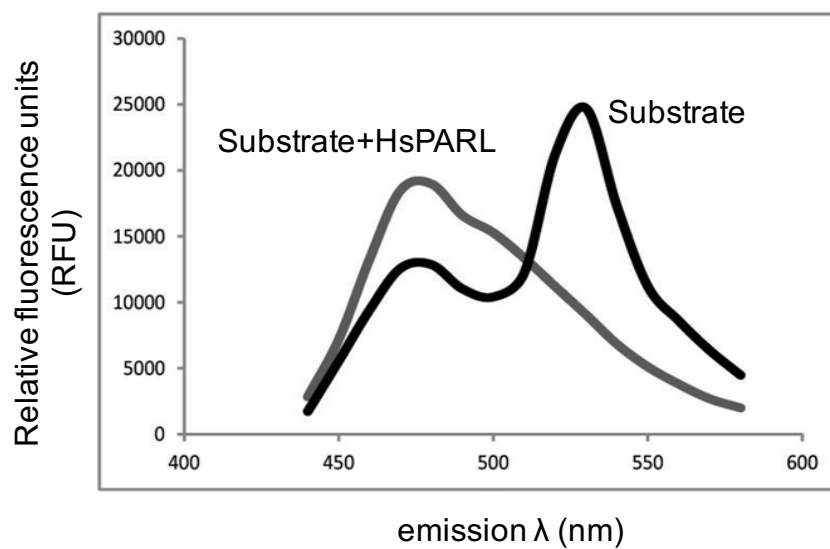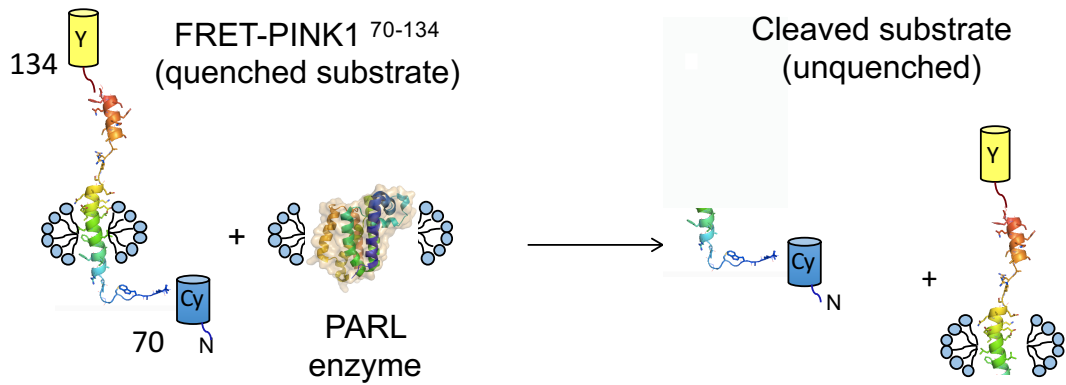
Figure 2.8: Proteolytic assay for HsFRET-PINK1(70-134) substrate with HsPARL. Detergent (DDM) solubilized HsFRET-PINK1(70-134) and HsPARL are incubated to initiate the cleavage reaction (top). Upon cleavage within the HsPINK1 TM region by the recombinant protease, the CyPet and YPet fluorophores are released, resulting in a measurable shift in fluorescence. The uncleaved HsFRET-PINK1(70-134) substrate shows partially quenched fluorescence of CyPet at 475 nm and full fluorescence of YPet at 530 nm (bottom, black curve). Upon cleavage by HsPARL, the emission of CyPet at 475 nm is increased while the emission of YPet at 530 nm is decreased due to a loss in FRET-based energy transfer (bottom, grey curve).

For HsFRET-PINK(70-134), λ_{ex} = 414 nm and λ_{em} = 530 nm. FRET-based kinetic cleavage assays were conducted for HsPARLΔ77 with each HsFRET-PINK substrate. The initial velocity was determined from the fluorescence readings over the time course; background fluorescence for each substrate concentration point over the time course was subtracted. Relative fluorescence units were converted to concentration (μM) by determining the maximum change in fluorescence observed for each substrate concentration when fully digested by trypsin. GraphPad Prism software was used for Michaelis-Menten and statistical analysis. One-way ANOVA with multiple comparisons was performed between the HsFRET-PINK1(70-134)-WT substrate and PD-associated variant to determine if differences observed were significant. The Dunnett method was used to correct for multiple comparisons and a cutoff of $p < 0.05$ was used to determine significance. A minimum of three experimental replicates were used for data analysis ($n \geq 3$).

2.4.3 Cardiolipin analysis with HsFRET-PINK1 and IQ4 substrates

For this assay, 1.5 μM HsFRET-PINK1(70-134)-WT substrate and 1 μM HsPARLΔ77 were used to assess proteolytic activity at each concentration of cardiolipin (CL). The activity assay was programmed as described above for the HsFRET-PINK1(70-134) substrate and the initial velocities for each condition were calculated. For the IQ4 peptide substrate, 3 μM IQ4 and 1 μM HsPARLΔ77 were used; λ_{ex} = 320 nm and λ_{em} = 400 nm. Because we are just looking at the activity of the enzyme towards one concentration of substrate, looking at velocity in units of RFU/h was sufficient for comparison between the lipid conditions. GraphPad Prism software was used to plot initial velocity values and one-way ANOVA with multiple comparisons was performed between the no-lipid condition and each molar ratio of CL:protein to determine if differences observed were significant. The Dunnett method was used to correct for multiple comparisons and a cutoff of $p < 0.05$ was used to determine significance. A total of five experimental replicates performed in duplicate were used for data analysis ($n = 5$).

2.4.4 IQ-PINK1-WT and IQ-PINK1-R98W substrates

Assays were performed as described in section *2.4.2* for the 10mer IQ peptides, with two minor modifications. Activity assay buffer #2 was used, containing 0.5% (w/v) DDM, as it was found that a higher detergent concentration was required to keep high concentrations of the peptides in solution. Fluorimeter sensitivity was set to 80 for all measurements of the IQ-PINK1(97-107)-WT and IQ-PINK1(97-107)-R98W peptides. Substrate concentrations assessed ranged from 0.05 µM – 25 µM. A minimum of eight experimental replicates performed in duplicate were used for data analysis (n ≥ 8).

2.4.5 Inhibitor assay with IQ-PGAM5 peptide

The IQ-PGAM5 substrate was used with three substrate concentrations tested, 0.64 µM, 3.2 µM, and 12.8 µM. The activity of HsPARLΔ77 was assessed in the presence of 1 mM PMSF, 0.25X protease inhibitor cocktail tablet, or 1 mM EDTA. The 0.25X protease inhibitor cocktail tablet was prepared from a 7X stock (one tablet dissolved in 1.5 mL ddH$_2$O). The IQ-PGAM5 peptide substrate was incubated with activity assay buffer #1 and DMSO in a 364-well black-bottomed plate at 37°C for 30 min in a multi-well plate reader (SynergyMx, BioTek). Control wells also contained the appropriate protease inhibitor. While the plate was incubating, HsPARLΔ77 was incubated with each protease inhibitor on ice for 30 min. Following pre-incubation, HsPARL+inhibitor was added to each well to a final enzyme concentration of 0.5 µM to initiate the cleavage reaction, final reaction volume was 100 µL. Fluorescence readings were taken every 3 min over a 3 h time course. GraphPad Prism software was used to plot initial velocity values and one-way ANOVA with multiple comparisons was performed between the no-inhibitor condition and each protease inhibitor. The Dunnett method was used to correct for multiple comparisons and a cutoff of $p < 0.05$ was used to determine significance. Two experimental replicates were performed with each inhibitor (n = 2).

2.5 Mass spectrometry based substrate-profiling

A multiplex peptide cleavage assay was established by our collaborator Dr. Anthony O'Donoghue (Skaggs School of Pharmacy and Pharmaceutical Sciences, UCSD) that can be used to generate the substrate specificity profile of a protease[184]. This method has been validated with bacterial rhomboid proteases and was adapted for use with PARL[185]. A peptide library composed of 283 unique peptide sequences was used to generate the substrate profile. Each sample contained 1-3 μg peptide total (500 nM of each unique peptide) and 50 nM HsPARLΔ77 in citrate phosphate buffer (20 mM citrate-phosphate pH 6.0, 150 mM NaCl, 1 mM MgCl$_2$, 1 mM CaCl$_2$, 20% glycerol, 0.1% DDM). The total reaction volume was 60 μL. Samples were incubated at 37°C and 10% of the reaction mixture was removed after 0.25, 1, 3, and 20 h of incubation. Reactions were quenched by addition of GuHCl to a concentration of 6.4 M and immediately flash frozen and stored at -80°C. Samples were desalted using C18 zip tips (Millipore) and rehydrated in 5% formic acid in 5% acetonitrile. Mass spectrometry analysis was performed using an Orbitrap Lumos Tribrid Mass Spectrometer (Thermo Fisher) equipped with an EASY-nLC 1000 (Thermo Fisher). Data were processed using Proteome Discoverer 2.1 (Thermo Fisher). A peptide fold-change > 4 and $p < 0.05$ (determined by ANOVA) indicated a significant change in peptide abundance and these peptides were then used to generate the substrate specificity plot using iceLogo software.

CHAPTER 3: PROTEOLYTIC ACTIVITY OF PARL

CONTRIBUTIONS

I would like to acknowledge the contributions of Dr. Anthony O'Donoghue and Zhenze Jiang (Skaggs School of Pharmacy and Pharmaceutical Sciences, UCSD). All mass spectrometry experiments were performed by Zhenze Jiang and all results shown in section *3.3.1* and *3.3.2* were obtained by Zhenze Jiang.

3.1 Introduction

The mammalian mitochondrial rhomboid protease, PARL, has an indispensable role in mitochondrial homeostasis and cellular health. Our knowledge of PARL to date has relied on cellular studies that have provided valuable insights into regulation and targets of PARL-mediated cleavage. Several different substrates of PARL have been identified, however, there has been no *in vitro* cell-free assay using recombinant protein to validate these substrates or to decipher mechanistic aspects of PARL-mediated cleavage[75]. Cellular studies in PARL-KO cells or cells expressing the catalytically inactive protein (PARL-S277A/G) can provide strong evidence for substrates of PARL-mediated cleavage. Though, with numerous other proteases both within the cell and within mitochondria that could be acting on these substrates there may be false evidence of PARL-mediated cleavage[186]. There have been several instances where new substrates of PARL were proposed, only for subsequent studies to show that their processing is not dependent on PARL being present or active. This was the case for OPA1, a protein involved in cristae maintenance. The yeast homologue of OPA1, Mgm1, is a bona fide substrate of the yeast mitochondrial rhomboid so it was presumed that in mammalian cells, PARL would be responsible for its processing[57,70]. Several early studies alluded to this based on genetic interactions, however, it was then observed that PARL was dispensable for OPA1 cleavage and that AAA proteases, such as YME1L, appeared to be responsible for its processing[57,59,187]. HTRA2 is another example of a substrate that was presumed to be cleaved by PARL, but no conclusive evidence could be provided as studies have produced contradicting results[188,189]. Using an assay with recombinant proteins eliminates doubt on if a substrate can be cleaved by PARL or not. Whether the processing that can be observed *in vitro* using recombinant protein is physiological or not requires further assessment, but this does allow us to validate identified substrates.

Comprehensive cellular studies have verified that PINK1, PGAM5, and, most recently, Smac are likely bona fide substrates of PARL[64,73-75]. However, without a cell-free assay system we

are unable to address several questions related to PARL-mediated cleavage. The benefit of a proteolytic assay system using recombinant protein is that it allows us to gather kinetic information about our enzyme and its specific enzyme-substrate interactions. Enzyme kinetics are invaluable tools in the study of proteases as the catalytic parameters obtained allow us to compare the cleavage of different substrates, reveal substrate specificity, and understand enzymatic regulatory mechanisms. In the protease field, enzyme kinetics and substrate specificity analyses have shed light on numerous factors in relation to the regulatory and mechanistic aspects of certain proteases. For example, extensive research towards the caspase family, the proteases responsible for driving apoptosis, has revealed highly conserved substrate recognition motifs for different members of the family and has allowed for characterization of cleavage rates and substrate preference between caspases, thus advancing our knowledge on how these proteins behave physiologically[190].

As highlighted in Chapter 1, several regulatory mechanisms have been proposed for PARL-mediated cleavage. Processing of PARL itself is suggested to be a major proponent of cleavage regulation. Several truncated forms of PARL have been identified *in vivo*, and cellular studies suggest that these different forms of the protease have differential cleavage abilities towards substrates such as PINK1[49,62,65]. PARL is most commonly found in the mature PARLΔ53 form, resulting after removal of its MTS, which recent studies demonstrate as being the more active form of the enzyme towards PINK1[65]. The PARLΔ77 truncation occurs after a cleavage event, called β-cleavage, that is proposed to be autocatalytic[62]. This β-cleavage event was suggested to be required for PARL activation as introduction of a mutation that prevented β-cleavage was associated with impaired functioning of PARL[49]. In light of the recent findings that suggest PARLΔ53 is more active, the function of these processed forms of PARL has become less clear[49]. These cleavages of PARL are suggested to be regulated by phosphorylation events that result in inhibited β-cleavage, though changes in cellular conditions also play a regulatory role as a decrease in mitochondrial membrane potential enhances β-cleavage[61]. A cell-free assay would allow for direct assessment of how PARL-

mediated cleavage is affected by the different truncations of PARL; cleavage rates could be compared for PARLΔ53 and PARLΔ77, and alterations in the enzyme-substrate interaction could be characterized based on catalytic parameters obtained. Furthermore, a direct comparison could be made between PARL-mediated cleavage of different substrates. The study that proposed PARL exists in complex with YME1L and SLP2 observed different cleavage patterns for PARL-mediated processing of PINK1 and PGAM5[66]. It is likely that the processing of each unique substrate has subtle differences in turnover, efficiency, and the affinity of the enzyme-substrate interaction which can all be elucidated from proteolytic kinetic assays, but not from cellular studies.

The lack of a cell-free system to assess the proteolytic activity of PARL has also impeded efforts to develop inhibitors that would be useful for further characterization of the protease with the ultimate goal of being used as targeted therapeutics. Inhibitor development for the rhomboid protease family has faced numerous challenges in regards to the development of inhibitors that are both specific and potent. Progress is being made, though, with the identification of chloro-isocoumarins, chloromethyl ketones, and β-lactams that inhibit rhomboid proteases[51]. While PARL has been implicated in diseases such as type 2 diabetes and Parkinson's, which make it an attractive target for therapeutic drug design, without an established cell-free method to monitor PARL-mediated cleavage, there is no way to screen proteolytic activity with a potential inhibitor library in an efficient manner. This greatly hampers our ability to make advancements towards both furthering our understanding of PARL-mediated cleavage and addressing PARL's activity in regards to physiological disease relevance.

We currently have only a speculative understanding of the mechanisms in place for regulation of PARL-mediated cleavage and how substrates may interact with the active site of the enzyme. The establishment of an *in vitro* assay to directly assess the proteolytic activity of PARL towards unique substrates is required to advance our knowledge on this protease and

determine regulatory and mechanistic aspects of its function. Cellular studies have provided a solid foundation of knowledge regarding PARL-mediated cleavage, however there are numerous questions that remain unanswered due their inability to be addressed in a cell-based system.

3.2 Objective

To date, there is no published kinetic data for HsPARL as cellular studies are unable to elucidate specific catalytic parameters associated with the cleavage of unique substrates. This chapter aims to address several facets in the characterization of PARL-mediated cleavage using a cell-free proteolytic assay system that employs recombinantly expressed and purified HsPARL.

Using mass spectrometry techniques in collaboration with Anthony O'Donoghue (Skaggs School of Pharmacy and Pharmaceutical Sciences, UCSD), we aimed to identify a model substrate of PARL, that is cleaved both specifically and efficiently, that could be used for rapid assessment of protease activity or for inhibitor screening. We also aimed to produce a substrate specificity profile for HsPARL that would provide information regarding substrate recognition and substrate preference.

Using small internally quenched peptides that contain the P5 to P5' residues of the identified PARL substrates PGAM5, PINK1, and Smac, we aimed to assess the proteolytic activity of HsPARL. Whether the truncations of PARL identified *in vivo* have an effect on proteolytic activity was assessed by monitoring cleavage mediated by either HsPARL∆55 or HsPARL∆77. We also looked at the difference between catalytic parameters obtained for cleavage of each peptide substrate to determine if there is an indication of a preferred PARL substrate. We hypothesized that the different truncations of PARL would result in altered catalytic parameters, indicating that the two forms of the protease lead to different enzyme-substrate

interactions. We also hypothesized that there would be notable differences between the cleavage of each unique substrate, again indicating that the enzyme-substrate interaction for each substrate is distinctive.

The final aim of this chapter was to assess the activity of HsPARLΔ77 with a panel of classic protease inhibitors. We hypothesized that the inhibitors would have no effect on the proteolytic activity of HsPARLΔ77, as rhomboids are known to be resistant to classical protease inhibitors, but that we would be able to eliminate any activity observed from a possible protease contaminant.

3.3 Results

3.3.1 Substrate profiling of HsPARL to identify model substrates

Mass spectrometry-based substrate profiling was performed by Zhenze Jiang with our collaborator Dr. Anthony O'Donoghue at UCSD to identify small soluble peptides that are preferentially cleaved by HsPARLΔ77 and to validate that our recombinant enzyme retains high levels of proteolytic activity, similar to substrate profiling performed for bacterial rhomboid proteases[185]. From a peptide library composed of 283 unique peptide sequences, the substrate profiling identified 139 peptides cleaved by HsPARLΔ77 with a fold-change > 4. Fold-change was calculated by comparing peptide abundance after a set time of incubation with the protease to the peptide abundance before addition of the protease; for peptides cleaved well by HsPARLΔ77, the amount of full-length peptide will be significantly reduced after incubation with the protease. The top-cleaved peptide had a fold-change of 780 after 60 min of incubation with HsPARLΔ77 while the second top-cleaved peptide had a fold-change of 295; the top five cleaved peptides are outlined in Table 3.1. Comparing the fold-change of the top-cleaved peptide to that of the second best, we see that the fold-change associated with the top-cleaved peptide is over 2.5 times greater. Upon obtaining sequences of the top-cleaved

Table 3.1: Top-cleaved peptides by HsPARLΔ77 identified through mass-spectrometry substrate profiling. The HsPARLΔ77 cleavage site is indicated by *.

PEPTIDE NAME	SEQUENCE	FOLD-CHANGE (60 MIN)	FOLD-CHANGE (180 MIN)
TDP94	MHSPWTMANF*LRGP	780	2860
TDP160	INDFLVR*TWKMPGL	295	1123
TDP89	GPKLTYDFWIQ*NLP	236	1015
TDP96	GQYPFVKIST*THW	230	932
TDP15	AMTDRGWYLAIQ*AV	231	674

peptides, the most preferred peptide was ordered to be synthesized as an IQ substrate with the EDANS/DABCYL fluorophore/quencher FRET-pair for kinetic analysis using the FRET-based protease kinetic assay described in Chapter 2.4. This model IQ peptide substrate will be used to determine the catalytic parameters associated with its cleavage.

3.3.2 Substrate specificity of HsPARL

The substrate specificity of HsPARLΔ77 was assessed using multiplex LC-MS/MS screening by Zhenze Jiang with our collaborator Dr. Anthony O'Donoghue at UCSD[184]. This screen revealed a distinct substrate specificity profile for PARL compared to that of the bacterial rhomboid protease HiGlpG (Figure 3.1). The bacterial rhomboid protease shows a preference for the small hydrophobic residue Ala in the P1 positon and bulky hydrophobic residues in P4 and P2', however the HsPARLΔ77 specificity profile reveals a bulky Phe residue in the P1 position. Homology modelling of the PARL core rhomboid domain with HiGlpG reveals that within the substrate binding pocket, there is sufficient space to facilitate a bulky amino acid such as phenylalanine in the P1 position (Figure 3.2). Proteolysis occurs at the peptide bond between the P1 and P1' residues. Like bacterial rhomboid proteases, a preference for a hydrophobic residue at the P4 position is conserved with HsPARLΔ77. Negatively charged residues are highly unfavourable throughout the length of the substrate profile from position P4 to P4'. C-terminal to the cleavage site, we observe a preference for helix-destabilizing residues like Arg and Pro. The majority of residues seen as favourable, though, are characteristic of TM segments. The substrate specificity plot for HsPARLΔ77 suggests that the enzyme has a broad recognition motif, preferentially for TM substrates; compared to HiGlpG, HsPARLΔ77 has a very broad substrate preference.

3.3.3 Truncations of HsPARL

Cellular studies have suggested that processing of PARL modulates its activity. To address
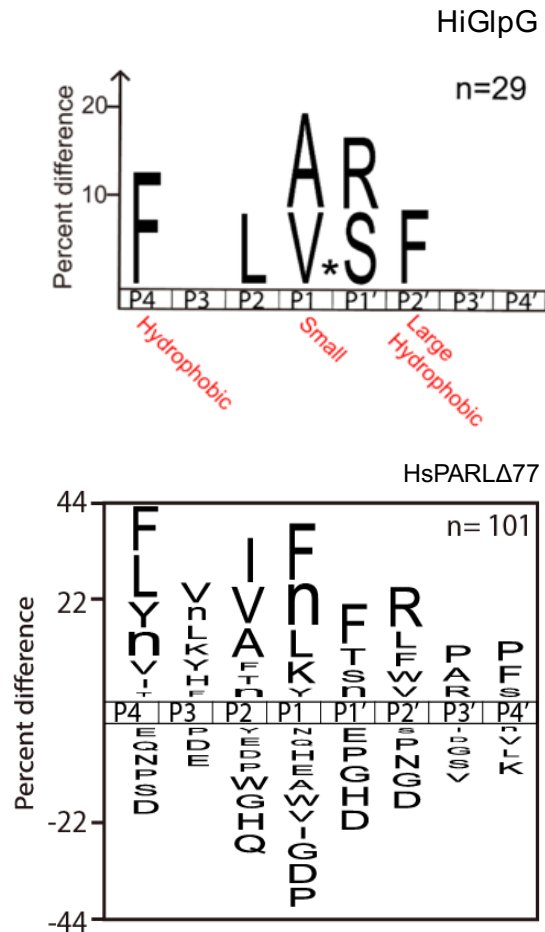
Figure 3.1: IceLogo substrate specificity plot for HiGlpG and HsPARLΔ77. Substrate specificity plot obtained from multiplex LC-MS/MS screening of HiGlpG (top) and HsPARLΔ77 (bottom) with a peptide library composed of 283 peptides. Specificity plot was based on cleavage of 29 unique peptides by HiGlpG and 101 unique peptides by HsPARLΔ77. P4 to P4' represent the amino acid residues of the substrate that would interact with the active site pocket of the enzyme. Hydrolysis of the peptide bond occurs between P1 and P1'. A preference for bulky hydrophobic amino acids is seen in position P4, P1, and P1' for HsPARLΔ77 while negative charged amino acids are unfavourable. A positive percent difference associated with a residue indicates that it is favourable in the position while a negative percent difference indicates an unfavourable reside.
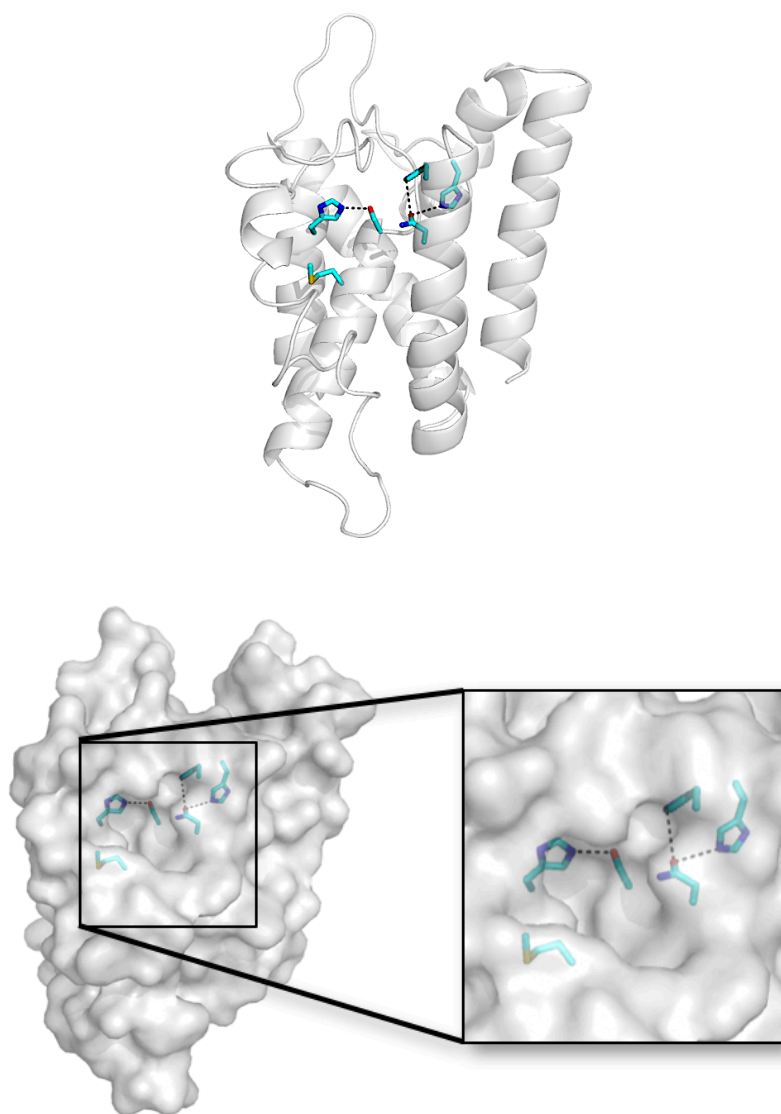
Figure 3.2: Homology model of HsPARL. A homology model of the HsPARL 6TM core based on the HiGlpG structure generated by Dr. M. Joanne Lemieux. Highlighted in cyan are the residues that comprise the catalytic dyad of the enzyme, Ser277 and His335. Flexible loops at the upper face of the active site likely allow access of the substrate to the catalytic core. The surface representation displays a large substrate binding pocket that could facilitate a bulky amino acid such as Phe in the P1 position of the substrate.

this, the activity of HsPARLΔ55 and HsPARLΔ77 was assessed towards the IQ-PINK1, IQ-PGAM5, and IQ-Smac peptide substrates (Table 2.7). The three peptide substrates were cleaved by both PARL truncations, indicating that processing to the Δ77 form is not necessary to activate the enzyme (Figure 3.3, 3.4, and 3.5). Catalytic parameters obtained for cleavage of the three peptide substrates by HsPARLΔ55 and HsPARLΔ77 are summarized in Table 3.2 and Figure 3.6. For cleavage of IQ-PGAM5, a significant increase in K_M, from 0.47 ± 0.07 μM to 1.6 ± 0.2 μM, is observed when cleaved by HsPARLΔ77 compared to HsPARLΔ55. There is also a significant increase in the IQ-PGAM5 turnover by HsPARLΔ77 as the k_{cat} value increases over two-fold, from 0.46 ± 0.02 h^{-1} to 0.98 ± 0.04 h^{-1}. While we observe a significant increase in the turnover of IQ-PGAM5 by HsPARLΔ77, the enzymatic efficiency of HsPARLΔ77 towards IQ-PGAM5 is significantly lower than that of HsPARLΔ55; the calculated k_{cat}/K_M value for cleavage of IQ-PGAM5 by HsPARLΔ77 is only 0.60 ± 0.09 $μM^{-1}h^{-1}$ compared to 0.98 ± 0.25 $μM^{-1}h^{-1}$ for HsPARLΔ55. A significant increase in both substrate turnover and enzymatic efficiency is observed for IQ-PINK1 cleavage by HsPARLΔ77 with the k_{cat} value increasing from 0.42 ± 0.03 h^{-1} to 1.3 ± 0.1 h^{-1} and the k_{cat}/K_M increasing from 0.22 ± 0.08 $μM^{-1}h^{-1}$ to 0.40 ± 0.12 $μM^{-1}h^{-1}$. There is a slight increase in K_M observed for HsPARLΔ77-mediated cleavage of IQ-PINK1, however this increase is not significant. No significant difference between HsPARLΔ55 and HsPARLΔ77 is observed in any of the catalytic parameters obtained for cleavage of IQ-Smac.

3.3.4 Differences between the PGAM5, PINK1, and Smac 10mer peptide substrates

Comparative analysis of the catalytic parameters obtained for cleavage of IQ-PINK1, IQ-PGAM5, and IQ-Smac shows that there are significant differences between cleavage of each unique substrate (Figure 3.7). A significant difference in K_M is observed between IQ-PGAM5 and IQ-PINK1 as well as IQ-PGAM5 and IQ-Smac for cleavage by both HsPARLΔ55 and HsPARLΔ77; IQ-PGAM5 consistently has the lowest K_M value, while IQ-Smac has the highest, out of the three peptide substrates assessed. A significant difference in K_M between IQ-PINK1

PARL☐55

PARLΔ77
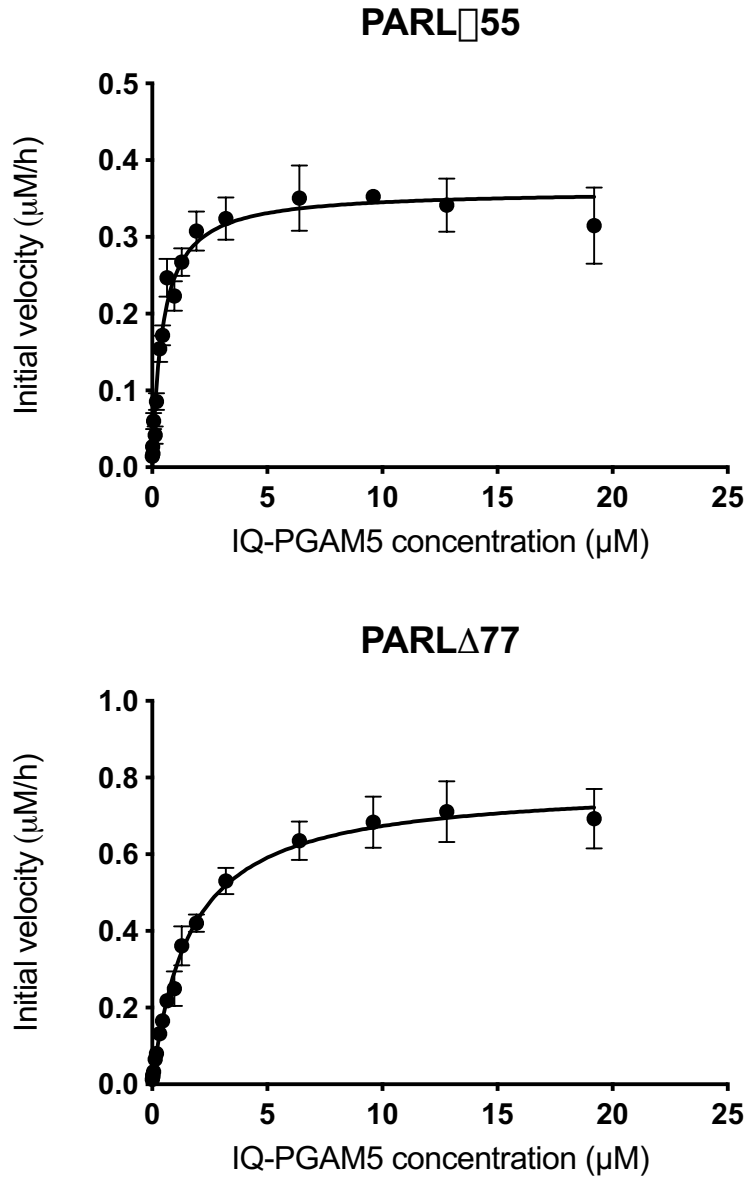
Figure 3.3: Michaelis-Menten kinetic curves for cleavage of IQ-PGAM5 by HsPARLΔ55 and HsPARLΔ77. Initial velocity values obtained were plotted for each concentration of IQ-PGAM5 tested. Curves were fit to the Michaelis-Menten equation using GraphPad Prism software and the catalytic parameters K_M and V_{max} were obtained. For cleavage of IQ-PGAM5 by HsPARLΔ55, n = 4. For cleavage by HsPARLΔ77, n = 5. Data are represented as mean ± SEM.

PARLΔ55

PARLΔ77
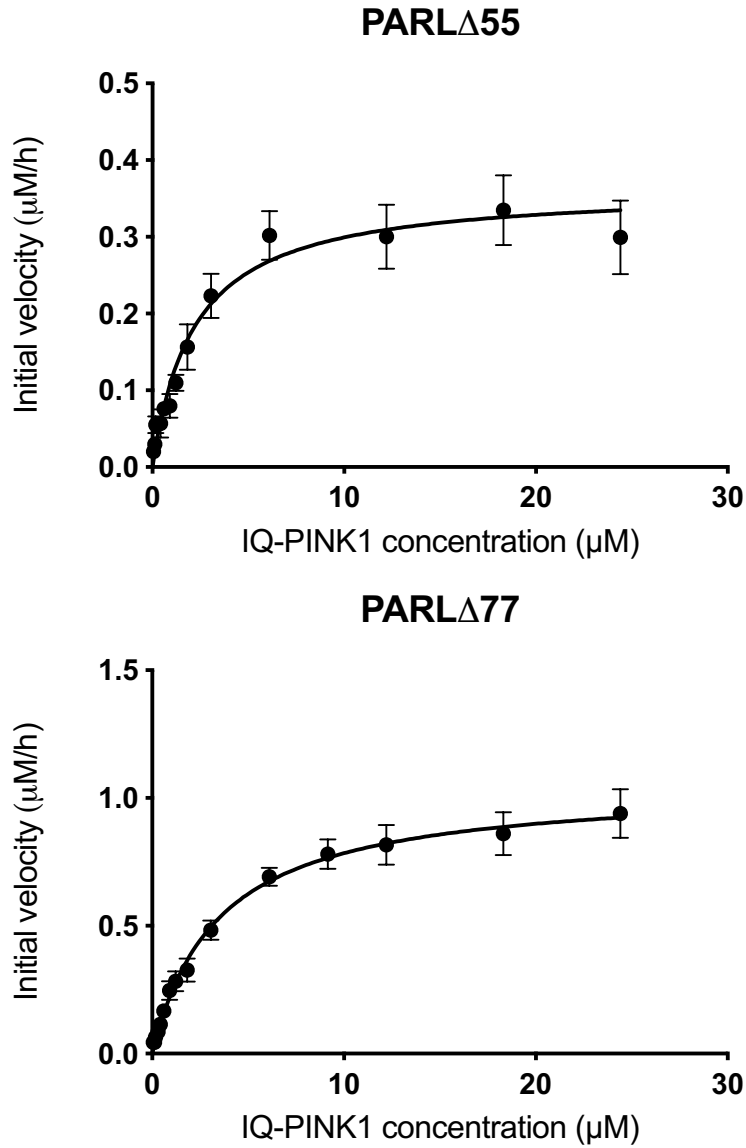
Figure 3.4: Michaelis-Menten kinetic curves for cleavage of IQ-PINK1 by HsPARLΔ55 and HsPARLΔ77. Initial velocity values obtained were plotted for each concentration of IQ-PINK1 tested. Curves were fit to the Michaelis-Menten equation using GraphPad Prism software and the catalytic parameters K_M and V_{max} were obtained. For cleavage of IQ-PINK1 by HsPARLΔ55, n = 3. For cleavage by HsPARLΔ77, n = 4. Data are represented as mean ± SEM.
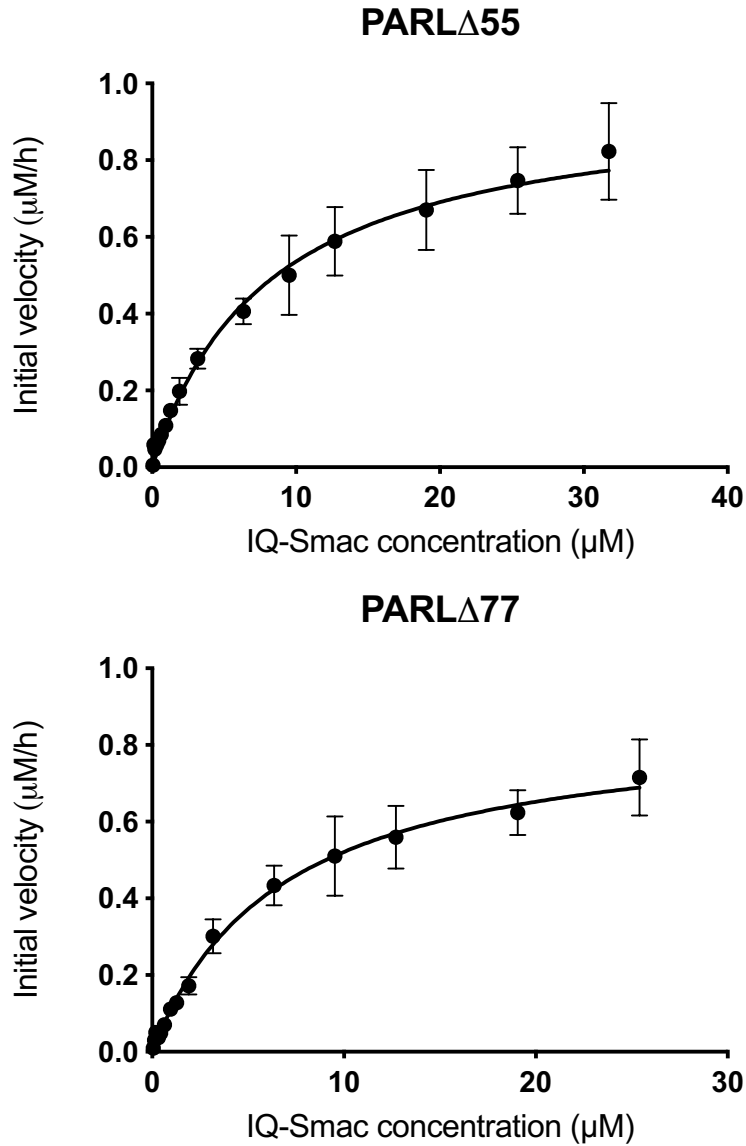
Figure 3.5: Michaelis-Menten kinetic curves for cleavage of IQ-Smac by HsPARLΔ55 and HsPARLΔ77. Initial velocity values obtained were plotted for each concentration of IQ-Smac tested. Curves were fit to the Michaelis-Menten equation using GraphPad Prism software and the catalytic parameters K_M and V_{max} were obtained. For cleavage of IQ-Smac by HsPARLΔ55 and HsPARLΔ77, n = 4. Data are represented as mean ± SEM.

Table 3.2: Catalytic parameters for cleavage of IQ-PINK1, IQ-PGAM5, and IQ-Smac by HsPARLΔ55 and HsPARLΔ77. Data are represented as mean ± SEM.

	PINK1		PGAM5		Smac	
	Δ55 n = 3	**Δ77** n = 4	**Δ55** n = 4	**Δ77** n = 5	**Δ55** n = 4	**Δ77** n = 4
K_M (µM)	1.9 ± 0.4	3.3 ± 0.5	0.47 ± 0.07	1.6 ± 0.2	6 ± 1	5 ± 1
k_{cat} (h^{-1})	0.42 ± 0.03	1.3 ± 0.1	0.46 ± 0.02	0.98 ± 0.04	1.3 ± 0.1	1.2 ± 0.1
k_{cat}/K_M ($\mu M^{-1}h^{-1}$)	0.22 ± 0.08	0.4 ± 0.1	1.0 ± 0.3	0.6 ± 0.1	0.3 ± 0.1	0.3 ± 0.1
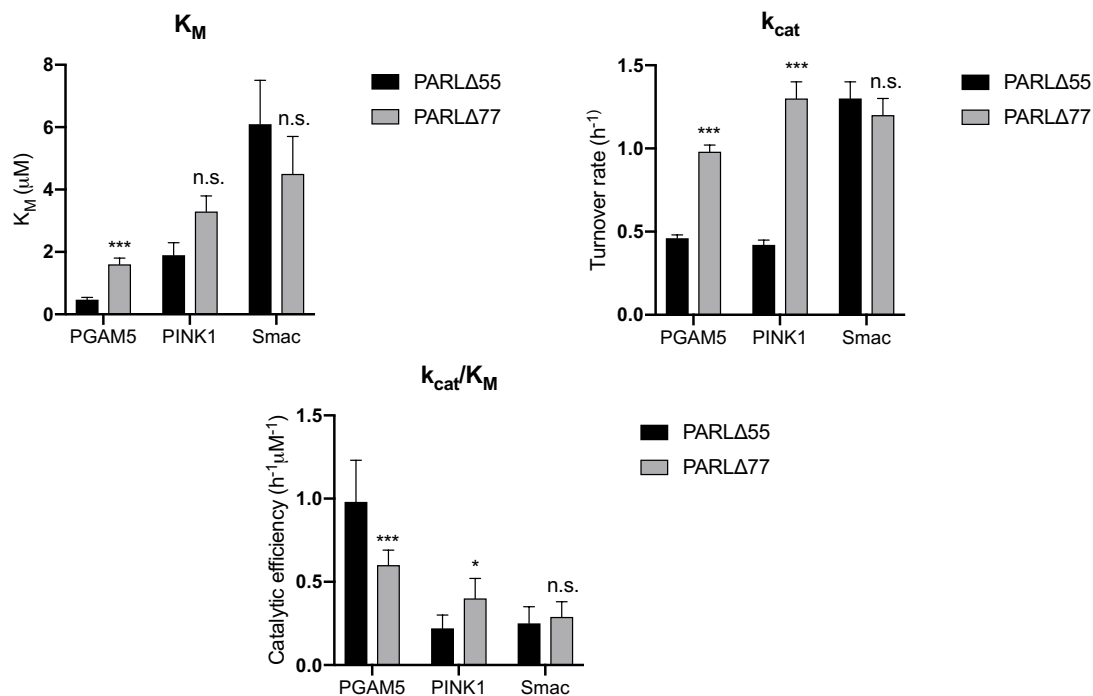
Figure 3.6: Catalytic parameters obtained for cleavage of IQ-PGAM5, IQ-PINK1, and IQ-Smac by HsPARLΔ55 and HsPARLΔ77. The Michaelis constant, K_M (µM), was obtained from Michaelis-Menten analysis of the kinetic curves obtained for cleavage of each internally quenched peptide substrate (Figure 3.3-3.5). K_M is the concentration of substrate at which there is half maximal enzymatic activity; it can also be thought of as the relative affinity of the enzyme for the substrate. From the V_{max} for cleavage of each substrate, the catalytic turnover, or k_{cat} (h^{-1}), is calculated (see *2.4.2*). The k_{cat}/K_M (h^{-1} $µM^{-1}$) is calculated to provide us with the enzymatic efficiency towards each substrate. Unpaired t-tests were performed to determine significant differences in parameters between cleavage mediated by HsPARLΔ55 and HsPARLΔ77. A cutoff of $p < 0.05$ indicated a statistically significant difference. (* $p < 0.05$, *** $p < 0.0005$, n.s. denotes no significance). Data are represented as mean ± SEM.

and IQ-Smac is only observed for cleavage by HsPARLΔ55. When looking at substrate turnover, the k_{cat} is significantly higher for IQ-Smac than IQ-PGAM5 when cleaved by both HsPARLΔ55 and HsPARLΔ77. Interestingly, the difference in turnover between IQ-PGAM5 and IQ-PINK1 is only significant when mediated by HsPARLΔ77. Whereas the difference between turnover of IQ-Smac and IQ-PINK1 is only significant when cleavage is mediated by HsPARLΔ55.

In regards to the k_{cat}/K_M, overall HsPARL cleaves IQ-PGAM5 the most efficiently as it consistently has the highest k_{cat}/K_M value. Catalytic efficiency is significantly decreased for cleavage of IQ-PINK1 and IQ-Smac compared to IQ-PGAM5 for HsPARLΔ55-mediated cleavage. Catalytic efficiency is decreased towards IQ-PINK1 and IQ-Smac compared to IQ-PGAM5 for HsPARLΔ77-mediated cleavage, however this decrease is only significant for IQ-Smac. The catalytic efficiency for cleavage of IQ-PINK1 and IQ-Smac is comparable when mediated by either HsPARLΔ55 or HsPARLΔ77 and we observe no significant difference between these two substrates.

3.3.5 HsPARL inhibitor study

Using a panel of protease inhibitors, we monitored cleavage of three concentrations of the IQ-PGAM5 peptide by HsPARLΔ77 (Figure 3.8). The protease inhibitors tested were PMSF, a serine protease inhibitor, a protease inhibitor cocktail tablet, to inhibit serine and cysteine proteases, and EDTA, to inhibit metalloproteases. None of the inhibitors tested influenced the activity of HsPARLΔ77, suggesting that no activity observed in our proteolytic assays is due to a potential contaminating protease of the serine, cysteine, or metalloprotease class.

3.4 Discussion

This chapter presents the first known kinetic analyses of recombinant HsPARL, providing a
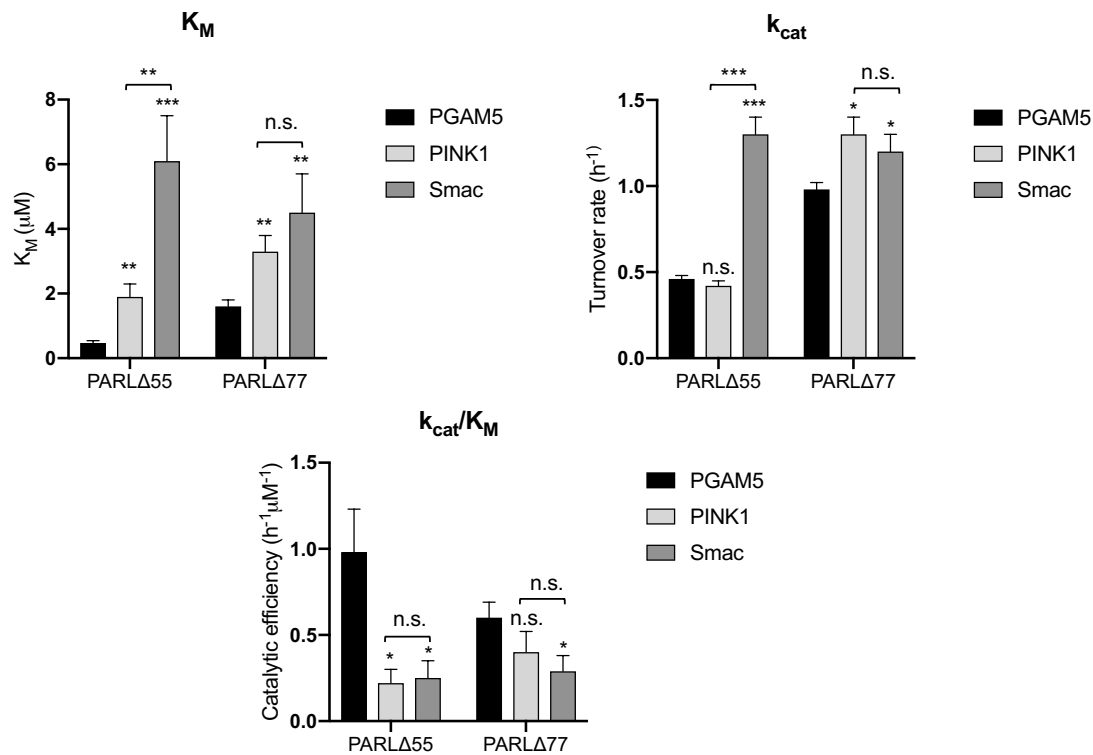
Figure 3.7: Comparative analysis of the catalytic parameters obtained for cleavage of IQ-PGAM5, IQ-PINK1, and IQ-Smac. The same parameters are displayed here as in Figure 3.6. Two-way ANOVA with multiple comparisons was performed between parameters obtained for IQ-PGAM5, IQ-PINK1, and IQ-Smac to determine if there were significant differences between the catalytic parameters for each unique substrate. The Tukey method was used to correct for multiple comparisons. A cutoff of $p < 0.05$ indicated a statistically significant difference. (* $p < 0.05$, ** $p < 0.005$, *** $p < 0.0005$, n.s. denotes no significance). Data are represented as mean ± SEM.
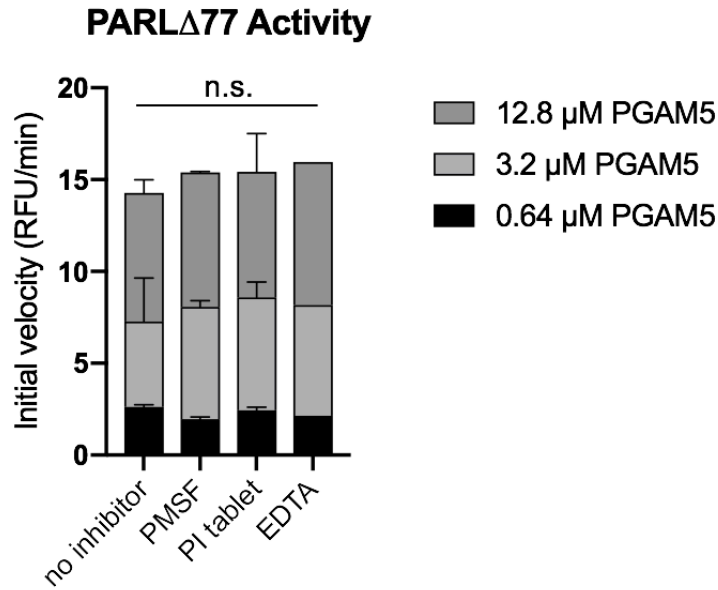
Figure 3.8: Relative activity of HsPARLΔ77 towards IQ-PGAM5 in the presence of standard protease inhibitors. Initial velocity values obtained were plotted for each concentration of IQ-PGAM5 tested in the presence of 1 mM PMSF, a Ser/Cys protease inhibitor cocktail tablet, or 1 mM EDTA. One-way ANOVA with multiple comparisons was performed between the no-inhibitor condition and each protease inhibitor. The Dunnett method was used to correct for multiple comparisons. A cutoff of $p < 0.05$ indicated a statistically significant difference (n.s. denotes no significance). Two experimental replicates were performed with each inhibitor (n = 2). Data are represented as mean $\pm$ SEM.

significant advance in our understanding of characteristics and regulation of PARL-mediated proteolytic activity.

The identification of substrates that are cleaved both rapidly and specifically by PARL is extremely beneficial in regards to their application in studying characteristics of PARL-mediated proteolytic activity. There are many commercial protease activity-probing kits that rely on model protease substrates, such as fluorescein-casein which has also been used in our lab[191]. While these commercially available kits provide a quick assessment of enzymatic activity, they are not specific to our protease of interest and provide no kinetic information relevant to the cleavage of preferred substrates. The mass spectrometry-based substrate profiling performed by Anthony O'Donoghue for HsPARLΔ77 revealed several peptide substrates that were preferentially cleaved by HsPARLΔ77 as revealed by their high fold-change. A paper recently published by our lab highlighted the multiple uses of model peptide substrates identified for bacterial rhomboid proteases, among others, using the mass spectrometry-based method employed here[39]. Small internally quenched peptides were synthesized based on the sequences of the top-cleaved peptides identified for three bacterial rhomboid proteases. These model peptide substrates were then able to be used to quickly compare catalytic parameters between the different rhomboid proteases. In regards to HsPARL, the top-cleaved peptide is in the process of being synthesized as an IQ peptide that is compatible with our FRET-based kinetic assay system. The model peptide will then allow us to confirm that our enzyme retains optimal activity before use in kinetic assays towards physiological substrates.

A further application of these peptides is their use for screening inhibitors[39,192]. As mentioned, inhibitor development towards HsPARL has been impeded due to there being no established *in vitro* method to assess HsPARL activity in a quick and reproducible manner. These model peptides can be used to assess the proteolytic activity of HsPARL while screening numerous inhibitors, allowing for a robust workflow. Model peptide substrates are becoming increasingly

attractive in assessing the functionality of rhomboid proteases and for high-throughput inhibitor screening, as demonstrated for the bacterial rhomboids[39]. The identification of model peptide substrates for HsPARLΔ77 through MS-based substrate profiling presents new ways for the proteolytic activity of HsPARL to be characterized and can mitigate the current limitations facing inhibitor design.

In addition to the identification of model peptide substrates for HsPARLΔ77, MS-based methods were also employed to determine the substrate specificity of HsPARLΔ77. The identified substrate specificity of HsPARLΔ77 presents many unexpected features. The preference for a large hydrophobic residue, particularly Phe, in the P1 position is in stark contrast to the substrate specificity of bacterial rhomboid proteases; bacterial rhomboids have been established as having a preference for the small hydrophobic Ala in the P1 position[31,183]. While there are these notable differences, a hydrophobic Phe residue is conserved in the P4 position between bacterial rhomboids and HsPARLΔ77. This substrate specificity of HsPARLΔ77 is in conflict with current literature that supports the idea of PARL preferring small hydrophobic amino acids in the P1 position like its bacterial family members, though this study used HEK293 cell lysates as opposed to purified protein[75]. In this proteomics study, of the six substrates of PARL identified, three were identified to have an Ala in the P1 position, while the others have either a Ser or Cys residue in the P1 position[75].

While the literature does not support the preference for a bulky amino acid at P1, structural modelling of PARL does. When looking at the surface representation of a homology model of PARL based on the HiGlpG structure, a large substrate binding pocket is observed (Figure 3.2). This pocket would easily facilitate the entrance of a bulky residue, such as a Phe, within the catalytic core of the enzyme. We see that negatively charged amino acids are highly unfavourable within the P4 to P4' positions; this is likely due to disruption of the oxyanion hole that would result from a negative charge entering into the catalytic core of the enzyme[193]. A study performed in SH-S5Y5 cells looked at PARL-mediated cleavage of PINK1-A103D and

PINK1-F104D (these mutations are in the P1 and P1' positions respectively) and found that there was an accumulation of the 63 kDa full-length form of PINK1 for both the A103D and F104D variants[67]. The accumulation of the full-length protein suggests that cleavage of PINK1-A103D and PINK1-F104D is impaired and supports the finding that Asp residues near the cleavage site are unfavourable, as shown by the negative percent difference associated with these residues (Figure 3.1). A different study looked at the cleavage of PINK1-F104M, a known polymorphism of the protein containing a Met residue in the P1' position. This variant had no cleavage defect when compared to PINK1-WT, though this study was again conducted using whole cell lysates of HeLa cells[77]. While the peptide library used for identifying the substrate specificity does not contain methionine, the norvaline residue is considered a methionine-mimic and is found as a preferred residue in the P1' site, thus providing an explanation for why this mutation does not impair PARL-mediated cleavage of PINK1. We do note that our observed cleavage by HsPARL occurs at a slow rate, similar to that reported for *in vitro* proteolytic studies with γ-secretase, though this MS analysis reveals substrates with Phe in the P1 position may cleaved at a faster rate[194]. This suggests that the cleavage of PINK1 is either slow *in vivo* or that it requires additional factors that enhance its rate of cleavage.

The substrate specificity profile obtained for HsPARLΔ77 suggests that the enzyme has an overall broad substrate specificity towards transmembrane substrates based on the preference for residues such as Phe, Ala, Val, Ile, and Pro which are commonly associated with TM regions of a protein. Furthermore, in the region directly C-terminal to the cleavage site, there is a preference for the helix-destabilizing or helix-breaking residues Arg and Pro. This supports evidence gathered for bacterial rhomboids that suggest that helix-destabilizing residues are required to facilitate unwinding of the helical TM segment so that the protease has access to the cleavage site[105]. The broad substrate specificity obtained for HsPARLΔ77 also supports previous work on the yeast mitochondrial rhomboid that demonstrated large sequence variability in cleavable substrates[195]. This broad specificity may indicate that there are numerous substrates that have yet to be identified for the mitochondrial rhomboids. The

substrate specificity of other intramembrane proteases, such as γ-secretase, have also been established to have broad specificity, with γ-secretase sometimes being referred to as the "proteasome of the membrane" due to the wide range of substrates, over 80 have been identified, that it is able to process[54,196]. These broad specificity patterns indicate that there are likely other factors that regulate intramembrane proteolysis, as opposed to a highly specific substrate recognition motif.

Processing of PARL, to either its mature Δ53 form or the further truncated Δ77 form, has been proposed to be a modulator of its enzymatic activity. Cellular studies have provided conflicting evidence as impaired PARL activity is observed when mutation at Ser77 prevents β-cleavage to the PARLΔ77 form, though the PARLΔ53 form appears to be more active towards the PINK1 substrate[49,65]. Using recombinant HsPARLΔ55 and HsPARLΔ77, we assessed the cleavage of three unique peptide substrates, IQ-PGAM5, IQ-PINK1, and IQ-Smac. The use of peptide substrates for proteolytic assays is well established and such substrates have been used for several intramembrane proteases[39,192,197]. Using a peptide substrate allows us to have the residues of a native substrate, but eliminates the efforts required to generate recombinant protein substrates, which is even more challenging when we are considering TM substrates. Additionally, peptides are easily synthesized with chemical fluorophore/quencher FRET-pairs so their cleavage can be monitored in a continuous assay format. We validated that HsPARL is catalytically active in either form, thus indicating that processing to the Δ77 form is not required for proteolytic activity or PARL functionality as was once speculated[49]. While these truncations do not serve as an activation switch for the protease, we found that there are measurable differences in the catalytic parameters of proteolytic cleavage mediated by either the Δ55 or Δ77 truncation of HsPARL. This suggests that these truncations of HsPARL identified *in vivo* do indeed regulate aspects of its activity. HsPARLΔ55 demonstrated significantly lower substrate turnover of IQ-PGAM5 and IQ-PINK. This can be reconciled with what is known in the literature for PGAM5 as it is suggested to be preferentially cleaved by PARL upon mitochondrial depolarization, when we also observe enhanced β-cleavage and

PARLΔ77 formation[65,74]. Is has been suggested that PARLΔ77 is catalytically less active towards PINK1 than the longer form of the protease, though our results suggest otherwise[65]. This may be due to these cellular studies being performed during times of mitochondrial stress in which PARLΔ77 formation is enhanced, but PINK1 import to the IMM is impaired, therefore even if PARLΔ77 would be more active towards PINK1, it does not have access to the substrate so we observe less cleavage. Interestingly, with the IQ-Smac peptide, no significant difference was observed in any of the catalytic parameters when cleaved by HsPARLΔ55 or HsPARLΔ77, indicating that cleavage of this substrate may not be regulated in a manner related to the different truncated forms of PARL. This supports a recent finding that Smac can be co-immunoprecipitated with PARL in both polarized and depolarized mitochondria[75]. If the truncations of PARL are proposed to mediate cleavage of substrates based on mitochondrial conditions, such as polarized or depolarized as observed for PINK1 and PGAM5 in cellular studies, and we see no difference in the PARL-Smac interaction in varying conditions, it is unlikely that its cleavage would be regulated by PARL truncation, as shown by our data.

While we were able to compare the cleavage of substrates mediated by either HsPARLΔ55 or HsPARLΔ77, many questions remain unanswered in regards to these different forms of PARL. It is important to note that varying amounts of the different truncations are detected in different tissues, suggesting that this processing of PARL occurs differentially in different tissues and may result in differing PARL function between tissues[62]. One obvious question is what could be the role of the roughly 20 amino acid N-terminal region that is removed upon β-cleavage? We can make several speculations on its potential function which may include protein stabilization or aiding in substrate recognition, though this is more unlikely unless this region is somehow able to embed into the membrane. Based on its localization to the matrix side of the IMM, it may be involved in mediating interactions with proteins that reside in the mitochondrial matrix. The paper that proposed the PARL-YME1L-SLP2 complex did not address what form of PARL resides in this complex; perhaps this N-terminal region is required for protein-protein interactions between PARL and the SLP2 scaffold protein, but because

there has been just the one published report on this complex, we can only make these preliminary speculations[66]. Additional assessment of the truncated forms of PARL is also necessary in the context of disease. Impaired processing of PARL to its truncated forms may be implicated in disease as the PARL-S77N mutation, albeit rare, has been identified in Parkinson's disease patients[49]. This mutation prevents β-cleavage and therefore abolishes PARLΔ77 formation. In our assay, the longer form of the enzyme, HsPARLΔ55, has significantly lower turnover rates, thus this mutation could inhibit PARL activity. Inhibition of PARL activity could lead to dysregulation of mitochondrial homeostasis if substrates are unable to be efficiently proteolysed, presenting a potential role for PARL in PD pathogenesis. This initial study addressing the truncations of PARL in an *in vitro* proteolytic assay system answers several questions that could not be conclusively addressed in cellular studies and presents new avenues of research regarding PARL and the regulatory roles of its truncated forms.

In addition to being able to address how truncations influence PARL-mediated cleavage, we were also able to gather kinetic information regarding the cleavage of specific substrates that have been identified as physiological substrates of PARL. These kinetic assays were the first *in vitro* assays using recombinant protein to validate that PARL is indeed able to cleave these proteins that have been identified as substrates in cellular studies. Comparing the catalytic parameters obtained for each substrate tells us that HsPARL does show differences in cleavage between the three substrates. This indicates that substrate specificity does have a role in regulating PARL-mediated cleavage. If there was no influence of substrate specificity or substrate recognition on cleavage, we would expect the catalytic parameters to be very similar for the three substrates. The catalytic parameters obtained suggest that of these three substrates assessed, PGAM5 is the preferred substrate of PARL. It is consistently seen that the K_M value is the lowest for PGAM5, indicating a higher affinity of the enzyme for this substrate, and that the catalytic efficiency towards PGAM5 is the greatest.

One substantial limitation of this assay, however, is that we are seeing cleavage events occurring at a substrate turnover rate of one per hour which is very slow for proteolytic reactions. This could be a factor of using a detergent-based reconstitution system for PARL, which is very different from the bilayer it natively resides in, or it could be a characteristic of the protein itself, though likely not to as great of an extent as seen here. The bacterial rhomboids HiGlpG and PsAarA cleave at a rate of roughly two per minute for their preferred substrates in DDM, while EcGlpG cleaves slowly in DDM, much like PARL, at a rate of approximately six per hour[39,177]. Studies on other intramembrane proteases also suggest that these slow turnover rates are standard for intramembrane proteolytic assays performed in DDM; intramembrane aspartyl proteases have been found to cleave a physiological FRET-peptide substrate at a rate of approximately two per hour which is not considerably different than what we see for HsPARL[197]. Regardless of the slow rate of substrate turnover, the catalytic parameters obtained are still able to provide valuable information regarding the unique enzyme-substrate interactions for each substrate assessed. Future studies will include an examination of PARL-mediated cleavage with our recombinant enzyme reconstituted into a membrane-mimetic system such as bicelles or liposomes, or with the development of an *in vivo* cleavage assay.

Another limitation to this *in vitro* assay is that we currently do not have a catalytically inactive mutant of HsPARL to serve as a negative control. As every protein preparation can vary slightly, including co-purifying contaminants, we wanted to assess whether contaminating proteases contribute to substrate cleavage. To mitigate the possibility that the proteolytic activity we are seeing is due to a potential contaminating protease, a proteolytic activity assay for HsPARLΔ77 was performed in the presence of a panel of protease inhibitors. This provides immediate and direct control for the purposes of our proteolytic assays. As others have reported, rhomboid proteases are resistant to inhibition by classical serine protease inhibitors and we see that this holds true with our recombinant HsPARLΔ77[17]. No inhibition of HsPARLΔ77-mediated proteolytic activity towards the IQ-PGAM5 peptide was observed in the

presence of PMSF, a serine protease inhibitor, a Ser/Cys protease inhibitor cocktail tablet, or EDTA, a metalloprotease inhibitor; while a specific aspartyl protease inhibitor was not tested, aspartyl proteases have optimal activity at acidic pH and should not be active at pH 7.0 used in our assays. This suggests that all proteolytic activity observed is a result of HsPARL-mediated cleavage.

This chapter highlights the many aspects of characterization of PARL-mediated cleavage that can be addressed by using *in vitro* proteolytic assays with a recombinant enzyme. Mass spectrometry-based methods allowed for the identification of peptides that were highly cleaved by HsPARLΔ77 which confirmed that our recombinant protease retained optimal activity after purification and provides substrates that can be used for downstream applications such as inhibitor screening. These mass spectrometry methods also enabled us to obtain a substrate specificity plot for HsPARLΔ77 which revealed unique features in regards to substrate recognition and preference that are not apparent for bacterial rhomboids. A FRET-based assay was established to monitor proteolytic activity of HsPARLΔ55 and HsPARLΔ77 in a continuous manner, allowing us to gather specific catalytic parameters for the cleavage of three unique substrates, IQ-PGAM5, IQ-PINK1, and IQ-Smac, by each HsPARL construct. We observed that the truncations of HsPARL do have a regulatory role in PARL-mediated cleavage along with substrate recognition and preference, as determined by the differences between catalytic parameters obtained for each substrate and each HsPARL construct. The establishment of this *in vitro* assay to directly measure proteolytic activity of HsPARL presents a large advance in the field as the majority of previous kinetic studies on rhomboid proteases have been limited to the bacterial rhomboids. These initial *in vitro* studies present a starting point for much new and exciting research on the mitochondrial rhomboid protease PARL and they provide us with new methods for characterizing regulatory and mechanistic aspects of PARL's proteolytic functions.

4.1 Introduction

Rhomboid proteases are integral membrane proteins composed of at least six TM segments. Due to their localization in cellular membranes, the lipid environment these proteins reside in is likely to regulate some aspect of their proteolytic function. The activity of numerous intramembrane enzymes has been demonstrated to be modulated by their lipid environment[198]. Two published crystal structures of bacterial rhomboid proteases exhibit a phospholipid that was bound and co-crystallized with the protease, though the specific function of the lipid remains unknown[25,26]. Studies on bacterial rhomboids have provided several lines of evidence that the proteolytic activity of rhomboids can be influenced by lipids. Reconstitution of EcGlpG into phosphatidylethanolamine (PE) liposomes resulted in increased proteolytic activity when compared to EcGlpG that was reconstituted into phosphatidylcholine (PC) liposomes[17]. Molecular dynamics simulations of GlpG in a lipid bilayer supported the *in vitro* evidence of lipids influencing activity as hydrogen bonding between the GlpG backbone and the lipid headgroups of its environment was observed, resulting in membrane thinning in the regions adjacent to the protein[33]. The greatest membrane perturbation was observed near the L1 loop that connects TM1 and TM2; the L1 loop of bacterial rhomboids contains numerous charged residues that interact with lipid headgroups and this region of the protein may act as a sensor for the lipid environment, providing specificity to rhomboids in different lipid environments[33,36]. Additional protein-lipid contacts were identified between TM5 and the lipid environment, suggesting stabilization of the protease in a confirmation conductive to substrate entry[199]. Perhaps the most striking evidence of lipids modulating rhomboid protease activity was the finding that non-substrates could become substrates and be cleaved simply by disruption of membrane composition[200]. The authors of this study concluded that the membrane environment in which the rhomboid protease resides imposes constraints and restricts the dynamics of substrate gating, thus providing specificity to the enzyme.

Studies on lipids influencing the activity of mitochondrial rhomboids have been performed in

yeast, however, the results of these have not provided evidence that the mitochondrial membrane lipid environment is regulating or influencing rhomboid activity. In mutant yeast strains with altered mitochondrial membrane lipid compositions, no differences in rhomboid-mediated cleavage were observed[86,201-204]. Given that the IMM has a unique lipid composition in comparison to that of other cellular membranes, it is unlikely that there would be no effect of the mitochondrial lipid environment on rhomboid activity. The main lipid species of the IMM are PC and PE, though phosphatidylinositol and cardiolipin (CL) make a significant contribution to the lipid milieu as well[205]. It should be noted that the IMM is the only eukaryotic cellular membrane that contains a significant amount of CL, with up to 20% of the total lipid content of the IMM being CL[206].

In bacterial membranes, PE and CL have been shown to assemble into lipid nanodomains, regions of the membrane enriched with a particular lipid species[207,208]. The identification of these lipid nanodomains in bacterial membranes suggest that lipid nanodomains composed of PE and CL could likely form in the mitochondrial membranes of eukaryotic organisms. A study looking at hydrophobic mismatch of rhomboid proteases due to membrane thinning found that rhomboid activity was inhibited in the presence of detergents or lipids with long alkyl chains, representative of a more ordered lipid bilayer[209]. This suggests that lipid nanodomains that are less ordered may compartmentalize rhomboid activity. The activity of mitochondrial rhomboids in particular may be compartmentalized as the mitochondrial membrane contains lipid species that have a higher propensity for clustering into lipid nanodomains[210]. Further supporting the idea that mitochondrial rhomboids may compartmentalize into lipid nanodomains is that a substrate of the yeast mitochondrial rhomboid was identified as localizing to cristae folds of the IMM, regions where these lipid nanodomains are proposed to exist[211]. Experimentally, the suborganellar localization of PARL within the IMM has not been determined.

Lipid nanodomains enriched with CL are of particular interest as it is known to be essential to the activity of numerous IMM proteins, particularly those of the electron transport chain. There
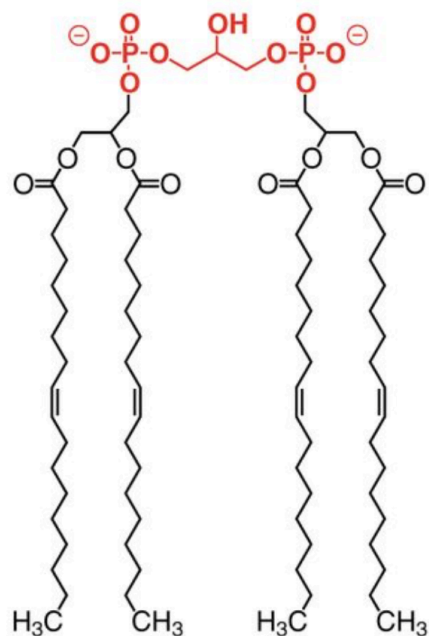
Figure 4.1: Cardiolipin structure. Cardiolipin (CL) is a diphosphatidylglycerol molecule. It is composed of four acyl chains and two polar headgroups. CL can hold up to two negative charges due its two phosphate groups. The headgroup is small compared to the bulky acyl tails allowing it to have unique properties regarding the structure of the IMM and its interaction with proteins that reside there. Because there are four distinct acyl tails, there is a large amount of complexity possible; most often, CL contains 18-carbon acyl chains with two unsaturated bonds each [(18:2)4][212-214]. From Oliver, P. M., *et al.* (2014). Localization of anionic phospholipids in Escherichia coli cells. *J Bacteriol 196*, 3386-98.

are currently 62 different proteins reported to interact with CL and high resolution structures of all respiratory complexes have been resolved with at least one CL molecule present[215]. Recent studies show that CL enhances electron transport between complex I and ubiquinone as well as directs ETC-modifying proteins to its targets, thus implicating the CL lipid species as a modulator of enzymatic activity as well[216,217]. CL is a structurally unique lipid composed of four acyl chains and two phosphate groups that can both potentially hold a negative charge (Figure 4.1). Due to these unique characteristics, CL can form lipid-protein interactions through phosphate binding, hydroxyl binding, or acyl binding patches on a membrane protein. Further adding to the complexity of CL and the lipid-protein interactions it can participate in, each acyl chain can have a distinct composition that can be remodeled in response to various physiological conditions[218]. This suggests that CL likely has many more unidentified interacting partners that may only present themselves under specific cellular conditions.

The unique architecture of CL promotes negative curvature of a membrane, electrostatic interactions, cohesiveness of the hydrocarbon chains, lipid clustering, and the formation of non-bilayer structures[219,220]. These features associated with CL are likely to be important in the dynamics and compartmentalization of mitochondrial membranes as well as in the stability of their high protein density, thus facilitating the formation of multi-protein complexes like those of the respiratory chain. Mitochondria have very high protein density within the cristae of the IMM where the ETC protein complexes are localized, require extensive membrane folding to support this high protein density, and are constantly undergoing dynamic fission and fusion events. These factors require non-bilayer lipid phases to facilitate the membrane dynamics and high negative curvature to promote cristae formation, all supporting the important roles of CL in the IMM[221].

CL is proposed to have defining roles in numerous mitochondrial processes including bioenergetics, apoptosis, mitophagy, and mitochondrial dynamics and membrane structure. Whether the role of CL in these processes is due to enhanced protein stabilization or by CL

eliciting a direct effect on target proteins is unclear. Much focus in regards to understanding the role of CL in these mitochondrial processes has been placed on the importance of CL in the context of the respiratory complexes, though with identification of numerous other proteins that interact with CL, our understanding of the role of CL in mitochondrial processes is bound to expand dramatically.

Membrane proteins are often sensitive to their lipid environments, and whether specific lipid-protein interactions result in increased stability of the membrane protein or an actual enhancement of protein function, or perhaps a combination of both, remains to be elucidated for the rhomboid proteases[198]. In the context of the IMM, unique lipid species such as CL have critical roles in mitochondrial morphology and membrane organization, thus imparting regulatory effects on the stability and function of numerous membrane-embedded proteins. It is likely that this regulation is extended to the mitochondrial rhomboid proteases, including PARL.

4.2 Objective

Numerous publications have shown that CL enhances the activity of proteins residing in the IMM[216,222-224]. Because PARL resides in the IMM and current evidence suggests that the activity of rhomboid proteases can be modulated by lipids, we hypothesized that CL would have an effect on the proteolytic activity of PARL. Previous work in our lab demonstrated that other lipids such as phosphatidylcholine do not influence the activity of PARL, thus we only aimed to assess the effect of CL. Using a mixed micelle system composed of the detergent DDM and the lipid CL, the activity of HsPARLΔ77 was assessed. Several lipid to protein molar ratios were tested to determine if there was an optimal lipid concentration that resulted in the greatest influence on activity. Activity of HsPARLΔ77 was assessed towards both a transmembrane substrate, HsFRET-PINK1(70-134)-WT, and a soluble model substrate, the internally quenched peptide IQ4. We assessed both a TM substrate that contains a complete

TM domain and a soluble substrate to see if any effect observed upon the addition of lipid was specific to the cleavage of TM substrates or if it was a general effect on the proteolytic activity of the enzyme.

4.3 Results

4.3.1 Effect of CL on HsPARL activity towards TM substrate HsFRET-PINK1(70-134)-WT

The activity of HsPARLΔ77 towards the FRET-PINK1(70-134)-WT transmembrane substrate was assessed in the presence of varying CL to PARL molar ratios (Figure 4.2). The no-lipid condition consists of HsPARLΔ77 reconstituted in detergent (DDM) micelles, while all CL lipid conditions consist of a mixed micelle system where both detergent (DDM) and lipid (CL) are present. Using the no-lipid condition as the baseline for proteolytic activity, a significant increase in activity was observed when the assay was carried out in the presence of 25:1 CL to PARL and 50:1 CL to PARL. The 25:1 CL to PARL condition resulted in a 1.8-fold increase in proteolytic activity of the enzyme, while the 50:1 CL to PARL condition resulted in a 1.4-fold increase in proteolytic activity. The activity of HsPARLΔ77 towards the FRET-PINK1(70-134)-WT substrate in the presence of a 5:1 molar ratio of CL to PARL resulted in no statistical difference in the activity of the protease when compared to the no-lipid control. Interestingly, this was also seen at the 100:1 molar ratio of CL to PARL, in which in the activity of HsPARLΔ77 returned to no-lipid baseline levels.

4.3.2 Effect of CL on PARL activity towards soluble model peptide substrate IQ4

The activity of HsPARLΔ77 towards the soluble IQ4 peptide substrate was assessed in the same conditions that were used for cleavage assessment of FRET-PINK1(70-134)-WT (Figure 4.3). A significant increase in the proteolytic activity of HsPARLΔ77 towards IQ4 was observed for the 5:1 and 25:1 CL to PARL molar ratios. Like the cleavage of HsFRET-PINK1, the greatest increase in proteolytic activity towards IQ4 was observed at the 25:1 CL to PARL ratio

HsFRET-PINK1(70-134)-WT
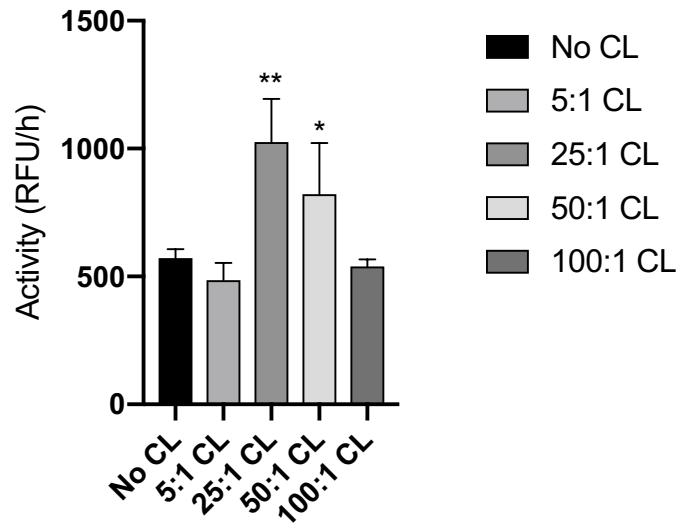
Figure 4.2: Effect of cardiolipin on HsPARLΔ77 activity towards HsFRET-PINK1(70-134)-WT. Cleavage of 1.5 μM HsFRET-PINK1(70-134)-WT by 1 μM HsPARLΔ77 in the presence of increasing cardiolipin concentrations was monitored for 3 h. Initial velocity was calculated for each lipid condition and values were plotted using GraphPad Prism software. The concentration of cardiolipin is displayed as a lipid to protein molar ratio. One-way ANOVA with multiple comparisons was performed between the no-CL condition and each CL:protein ratio. The Dunnett method was used to correct for multiple comparisons. A cutoff of $p < 0.05$ indicated a statistically significant difference. Five experimental replicates were used for data analysis (n = 5). Data are represented as mean $\pm$ SEM (** $p < 0.005$, * $p < 0.05$).

IQ4 Peptide
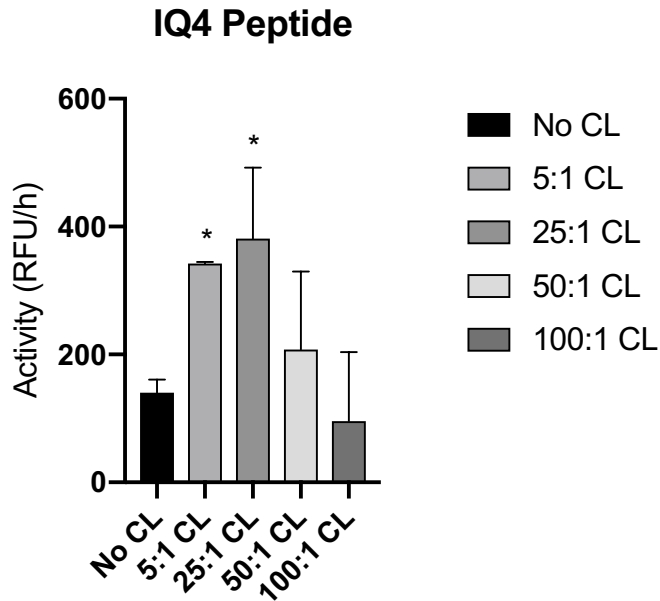
Figure 4.3: Effect of cardiolipin on HsPARΔ77 activity towards internally quenched peptide substrate IQ4. Cleavage of 3 μM IQ4 by 1 μM HsPARLΔ77 in the presence of increasing cardiolipin concentrations was monitored for 3 h. Initial velocity was calculated for each lipid condition and values were plotted using GraphPad Prism software. The concentration of cardiolipin is displayed as a lipid to protein molar ratio. One-way ANOVA with multiple comparisons was performed between the no-CL condition and each CL:protein ratio. The Dunnett method was used to correct for multiple comparisons. A cutoff of $p < 0.05$ indicated a statistically significant difference. Two experimental replicates were used for data analysis (n = 2). Data are represented as mean ± SEM (* $p < 0.05$).

with a 2.7-fold increase in proteolytic activity. Unlike the TM substrate though, we also see an increase in activity at the lower 5:1 CL to PARL molar ratio, with a 2.4-fold increase observed. At cardiolipin concentrations exceeding 25:1 CL to PARL, proteolytic activity of the enzyme begins to decrease back to the no-lipid baseline levels. The 100:1 CL to PARL molar ratio appears to have an inhibitory effect on the activity of the enzyme towards the soluble peptide substrate as the initial velocity measured is below baseline levels. There are large errors in the calculated velocities for the higher concentrations of CL that could be due to the smaller sample size (n=2) in comparison to that for the HsFRET-PINK1 study (n = 5).

4.4 Discussion

Cardiolipin has a significant effect on the activity of HsPARLΔ77 towards the HsFRET-PINK1(70-134)-WT transmembrane substrate and the soluble IQ4 peptide substrate. The results of this assay present the first direct evidence suggesting that lipids may modulate the activity of the mitochondrial rhomboid protease PARL. Cardiolipin was the lipid chosen to be assessed due to its exclusivity to the IMM of eukaryotic cells, the membrane in which PARL is localized, and substantial evidence supporting its role in protein function. The finding that CL can influence the proteolytic activity of PARL is not overly surprising as there is considerable evidence that the activity of rhomboids can be modulated by lipids and that proteins of the IMM are influenced by the presence of CL. It was determined that a 25:1 molar ratio of CL to PARL results in the greatest increase in proteolytic activity compared to the no-lipid condition. We see the effect of this CL condition on enhanced proteolytic activity of HsPARLΔ77 towards both a transmembrane substrate and a soluble peptide substrate. This indicates that CL is facilitating a general enhancement of PARL activity. There are several probable explanations for this observed proteolytic enhancement. The first, and most simple, is that CL may enhance the stability of PARL, thus enhancing its activity. Because we are working with an integral membrane protein that is removed from its native lipid environment, the presence of any lipid species may help to stabilize the protein through non-specific protein-lipid interactions. A

second explanation for the proteolytic enhancement is that CL may bind to a specific site on PARL, thereby inducing subtle conformational changes that facilitate substrate binding or substrate entrance to the active site, again resulting in enhanced activity.

From this assay, we cannot elucidate if CL has a stabilizing effect on PARL, allowing it to retain some activity that it would have when constricted in a lipid bilayer, or if a direct lipid-protein interaction at a specific CL-binding site on PARL results in enhanced activity. Several methods could be utilized to determine the mechanism by which CL exerts its effects on the proteolytic activity of PARL. If CL is merely acting as a stabilizing agent, a simple thermal shift assay performed in the presence or absence of CL could indicate the extent to which CL stabilizes the protein, observed by an increased melting temperature if the protein is more stable. Deciphering if there is a specific CL-binding site on PARL requires significantly more effort. A lipid-binding assay could be performed to validate specific binding between CL and PARL. These assays are based on a premise similar to either a pull-down assay or a Western blot in which we probe for a lipid-protein interaction with our lipid of interest and visualize bound protein by immunoblotting[217]. However, CL is known to bind many proteins, including non-mitochondrial and cytosolic proteins *in vitro*, thus such lipid-binding assays could present false positive results for CL-protein interactions. Ultimately, a high resolution structure of the PARL protease would be the best way to confirm or reject the existence of a specific CL-binding site.

An unexpected and interesting finding of this study was that as the concentration of CL was increased beyond a certain point (in this case, beyond the 25:1 lipid to protein molar ratio), we begin to see the activity of HsPARLΔ77 return to baseline levels. This could be due to the lipid restricting the dynamics of the protein and thus inhibiting its ability to facilitate the cleavage of different substrates. In a bilayer with this excessive numbers of cardiolipin molecules adjacent to the protein, as mimicked by the 100:1 CL to PARL molar ratio in this assay, protein dynamics would be constricted, thus providing an explanation for the reduced proteolytic activity in these conditions. This effect was more evident with the soluble IQ4 substrate than the TM substrate,

perhaps indicating that excess lipid restricts access of the active site to soluble substrates, but not substrates that would access the catalytic core by lateral diffusion in the membrane. Placing these findings in a physiological context, this alteration of PARL activity may imply that PARL resides in compartmentalized regions of the IMM that have a defined amount of CL present. Intramembrane translocation of CL could potentially be a sophisticated mechanism used to modulate the activity of PARL depending on cellular conditions and proteolytic requirements. For example, if decreased PARL activity was required, the concentration of CL in close proximity to the enzyme could be increased or decreased to minimize the activity of the protein.

Other implications of CL-PARL lipid-protein interactions could be in the context of PARL's place in larger protein complexes within the IMM. The recent evidence that PARL may reside within a proteolytic hub consisting of another protease and a scaffold protein within the IMM supports the notion of CL participating in lipid-protein interactions with PARL to facilitate the formation, stability, and organization of such a complex. CL is often seen as an interactor within protein complexes in the IMM, exemplified by its critical role in both stability and function of the respiratory supercomplexes; there are predicted to be 200-400 cardiolipin molecules associated with the respiratory supercomplexes from bovine heart[225]. If PARL activity is modulated by or dependent on its localization to a larger protein complex as recently suggested, there is a high probability that CL is present and promotes the clustering of proteins into this complex, thus positively regulating the stability and function of PARL.

While the mixed micelle reconstitution system used in this assay provides initial evidence of lipids being a modulator of mitochondrial rhomboid activity, these mixed micelles have very little resemblance to the actual membrane environment of the IMM. To assess if the trend observed in the micellar system is relevant to the physiological environment of the IMM, activity of HsPARL could be assessed in a liposome-based reconstitution system. Proteoliposomes are considered a more membrane-mimetic system due to their ability to form a lipid bilayer

structure, have a tailored or defined lipid composition, and present curvature that would occur in a native bilayer. Proteoliposome-based proteolytic assays have been performed with bacterial rhomboids to assess the influence of specific lipids on rhomboid activity indicating that this assay system could be translated for use with the mitochondrial rhomboid PARL. Furthermore, with proteoliposomes we would be able to assess not just the effect of lipids on proteolytic activity, but also membrane curvature. CL promotes negative curvature of membranes which is a feature in localized regions of the IMM such as cristae junctions. If PARL localizes to a region of the IMM characterized by increased negative curvature, it further supports the indication that CL enhances the activity of PARL.

The ability of CL to modulate the activity of PARL may have implications in regards to mitochondrial dysfunction and disease pathogenesis. In the context of Parkinson's disease, it is known that CL levels decline with age and that lipid modulation, such as peroxidation of CL due to oxidative stress, is extensive[226]. These modulations may result in compounding factors that accelerate mitochondrial dysfunction leading to neurodegeneration. If extensive CL peroxidation occurs, its interaction with PARL could be altered and, thus, the proteolytic activity of PARL may be compromised. If PARL cannot maintain optimal activity, it may be unable to cleave substrates such as PINK1 efficiently, leading to the upregulation of mitophagy and an overall imbalance in mitochondrial homeostasis. In addition to upregulated mitophagy, CL peroxidation could lead to impairments in oxidative phosphorylation as CL would be unable to stabilize or enhance activity of the respiratory complexes, further contributing to mitochondrial dysfunction. A recent study implicated both PINK1 and CL in the optimal function of complex I[216]. PINK1-mediated phosphorylation of a subunit of complex I is required for efficient electron transport between complex I and ubiquinone[130]. In a PINK1-deficient scenario, electron transfer was impaired, however upon increased CL synthesis, efficient transfer was restored[216]. Comparison of the PINK1-deficient scenario with a situation in which PARL-mediated processing of PINK1 is altered could be paralleled, with CL enhancing both proteolytic activity of PARL and electron transfer at complex I. This study provided a new link

between lipid homeostasis and mitochondrial homeostasis that could potentially be exploited as a therapeutic target for neurodegenerative disorders. While there is mounting evidence that lipids or lipid-modulating proteins can be good therapeutic targets, studies performed with bacterial rhomboid proteases emphasize the importance of understanding protein-lipid interactions before therapeutic design begins. It was discovered that several non-steroidal anti-inflammatory drugs can alter membrane characteristics which then induced non-specific cleavage by rhomboid proteases[200]. These off-target effects of a potential therapeutic could unnecessarily contribute to disease pathogenesis in ways not realized if the full interactome of a drug target is not well characterized.

The study presented in this thesis focused on observing the effect of the lipid CL on the proteolytic activity of HsPARLΔ77 towards two different substrates. This study provides direct evidence to support the notion that the lipid environment in which the PARL protease resides in within the IMM does indeed have a modulating effect on its activity. While we cannot confirm or deny the existence of specific lipid-protein binding sites or even a specific interaction between CL and PARL, these results do suggest that aspects of the IMM lipid environment are able to modulate the activity of HsPARL. The findings illustrated here and the current knowledge in the field regarding mitochondrial protein interactions with CL present interesting new avenues of research that will enhance our understanding of mechanisms of regulation of the mitochondrial rhomboid protease PARL and its links to disease pathogenesis.

Parkinson's disease is the second most common neurodegenerative disorder. Most commonly presented in the sporadic form, mutations in several genes have been implicated in inherited forms of the disease and this has sparked new avenues of research into determining the molecular etiology of PD. One of these genes is located within the *PARK6* locus, encoding for the PINK1 protein; PARK6 parkinsonism is the second most common autosomal recessive form of the disease[149]. As stated in the introduction chapter, PINK1 is a key protein in the mitophagy pathway and acts as a sensor of mitochondrial health. The identification of PD-associated mutations in PINK1 adds to a growing body of evidence that highlights mitochondrial dysfunction as an underlying cause of PD.

PD-associated mutations in PINK1 have been identified throughout the span of the entire protein and result in an early-onset form of the disease that is otherwise indistinguishable from the sporadic form of PD (Figure 5.1). The majority of the identified mutations in PINK1 reside in the large kinase domain that spans residues 156-511, with many causing an alteration or impairment of PINK1's kinase functionality[227]. Based on substrates of PINK1 that are currently known, an impairment of PINK1 kinase activity could have a detrimental impact on several mitochondrial processes. Studies performed with loss-of-function PINK1 variants observe altered complex I function, due to an inability to maintain phosphorylation of the NdufA10 subunit, thus resulting in weakened mitochondrial bioenergetics and decreased mitochondrial membrane potential[130]. Loss of PINK1 kinase function also results in impaired mitophagy initiation as ubiquitin and Parkin cannot be efficiently phosphorylated. Together, these two factors would lead to a state of increased numbers of damaged mitochondria that cannot be efficiently removed from the cell, prompting cell death mechanisms such as apoptosis.

Several PINK1 mutations implicated in the autosomal recessive early-onset phenotype, however, are not located within the kinase domain, and thus must have a different role in PD
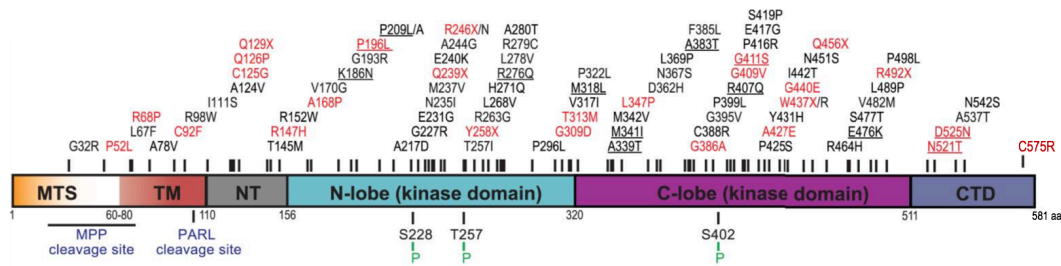
Figure 5.1: PINK1 domain schematic highlighting PD-associated mutations. Domain representation of PINK1 with locations of PD-associated mutations identified in the PD Mutation Database (http://www.molgen.vib-ua.be/PDMutDB/). Mutations highlighted in red have been experimentally verified as loss-of-function mutations and are classified as pathogenic, while mutations highlighted in black have an uncharacterized functional defect. Mutations that are underlined are considered common, with an allele frequency greater than 1:10 000. We will be assessing cleavage of PD-variants R98W and I111S which are currently uncharacterized in terms of their pathogenicity, as well as C92F and Q126P which are considered pathogenic. The four mutations we will assess are heterozygous mutations, with PINK1-C92F being a compound heterozygous mutation presenting with R464H. Domain structure of PINK1: mitochondrial targeting sequence (MTS, residues 1 to approximately 80), transmembrane region (TM, speculated to be residues 90-110), N-terminal regulatory region (NT, residues 111-156), N-lobe of the kinase domain (residues 157-320), C-lobe of the kinase domain (residues 321-511), and C-terminal domain (CTD, residues 512-581)[163]. From Truban, D., *et al*. (2017). PINK1, Parkin, and Mitochondrial Quality Control: What can we Learn about Parkinson's Disease Pathobiology? *J Parkinsons D 7*, 13-29.

pathogenesis than altering kinase function. There are several mutations that lie within or near the TM region of PINK1, placing them in close proximity to the proposed PARL cleavage site at Ala103 (Figures 5.1 and 5.2). Mutations within the TM region include C92F, R98W, and I111S. The C92F mutation was identified in the genetic analysis of a 60 year old woman as a heterozygous compound mutation with R464H; she presented disease symptoms at 37 years of age with a resting tremor of the upper right limb[228]. There are conflicting results from cellular studies analyzing the C92F mutation; in SH-SY5Y whole cell lysates, an accumulation of full-length PINK1-C92F was observed in comparison to PINK1-WT, while in whole cell lysates derived from HeLa cells transfected with PINK1-YFP mutants, there is no apparent difference between the turnover of PINK1-C92F and PINK1-WT[67,73]. Unfortunately, neither study looked at the localization of the PINK1-C92F mutant so it is not clear if the accumulation seen in the SH-SY5Y cells is due an altered subcellular localization or impaired processing within the mitochondria.

The R98W and I111S mutations were identified through retrospective genetic analysis of over 1100 sporadic and familial cases of PD[229]. One study demonstrated significantly altered processing of PINK1 when a Phe was introduced at residue 98 (PINK1-R98F), however they did not examine the R98W PD-variant[73]. This result suggested that mutations within the TM region of PINK1 could lead to impaired processing and perhaps dysfunctional mitophagy, resulting in the PD phenotype; this study, however, does not confirm a cleavage defect. More recent cellular studies have looked at the R98W and I111S PD mutations, first looking at impairment in PARL-mediated cleavage and subsequently in the context of Parkin recruitment and mitophagy initiation[64,78]. In inducible stable cells lines expressing the PINK1-R98W mutation, a very clear altered processing pattern is observed in comparison to PINK1-WT-expressing cells[64]. Altered processing of PINK1-R98W is also observed when cells are treated with CCCP, indicating that proteases within the OMM could be cleaving this variant as CCCP disrupts the electrochemical gradient, and inhibits the import of PINK1 to the IMM; PINK1-WT appears as a single band at 66 kDa when CCCP is present[78].The final PD-associated variant
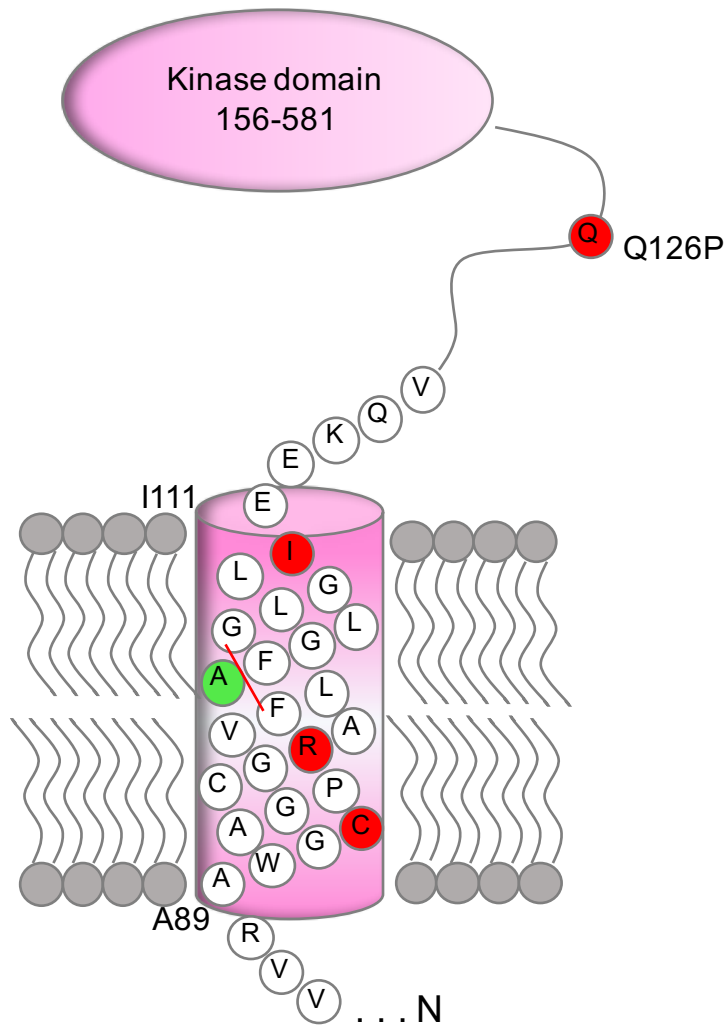
Figure 5.2: Topological diagram of the PINK1 transmembrane domain. Topological representation of the PINK1 transmembrane region. Highlighted in green is Ala103, where PINK1 is proposed to be cleaved by PARL. Highlighted in red are the PD-associated variants of PINK1. Mutations within the TM region include C92F, R98W, and I111S. We will also look at the Q126P mutation located in the juxtamembrane region of PINK1.

that harbours a mutation within the TM region is I111S. This mutation was also looked at in the study with PINK1-R98W; the authors state that PINK1-I111S blocks PARL-mediated cleavage, though analysis shows only a mild cleavage defect when compared to PINK1-WT[64]. Furthermore, the authors conclude that PINK1-I111S has impaired retrotranslocation and release to the cytosol as there was no recruitment of Parkin to mitochondria when cells were cotransfected with catalytically inactive PARL, though PINK1-WT also demonstrated this so it is not clear how the conclusion was reached[78]. These PD-linked mutations have not been further characterized and thus it remains difficult to conclude that a processing defect may play a role in PD pathogenesis.

To provide further support to the possibility of aberrant PARL-mediated cleavage towards the PD-associated variants of PINK1 that contain a mutation within the TM region, there have been cellular studies performed on other PINK1 TMD mutations. These TM mutations have not been identified in PD patients, but they provide additional evidence of PINK1 processing alteration as a factor in mitochondrial dysfunction. Studies on SH-SY5Y whole cell lysates expressing PINK1-P95A demonstrate an accumulation of full-length PINK1 in comparison to PINK1-WT, suggesting impaired processing when this TM mutation is present. Expression of PINK1 carrying this mutation also results in an increase in ROS production, decreased mitochondrial membrane potential, and an overall decrease in mitochondrial mass which are all indications of mitochondrial dysfunction[67]. Proline residues are considered helix-breaking and may play a role in substrate recognition by rhomboids. Helix-breaking or helix-destabilizing residues are suggested to be a requirement for efficient cleavage by rhomboids as they facilitate the helix unwinding needed for cleavage to occur; in the rigid α-helical conformation, it is unlikely that cleavage would occur as the cleavage site would be shielded from the catalytic residues by the hydrogen bonding that stabilizes the helix[105]. With the PINK1-P95A mutation, helix unwinding is disfavoured, thus impairing cleavage. Studies on HEK293 whole cell lysates expressing PINK1-G107L or PINK1-G109L also demonstrate impaired cleavage as seen by an increase in full-length PINK1 compared to PINK1-WT; these mutations are also considered

helix-stabilizing and thus disfavourable for rhomboid-mediated cleavage[64]. Expression of the PINK1-G109L mutation also resulted in enhanced Parkin recruitment and autophagosome formation, indicating that this mutation can induce mitophagy without mitochondrial depolarization which may be due to its impaired processing[78]. These two studies indicate that mutations within the TM region of PINK1 are likely to cause impaired processing by PARL and that this can lead to mitochondrial dysfunction, thus providing support to the possibility of aberrant PARL-mediated cleavage towards the PD-associated variants.

It is speculated that there are two main aspects of the PINK1-PARL interaction that may be altered by the mutations within the PINK1 TM region. These mutations may disrupt the localization of PINK1 to the IMM, thus preventing PARL from having access to PINK1 in the first place, or they may directly impair PARL-mediated cleavage of PINK1 either by preventing substrate recognition or by inhibiting cleavage. Both of these scenarios could be due to changes in the secondary structure of the PINK1 TM region that arise from these mutations. If PARL-mediated cleavage of PINK1 is impaired, PINK1 will accumulate on all mitochondria, including what are otherwise healthy mitochondria. This will result in increased mitophagy of the entire mitochondrial pool, and if all mitochondria are being targeted for degradation, the cell will no longer be able to support its energy demands and thus cell death mechanisms will be triggered. This dysregulation of mitophagy resulting from impaired PARL-mediated cleavage of PINK1 may be a contributing factor to the PD pathogenesis associated with PINK1 PD-associated TM variants.

5.2 Objective

Cellular studies have demonstrated altered processing of PINK1 when a mutation is present in the TMD. We propose that the PD pathophysiology associated with PINK1 PD variants that contain a mutation within or near the TMD of PINK1 may be due to two scenarios that could contribute to a dysregulation of mitophagy and overall mitochondrial dysfunction (Figure 5.3).

The first possible scenario is that PD-associated variants of PINK1 are no longer able to be translocated through the TOM and TIM complexes, thus not being integrated into the IMM and not meeting the PARL protease. This would result in an accumulation of PINK1 on the OMM because the protein is not being turned over and released to the cytosol, thus initiating mitophagy. The second potential scenario is that the PINK1 PD-associated variants localize correctly to the IMM, however these mutations cause an impairment in PARL-mediated cleavage or an inability of PARL to recognize PINK1 as a substrate. With PARL not being able to recognize or cleave PINK1, this would again result in an accumulation of the PINK1 kinase domain on the surface of the mitochondria and the initiation of mitophagy. In either scenario, the cleavage of PINK1 is impaired. Thus, the rapid turnover of PINK1 required to signal that the mitochondrial pool is healthy is compromised, resulting in an upregulation of mitophagy.

Given that all studies to date on the processing of PINK1 TMD PD variants have been conducted using whole cell or mitochondrial lysates which contain a wide variety of proteases, we aim to assess the direct cleavage of PINK1 PD-associated variants using recombinantly expressed and purified HsFRET-PINK1, as well as small synthesized IQ peptides to determine if PARL-mediated cleavage is altered by the presence of TM mutations in PINK1. We hypothesize that the TMD PD-associated variants of PINK1 – C92F, R98W, and I111S – will have altered PARL-mediated cleavage when compared to the cleavage of wtPINK. We hypothesize that the mutation PINK1-Q126P, which lies in the juxtamembrane region, will be cleaved in a manner comparable to PINK1-WT, as this residue lies far enough from the cleavage site that it should not interfere with processing.
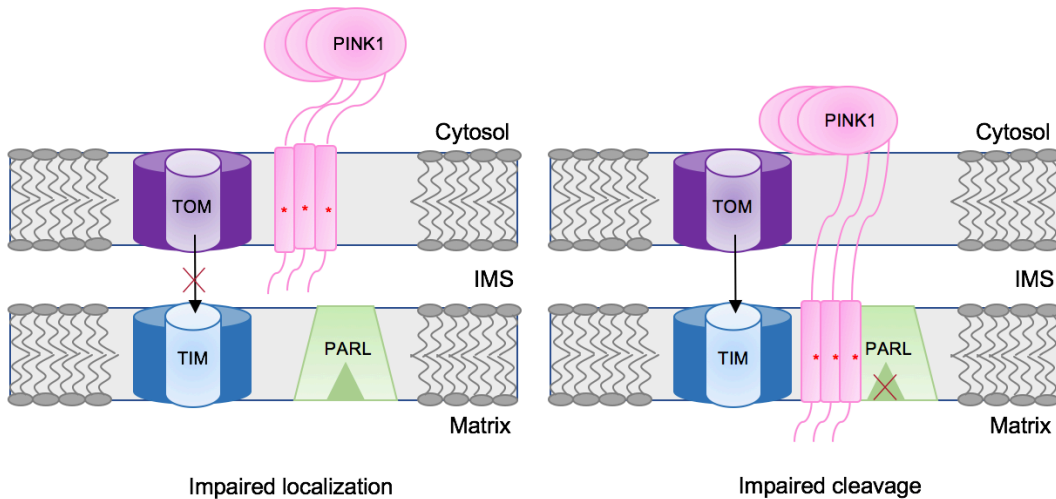
Figure 5.3: Proposed models for pathology of PINK1 TM PD-associated variants. In healthy mitochondria, PINK1 is translocated to the IMM where it meets PARL and is rapidly turned over. In damaged mitochondria, PINK1 accumulates on the OMM and recruits Parkin to initiate mitophagy (see Figure 1.8). We propose that the pathology of PINK1 PD-associated variants that harbour a mutation within the TM region is due to one of two possible scenarios that lead to a dysregulation of mitophagy. In the first model (left panel), PINK1 variants are unable to be translocated to the IMM and therefore do not meet PARL. In this scenario, PINK1 will accumulate on the OMM whereby mitophagy will be initiated by the recruitment of Parkin. The second model (right panel) occurs upon a PARL-mediated cleavage impairment. These PINK1 variants are able to localize correctly to the IMM, however PARL is unable to recognize or cleave PINK1. The kinase domain of PINK1 will then accumulate on the OMM and again Parkin will be recruited and mitophagy initiated. In either scenario, the rapid turnover of PINK1 required to signal that mitochondria are healthy is impaired and therefore otherwise healthy mitochondria will be subject to mitophagy.

5.3.1 HsFRET-PINK1(70-134) substrates

HsPARLΔ77 was used to analyze all FRET-PINK1 PD-associated variants as it was observed that this truncation of HsPARL had a significantly higher turnover of and catalytic efficiency towards the IQ-PINK1 substrate compared to HsPARLΔ55 (see Figure 3.6).

HsPARLΔ77 was able to cleave all PD-associated variants of PINK1, however, there are notable differences in the catalytic parameters obtained for the variants compared to that of PINK1-WT. Michaelis-Menten kinetic curves obtained for the cleavage of each variant are found below (Figure 5.4). The catalytic parameters obtained from the Michaelis-Menten analysis are summarized in Table 5.1 and a graphical representation of these values is shown in Figure 5.5. No significant difference in K_M is observed for the FRET-PINK1 substrates; the K_M for WT, C92F, and I111S are all roughly 3 µM. The K_M of the FRET-PINK1-Q126P variant does appear slightly decreased, being only 0.7 ± 0.5 µM, however this difference was not determined to be statistically significant, likely due to the large error associated with the K_M value for the Q126P substrate. The three PD-associated variants of PINK1 have a significantly decreased turnover rate compared to the WT construct. This indicates that PARL is not able to cleave these PD-associated variants as quickly as it can PINK1-WT; all PD-associated variants have approximately a 7-fold decrease in turnover rate. All PD-associated variants are turned over very slowly, with less than 0.1 of a single substrate molecule being processed per hour. Because we are using a fluorescence-based assay to observe proteolytic activity, it is very sensitive to even these extremely minor changes in substrate decrease and product production. Looking at the catalytic efficiency of PARL toward the PD-associated variants, we see that efficiency is decreased towards the three variants, however this decrease was not determined to be statistically significant in any of the cases. This lack of significance, can once again likely be attributed to the large errors associated with the K_M values that are skewing the
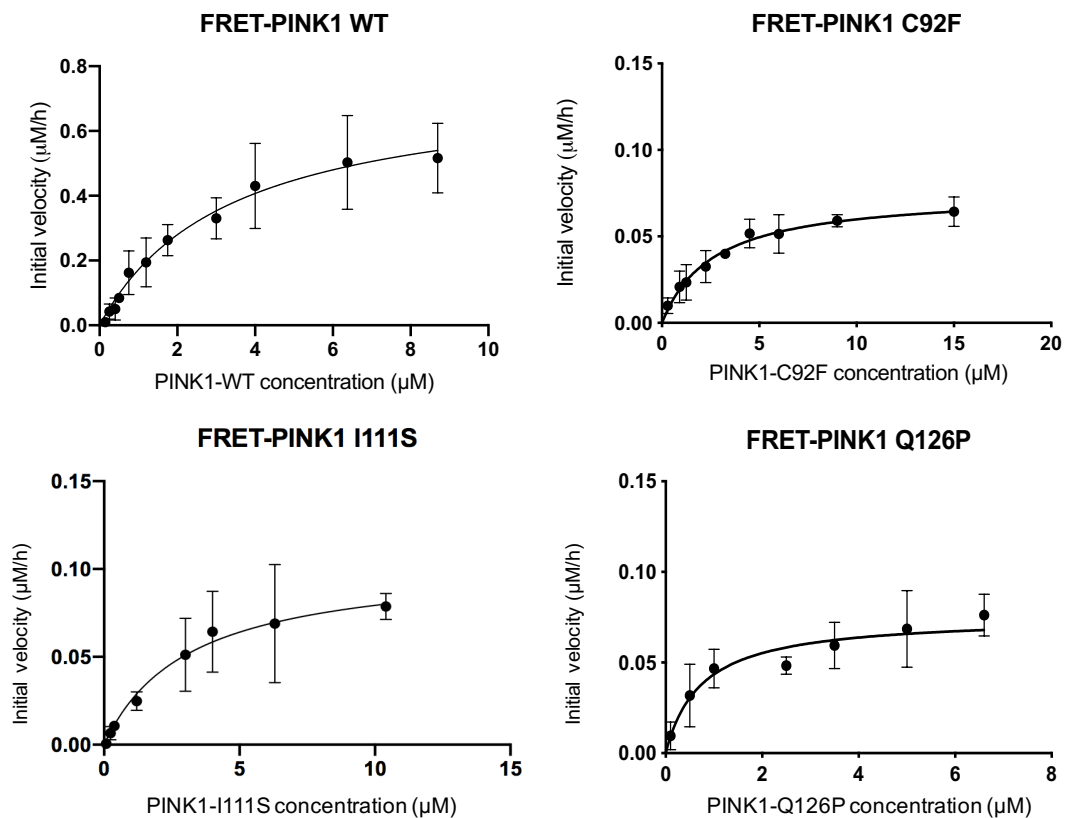
Figure 5.4: Michaelis-Menten kinetic curves for cleavage of HsFRET-PINK1(70-134) substrates by HsPARLΔ77. Initial velocity values obtained were plotted for each concentration of HsFRET-PINK1(70-134) tested. Curves were fit to the Michaelis-Menten equation using GraphPad Prism software and the catalytic parameters K_M and V_{max} were obtained. For cleavage of HsFRET-PINK1(70-134)-WT, n = 4, for C92F n = 3, for I111S n = 3, and for Q126P n = 3. Data are represented as mean ± SEM.

Table 5.1: Catalytic parameters for cleavage of HsFRET-PINK1(70-134) PD-associated variants by HsPARLΔ77. Data are represented as mean ± SEM. PINK1 accumulation was determined by quantifying the ratio of PINK1 localizing in and out of mitochondria in HeLa cells; a ratio > 1 indicated mitochondrial accumulation. Accumulation data was gathered by graduate student Raelynn Brassard and Dr. Nicolas Touret.

	K_M (µM)	k_{cat} (h^{-1})	k_{cat}/K_M ($µM^{-1} h^{-1}$)	Accumulation
WT (n= 4)	3 ± 1	0.46 ± 0.09	0.16 ± 0.09	No
C92F (n = 3)	3 ± 1	0.06 ± 0.01	0.02 ± 0.01	No
I111S (n = 3)	3.1 ± 1.5	0.08 ± 0.02	0.03 ± 0.02	No
R98W	---	---	---	Yes
Q126P (n = 3)	0.7 ± 0.5	0.06 ± 0.01	0.08 ± 0.07	No
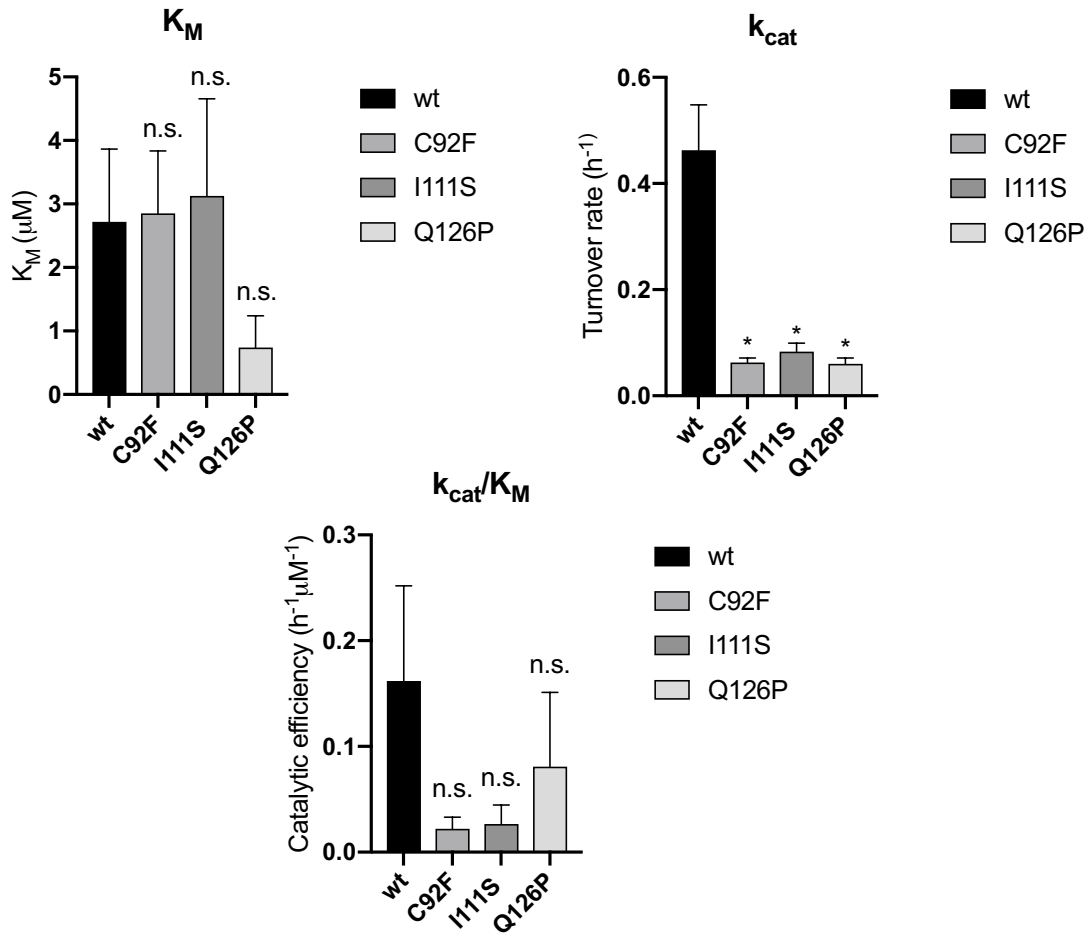
Figure 5.5: Catalytic parameters obtained for cleavage of FRET-PINK1(70-134) substrates by HsPARLΔ77. The catalytic parameters K_M (µM), k_{cat} (h^{-1}), and k_{cat}/K_M ($h^{-1}µM^{-1}$) were obtained from Michaelis-Menten analysis of the kinetic curves obtained for cleavage of each HsFRET-PINK1(70-134) substrate (Figure 5.4). One-way ANOVA with multiple comparisons was performed between WT and each PD variant. The Dunnett method was used to correct for multiple comparisons. A cutoff of $p < 0.05$ indicated a statistically significant difference. Data are represented as mean ± SEM (* $p < 0.05$, n.s. denotes no significance).

statistical analysis of the k_{cat}/K_M parameter. Taken together, these results suggest that PARL-mediated cleavage of the PINK1 PD-associated variants PINK1-C92F, -I111S, and –Q126P is impaired to some extent.

5.3.2 IQ-PINK1(97-107)-WT and IQ-PINK1(97-107)-R98W

Due to an inability to produce recombinant HsFRET-PINK1-R98W of sufficient yield or purity, a small fluorogenic peptide harbouring the R98W PD mutation was synthesized and used for cleavage analysis. An IQ-PINK1(97-107)-WT peptide was also synthesized to serve as the control. These IQ-PINK1(97-107) peptides are similar to the IQ peptides analyzed in Chapter 3, as they also employ the EDANS/DABCYL fluorophore/quencher FRET-pair. To increase the solubility of these peptides, they are flanked by Arg residues at the N- and C-termini (see Table 2.7). To validate the use of this peptide substrate, catalytic parameters for cleavage of the IQ-PINK1(97-107)-WT peptide by HsPARLΔ77 were compared to the parameters obtained for HsFRET-PINK1(70-134)-WT (Figure 5.6). No significant difference was seen between the K_M and k_{cat}/K_M parameters for the PINK1-WT substrates. The turnover rate of the IQ peptide, however, was significantly lower than that of the HsFRET-PINK1(70-134) substrate. As the catalytic parameters obtained for cleavage of HsFRET-PINK1(70-134)-WT and IQ-PINK1(97-107)-WT were similar or showed no significant difference, this indicated that results obtained from cleavage analysis of the mutant peptide, IQ-PINK1(97-107)-R98W, could be used with confidence.

Michaelis-Menten kinetic curves for the cleavage of IQ-PINK1(97-107)-WT and IQ-PINK1(97-107)-R98W by HsPARLΔ77 are shown in Figure 5.7. The catalytic parameters obtained from the Michaelis-Menten analysis are summarized in Table 5.2 and displayed in a graphical representation in Figure 5.8. Cleavage of the IQ-PINK1(97-107)-R98W peptide results in significantly increased K_M and k_{cat} values compared to those obtained for the cleavage of the IQ-PINK1(97-107)-WT peptide. There is a 2.9-fold increase in the K_M for cleavage of the R98W
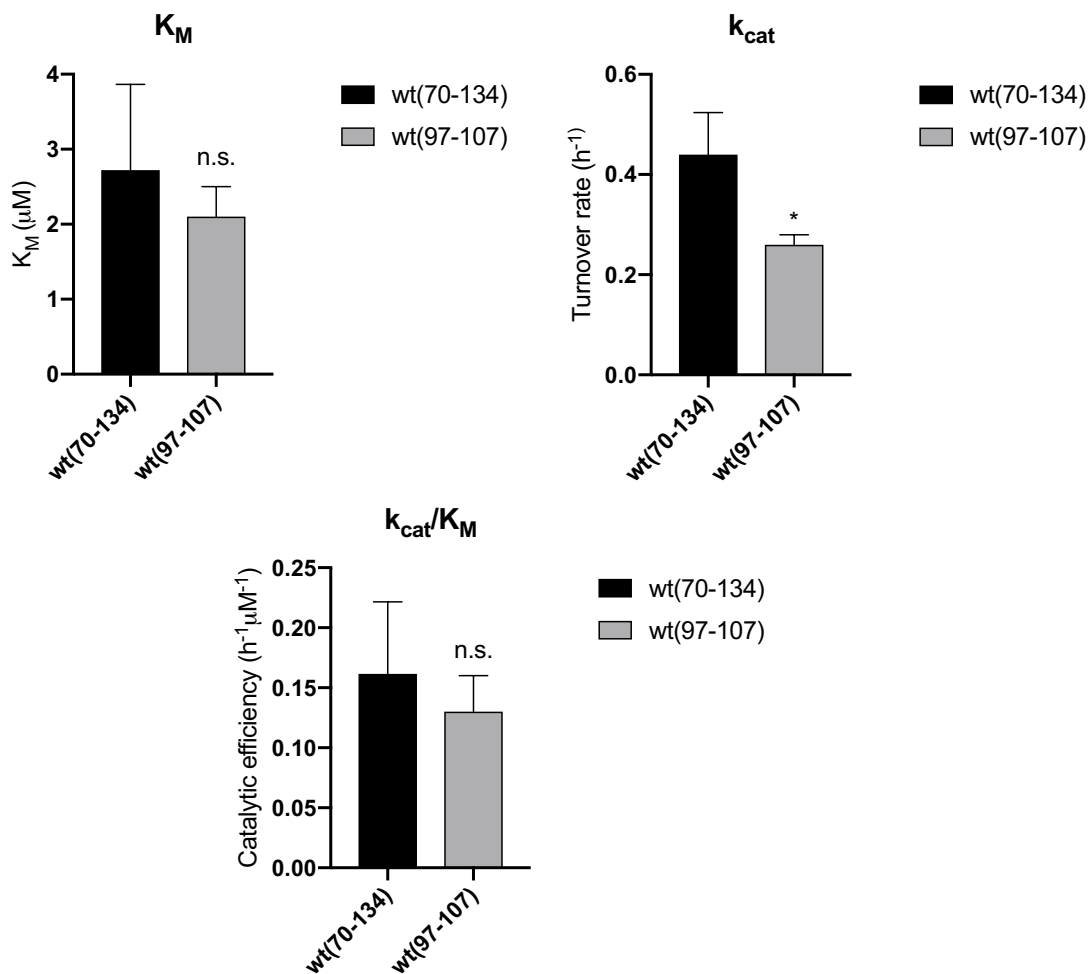
Figure 5.6: Validation of the IQ-PINK1(97-107) peptide for kinetic analysis of PD-mutation PINK1-R98W. Catalytic parameters for the HsFRET-PINK1(70-134)-WT and IQ-PINK1(97-107)-WT substrates were compared to validate the use of the IQ-PINK1(97-107) substrate for analysis of the PINK1-R98W PD-associated mutation as FRET-PINK1-R98W was unable to be recombinantly expressed and purified to sufficient quality for analysis. Unpaired t-tests with a $p < 0.05$ cutoff were performed to determine significant differences. Data are represented as mean $\pm$ SEM (* $p < 0.05$, n.s. denotes no significance).

IQ-PINK1(97-107)-WT
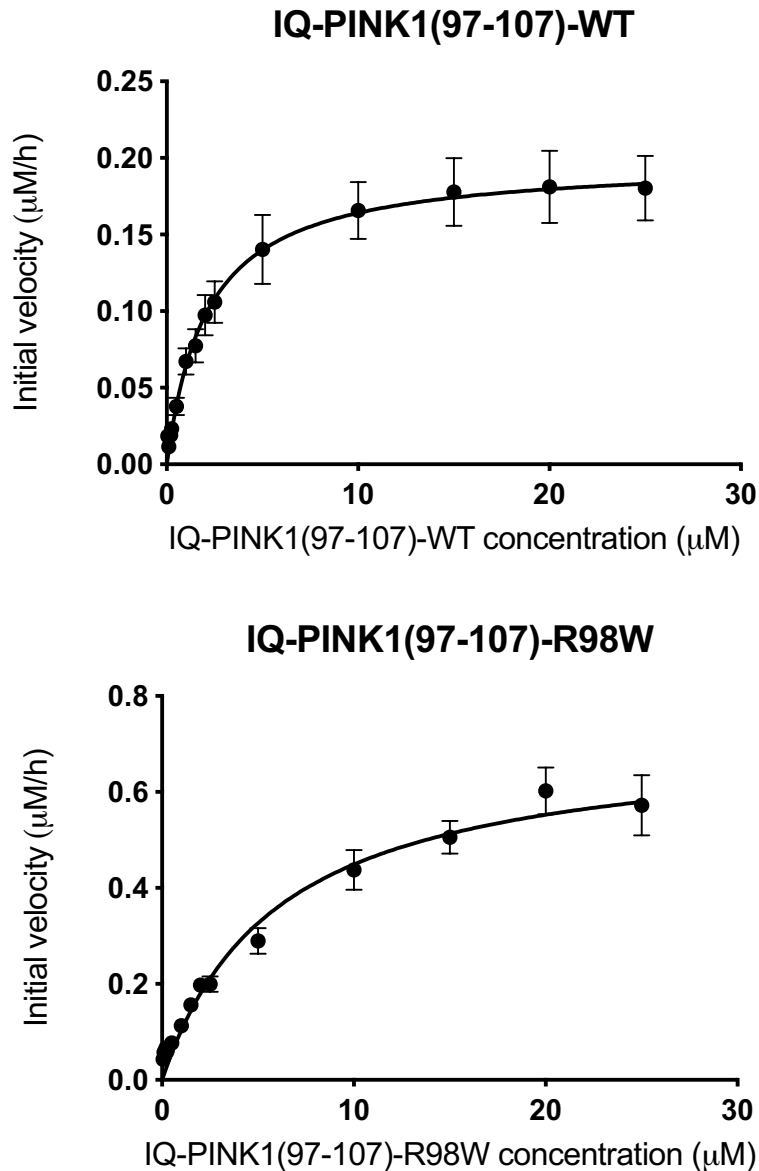
IQ-PINK1(97-107)-R98W

Figure 5.7: Michaelis-Menten kinetic curves for cleavage of IQ-PINK1(97-107)-WT and IQ-PINK1(97-107)-R98W by HsPARLΔ77. Initial velocity values obtained were plotted for each concentration of IQ-PINK1(97-107) tested. Curves were fit to the Michaelis-Menten equation using GraphPad Prism software and the catalytic parameters K_M and V_{max} were obtained. For cleavage of IQ-PINK1(97-107)-WT, n = 10, while for cleavage of IQ-PINK1(97-107)-R98W, n = 8. Data are represented as mean $\pm$ SEM.

Table 5.2: Catalytic parameters for cleavage of IQ-PINK1(97-107)-WT and IQ-PINK1(97-107) -R98Wby PARLΔ77. Data are represented as mean ± SEM.

	K_M (µM)	k_{cat} (h^{-1})	k_{cat}/K_M ($\mu M^{-1} h^{-1}$)
IQ-PINK1(97-107)-WT n = 10	2.1 ± 0.4	0.26 ± 0.02	0.13 ± 0.03
IQ-PINK1(97-107)-R98W n = 8	6.0 ± 0.9	0.96 ± 0.05	0.16 ± 0.03
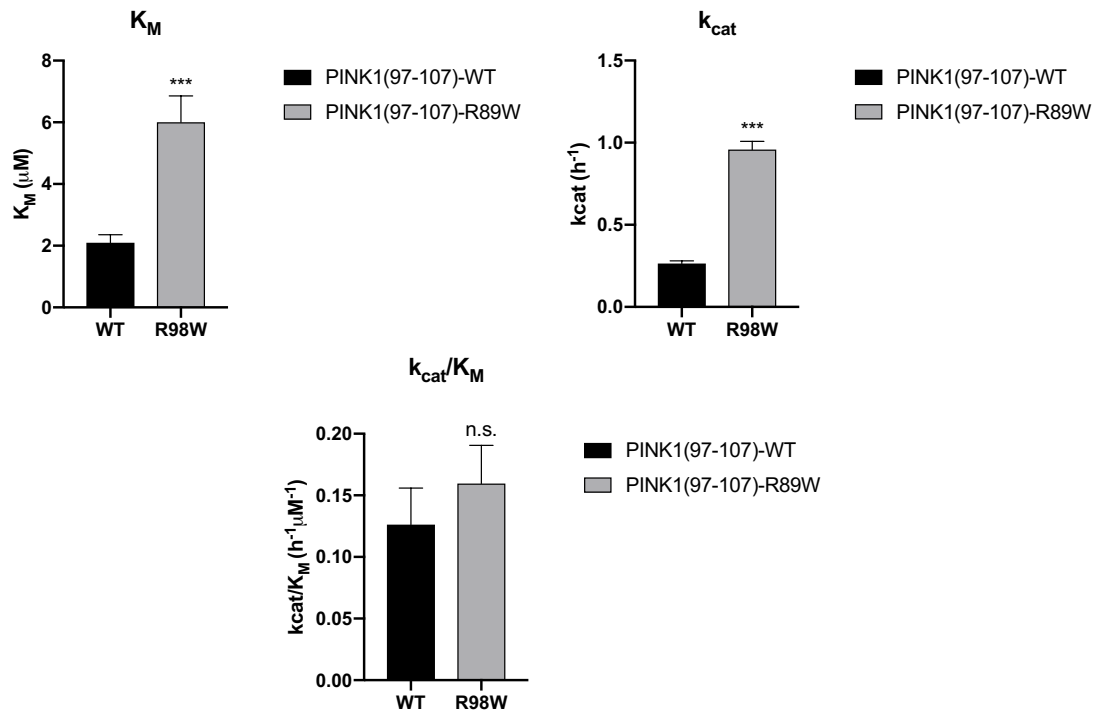
Figure 5.8: Catalytic parameters obtained for cleavage of IQ-PINK1(97-107)-WT and IQ-PINK1(97-107)-R98W by HsPARLΔ77. The catalytic parameters K_M (μM), k_{cat} (h^{-1}), and k_{cat}/K_M ($h^{-1}μM^{-1}$) were obtained from Michaelis-Menten analysis of the kinetic curves obtained for cleavage of each internally quenched peptide substrate (Figure 5.7) by HsPARLΔ77. Unpaired t-tests were performed with a cutoff of $p < 0.05$ to indicate a statistically significant difference. Data are represented as mean ± SEM (*** $p < 0.0005$, n.s. denotes no significance).

peptide compared to the WT peptide. The K_M for IQ-PINK1(97-107)-R98W is 6.0 ± 0.9 μM, while the K_M for IQ-PINK1(97-107)-WT is only 2.1 ± 0.4 μM. This indicates that the affinity of HsPARLΔ77 for the substrate is significantly reduced when this R98W mutation is present; a higher K_M value tells us that more substrate is required for the enzyme to reach half-maximal activity. For the k_{cat}, we also see a 3.6-fold increase for the R98W peptide compared to WT, indicating a more rapid turnover of the R98W variant by HsPARLΔ77. No significant difference is observed for the k_{cat}/K_M, as a comparable increase in both the K_M and k_{cat} values for the R98W peptide negate there being a shift in enzymatic efficiency. In the context of the other PD-associated variants, the R98W mutation appears to be the only mutation that results in a significantly increased turnover rate. This suggests that while all other PD-associated variants have a cleavage impairment, the cleavage of the R98W variant is actually enhanced and does not display a cleavage defect.

5.4 Discussion

PD-associated variants of PINK1 that harbour a mutation within the TM region display altered processing by HsPARLΔ77 when compared to the processing of PINK1-WT. This chapter presents the first direct evidence of PARL-mediated cleavage impairment or alteration towards PD-associated variants of PINK1. Cellular studies have provided initial evidence suggesting that impaired PINK1 processing due to mutations within the TM region can lead to mitochondrial dysfunction[67,78]. In the context of mitochondrial dysfunction in Parkinson's disease, we analyzed four PD-associated mutations found either in the PINK1 TM or juxtamembrane regions (Figure 5.2). PINK1-C92F, -I111S, and -Q126P were analyzed using the HsFRET-PINK1(70-134) construct while the PINK1-R98W variant was analyzed by using the IQ-PINK1(97-107) peptide. Catalytic parameters obtained for the cleavage of Hs-FRET-PINK1(70-134)-WT and IQ-PINK1(97-107)-WT by HsPARLΔ77 were comparable, indicating that we could be confident in the results gathered from kinetic analysis of either the FRET or IQ substrates. We hypothesized that the mutations found within the PINK1 TM region would alter PARL-mediated cleavage due to their proximity to the cleavage site at Ala103, while the

juxtamembrane region mutant, Q126P, would be cleaved in a manner comparable to PINK1-WT as this mutation is located quite distant from Ala103.

All PINK1 variants analyzed using the HsFRET-PINK1(70-134) substrate display a cleavage defect as revealed by the significantly decreased turnover rate for each of the variants compared to WT. We observe an approximate 7-fold decrease in the turnover rate of HsFRET-PINK1(70-134)-C92F, I111S, and Q126P compared to the turnover rate of HsFRET-PINK1(70-134)-WT by HsPARLΔ77. Rationalizations for the decreased turnover include alterations of secondary structure characteristics that impede PARL-mediated cleavage. As has been previously stated, rhomboid protease substrates typically have helix-destabilizing features that facilitate the unwinding of the TM substrate, therefore allowing access of the catalytic residues to the cleavage site[105]. The C92F mutation would enhance PINK1 TM helix stability as the large aromatic Phe residue is considered helix-stabilizing compared to the Cys residue in the native protein[230]. With a stabilized α-helical TM region, cleavage at Ala103 is impaired as helix unwinding becomes disfavourable. The I111S mutation may result in additional hydrogen-bonding due to the introduction of a Ser residue, altering the stability of this region of the protein and disfavouring helix unwinding to facilitate cleavage. The reasoning for the cleavage defect seen with the Q126P mutation is less clear as this mutation occurs in the juxtamembrane region over twenty residues away from the cleavage site and would likely not result in structural perturbations in the TM region around the cleavage site. Proline is considered a helix-breaking residue and most commonly introduces a kink to helical segments of a protein. It may be that when this mutation is introduced in our construct, a kink in the linker region between the PINK1 TM and the YPet fluorophore is produced. This kink could cause the spatial localization of the YPet fluorophore to be altered, and potentially restrict access of PARL to the cleavage site. Translating this speculation to the full-length PINK1 protein, this Q126P mutation could result in the kinase domain of PINK1 being restricted in a spatial localization closer to the PINK1 TM region which could impair either translocation of the protein through the TOM and TIM complexes or the insertion of the protein into the IMM. The

significant decrease in turnover observed for HsFRET-PINK1(70-134)-C92F, -I111S, and -Q126P can be rationalized by structural changes in the protein that alter helical stability of the TM region or spatial rearrangement of the protein domains, with either being disfavourable for cleavage mediated by HsPARLΔ77.

The k_{cat}/K_M was also decreased for each of the PD-associated variants assesses using the HsFRET-PINK1(70-134) construct compared to WT, however, these differences in catalytic efficiency were not determined to be statistically significant. This is most likely due to large standard errors associated with the values calculated for each catalytic parameter. There are several explanations for why such large errors may be associated with the catalytic parameters obtained for cleavage of the HsFRET-PINK1(70-134) substrates. Because we are working with a recombinant enzyme and a recombinant substrate, in which both are membrane proteins, this is a relatively complicated assay system. As membrane proteins are challenging to express and purify, the homogeneity of the purified proteins being used for the assay is likely to vary between each protein preparation. From the purification gels for HsPARLΔ77 and HsFRET-PINK1(70-134) (Figure 2.3 and 2.5), we can clearly see that there are other proteins that co-purify with our proteins of interest. For FRET-PINK1, these co-purifying proteins may be interacting with the TM region in such a way that the cleavage site becomes occluded in some cases. It is proposed that the proteins that co-purify with FRET-PINK1 are chaperones that assist in the proper folding of the protein; in cellular studies, PINK1 has been associated with the mitochondrial chaperone HSP90 so it is highly probable that it would be interacting with bacterial chaperones when recombinantly expressed in *E. coli*[149]. The purification of recombinant HsFRET-PINK1(70-134) required extensive optimization to produce protein of sufficient purity, indicating that residues 70-134 of PINK1, due to their strong hydrophobic nature, likely enable non-specific protein-protein interactions.

Aside from co-purifying proteins potentially increasing the variability, and thus error, in the catalytic parameters obtained for FRET-PINK1 substrates, the introduction of these mutations

may also cause structural changes in the protein that increase protein aggregation. If the substrate is aggregating, only a fraction of the substrate will be available for cleavage, again introducing excess variability between each assay performed. Previous analysis of these PD-associated mutations using AGGRESCAN, an algorithm that predicts a protein's propensity to aggregate based on its sequence, demonstrated that PINK1 has an intrinsic propensity to self-associate and that these mutations enhance this, supporting the notion that substrate aggregation may contribute to variability in assay outcomes[231]. However, we assessed PINK1 peptides by electron microscopy, in collaboration with Dr. Howard Young, and did not see any aggregation or fibril formation with the PINK1 TM domain. The final, and more likely factor that may contribute to the high variability and error obtained for the catalytic parameters associated with cleavage of HsFRET-PINK1(70-134) substrates is the use of the CyPet-YPet FRET-pair. These bulky fluorophores may be non-specifically interacting with the PINK1 region they flank, again resulting in occlusion of the cleavage site and contributing to the large variability in catalytic parameters obtained that contribute to the standard error of the values.

These first analyses of HsPARL activity allow us to reveal shortcomings of different assay systems used to measure proteolytic activity. Given the variability observed with the HsFRET-PINK1(70-134) construct, the IQ peptides appear to be the preferred way to assess if mutations impair PARL-mediated cleavage. Cleavage of the WT IQ peptide, IQ-PINK1(97-107)-WT, is comparable to cleavage of the longer WT FRET substrate, indicating that HsPARLΔ77 is likely recognizing and cleaving these substrates in a similar manner. The peptide substrate may also be favourable as very small standard errors are associated with the catalytic parameter values obtained, indicating that these substrates provide results that are more reproducible than those obtained for cleavage of the FRET-PINK1 substrates.

In our assessment of the cleavage of the R98W PD-associated mutation using an IQ peptide, it is interesting that we actually see enhanced cleavage of the IQ-PINK1(97-107)-R98W substrate by HsPARLΔ77 in our assay system. The turnover of IQ-PINK1(97-107)-R98W is

nearly 3-fold greater than the turnover of IQ-PINK1(97-107)-WT, with the $p < 0.0005$ for this difference. While we see significantly increased turnover of the mutant peptide, the catalytic efficiency of HsPARLΔ77-mediated cleavage towards IQ-PINK1(97-107)-R98W is not significantly difference than cleavage of the WT peptide because the K_M associated with cleavage of the mutant peptide is also significantly increased. The significantly increased K_M for cleavage of IQ-PINK1(97-107)-R98W indicates that the interaction between this variant and HsPARLΔ77 is altered, but this does not impair cleavage. These results strongly point to the R98W mutation leading to a trafficking defect in a physiological setting, with the protein stuck in the OMM. In cellular studies, PINK1-R98W displays an altered cleavage pattern in the presence or absence of CCCP, indicating that it is likely stuck in the OMM in either scenario, where it can be mildly processed by other proteases, but not efficiently enough for clearance from the mitochondria as there is an accumulation of both FL-PINK1-R98W and cleaved forms, thus providing a molecular rationale for this mutation and the etiology of PD[73,78].

Confocal microscopy studies on HeLa cells expressing these PD-associated variants of PINK1 provide further supporting evidence for the pathology these mutations may have in PD (performed by graduate student Raelynn Brassard with Dr. Nicolas Touret). HeLa cells naturally lack Parkin, thus if there is any accumulation of these PINK1 variants, we can observe their accumulation without mitophagy being initiated. PINK1-R98W was the only PD-associated variant that demonstrated high levels of mitochondrial accumulation, further supporting the mitochondrial import defect proposed to be associated with this mutation (Table 5.1). The other three variants did not display increased levels of mitochondrial accumulation when compared to PINK1-WT, indicating that while there is a decrease in the PARL-mediated cleavage rate for these variants in our kinetic assay, other proteases in the mitochondria may be able to compensate for a loss of PARL-mediated cleavage *in vivo*.

The results presented here suggest that all PD-associated variants of PINK1 that harbour a mutation within the TM region demonstrate some alteration in PARL-mediated cleavage. The

C92F, I111S, and Q126P mutations all result in a cleavage defect with significantly decreased substrate turnover compared to PINK1-WT. Interestingly, in cellular studies the R98W mutation demonstrates impaired or altered processing, yet our *in vitro* study shows a significant increase in turnover compared to PINK1-WT. The cleavage defect observed for C92F, I111S, and Q126P suggests that this impaired cleavage could be a mechanism by which the dysregulation of mitophagy occurs that contributes to overall mitochondrial dysfunction in Parkinson's disease. While a cleavage defect is observed for these variants in our assay system, we cannot discount that in a physiological setting, these mutations could also lead to a mitochondrial import defect, a possibility that our cleavage assay is unable to address. The increased turnover rate observed for R98W and its mitochondrial accumulation in HeLa cells strongly suggests that this mutation impairs translocation of the protein to the IMM. Thus, PINK1 never meets PARL and again mitophagy becomes dysregulated. Both a cleavage defect or an import defect associated with these PINK1 variants has the potential to lead the dysregulation of mitophagy and mitochondrial dysfunction, providing a rationalization for their pathology in PD. Importantly, individuals with *PINK1* mutations tend to be diagnosed with PD earlier, though the progression of the disease is substantially slower compared to the idiopathic late-onset form. Our observations for PINK1-C92F, R98W, I111S, and Q126P likely manifest this slow-progressing PD phenotype related to mitochondrial membrane trafficking and cleavage defects.

CHAPTER 6: CONCLUSION

This thesis aimed to address questions regarding the molecular determinants and regulators of PARL-mediated intramembrane proteolysis. To date, our knowledge on the mitochondrial rhomboid protease PARL has been limited to results obtained from cellular studies. While cellular studies have provided extensive insights into the roles PARL plays in mitochondrial homeostasis, an *in vitro* assay with recombinant protein is needed to provide direct insights regarding proteolytic regulation and characteristics.

We cloned HsPARL as a GFP-fusion protein and utilized *P. pastoris* as our expression system, which enabled us to screen for colonies that highly expressed HsPARL-GFP in a rapid and high-throughput manner. This allowed us to begin our large-scale expression with the significant advantage of already knowing that we would be expressing our protein of interest to a high degree, ultimately leading to an increased final protein yield. Upon successful expression and purification of HsPARL, we were able to assess its proteolytic activity using a highly sensitive and robust FRET-based proteolytic kinetic assay. As outlined in Chapter 2, fluorescence-based assays are well-suited to monitoring proteolytic activity due to the ability to detect very small changes in fluorescence intensity, which directly corresponds to substrate depletion or product formation, in a continuous manner. From these FRET-based proteolytic assays we were able to obtain specific catalytic parameters, such as the K_M, k_{cat}, and k_{cat}/K_M, associated with the cleavage of unique substrates of HsPARL which can provides insights on these PARL-mediated cleavage events.

Because there is no published kinetic data for HsPARL, we aimed to examine and characterize several aspects of PARL-mediated cleavage, as outlined in Chapter 3. We were able to obtain the substrate profile and specificity of our recombinant enzyme in collaboration with Dr. Anthony O'Donoghue. The HsPARLΔ77 substrate profiling demonstrated that our recombinant enzyme retained optimal activity as evident by the high fold-change gathered for the most highly-cleaved peptides, while the substrate specificity plot identified substrate recognition features unique to HsPARLΔ77, but not present in other rhomboid proteases. A bulky

hydrophobic Phe residue was observed in the P1 position for HsPARLΔ77, while bacterial rhomboid proteases prefer the small Ala. The overall broad substrate specificity obtained for HsPARLΔ77 suggests that it may a cleave a multitude of proteins within the IMM that have yet to be identified.

We looked at the influence of the PARL truncations identified *in vivo* on proteolytic activity of the enzyme, as processing of PARL to its truncated forms is proposed to be a regulatory mechanism of PARL-mediated cleavage. Both HsPARLΔ55 and HsPARLΔ77 were active towards three internally quenched substrate peptides, IQ-PGAM5, -PINK1, and -Smac, though we do observe differences between the catalytic parameters obtained for cleavage mediated by HsPARLΔ55 or HsPARLΔ55. These differences suggest that these truncations do indeed serve as a regulator of PARL activity, which may occur as a response to cellular conditions. Furthermore, there are differences between catalytic parameters obtained for each substrate, indicating that substrate specificity, as mediated by the enzyme-substrate interaction, do contribute to the regulation of PARL-mediated proteolysis.

Another regulatory element of intramembrane proteolysis is the lipid environment in which the protein resides as highlighted in Chapter 4. Because the proteolytic activity of other rhomboid proteases has been shown to be influenced by lipids, we hypothesized that cardiolipin, a lipid specific to the IMM, would have an effect of HsPARL activity. We observed that the activity of HsPARLΔ77 was increased towards both a TM substrate and a soluble peptide substrate when in the presence of a 25:1 lipid to protein (cardiolipin to HsPARL) molar ratio. The proteolytic assays described in Chapter 3 and 4 of this thesis present the first kinetic assays of HsPARL and provide a starting point for characterizing and understanding regulatory and mechanistic features of PARL-mediated proteolysis.

In addition to regulatory and mechanistic features of PARL-mediated cleavage that were explored, we have begun to elucidate a role of PARL in Parkinson's disease pathogenesis.

The results of Chapter 5 demonstrate that the PINK1-C92F, I111S, and Q126P mutations identified in PD patients result in impaired PARL-mediated cleavage. These mutations, however, do not result in mitochondrial accumulation of PINK1 as observed in the confocal microscopy studies, suggesting that other proteases may be able to compensate for the impaired PARL-mediated cleavage. These compensatory proteases, however, may not be able to cleave PINK1 as efficiently as PARL, thus contributing to mitophagy dysregulation in PD. Interestingly, we observed that the PINK1-R98W mutation significantly enhanced the catalytic turnover rate of PARL-mediated cleavage, though R98W is the only PD-associated variant for which we observed mitochondrial accumulation. This mitochondrial accumulation suggests that PINK1-R98W may get stuck in the OMM, thus preventing PARL-mediated cleavage. Rapid turnover of PINK1 is required to signal that the mitochondrial pool is healthy and to prevent mitochondrial degradation. These results suggested that both impaired PARL-mediated cleavage or impaired localization of PINK1 may contribute to PINK1 accumulation and a dysregulation of mitophagy, providing a rationale for the molecular etiology of PD associated with the PINK1 variants that harbour a mutation within or near the PINK1 TM region.

The work presented in this thesis provides a strong foundation for characterizing PARL-mediated cleavage in an *in vitro* capacity. Using a recombinant enzyme allows us to gather information on specific enzyme-substrate interactions that cannot be elucidated from cellular studies, yet there are several limitations to detergent-based *in vitro* proteolytic assays. Because we are working with a membrane protein, it is difficult to validate that our recombinant enzyme is folded and functional similar to that *in vivo*. Being situated in a lipid bilayer places spatial constraints and mobility restrictions on the protein that are not present when the protein is reconstituted in a detergent micelle. Additionally, the IMM is a very protein-dense membrane and the protein-protein contacts that arise may greatly affect PARL activity. Due to these limitations, it can be difficult to place the results obtained from our proteolytic assays in a physiological context, particularly when we observe cleavage on the order of a single substrate

molecule per hour. However, similar slow cleavage rates were observed both *in vitro* and *in vivo* for γ-secretase[194]. Since no catalytic data exists for PARL, we cannot ascertain whether detergent-based systems accurately represent the catalytic rates that would be observed in a cell. However, our assays can still provide valuable information such as the observed differences for the truncations of PARL and differences in catalytic turnover rate associated with substrate variants.

In order to overcome the limitation of a detergent-based assay system, future directions for this project include performing proteolytic assays in membrane mimetic systems such as bicelles or proteoliposomes. This will help with translating the results obtained from *in vitro* assays using detergent-solubilized recombinant protein to a more physiological context. When the protein is reconstituted in a more constrained lipid environment, such as a proteoliposome, we may observe higher enzymatic activity or altered catalytic parameters in regards to substrate cleavage.

From the substrate profile obtained, we hypothesize that there may be numerous unidentified substrates of PARL. Using proteomics methods, we can further explore this possibility. A search of mitochondrial proteins that contain the motif identified in the substrate profile can be a starting point for the identification of novel PARL substrates and may reveal additional roles of PARL in mitochondrial homeostasis. Additionally, we would like to explore the sub-mitochondrial localization of PARL. It is currently unknown what region of the IMM PARL localizes to, though its sub-mitochondrial localization could suggest interacting partners or aid in identifying substrates of PARL. Furthermore, obtaining a high resolution structure for HsPARL would provide a significant advancement in our understanding of the mechanism of PARL-mediated cleavage. A high resolution structure would enable us to visualize how a substrate may dock within the catalytic core of the protein and how factors such as the lipid cardiolipin or additional proteins may interact with PARL, ultimately providing a more detailed understanding of the mechanism and regulation of PARL-mediated proteolysis.

In regards to the role of PARL in PD pathogenesis, we would like to further explore the variants near the PINK1-Q126P mutation. This mutation impaired PARL-mediated cleavage even though the mutation is quite distal to the cleavage site. This suggests that this mutation is altering the enzyme-substrate interaction, though the manner by which remains to be elucidated. Interestingly, the Q126P mutation resides in region of PINK1 that is a hotspot for PD mutations. PD-associated mutations of PINK1 also include A124V, C125G, and Q129X, suggesting that this region of PINK1 plays a role in the function of PINK1 or its ability to be efficiently turned over. A better understanding of mutations within this region and their influence on PARL-mediated cleavage will help to rationalize their PD pathogenicity.

This thesis presented the first known kinetic analyses of HsPARL and highlights the importance of *in vitro* assays that utilize recombinant protein to decipher regulatory and mechanistic aspects of proteolysis mediated by the mitochondrial rhomboid protease PARL. As methodologies utilized to study intramembrane proteolysis advance, we can expect PARL to remain an exciting target for its role in mitochondrial homeostasis and cellular pathways in the context of health and disease.

BIBLIOGRAPHY

1   Lopez-Otin, C. & Bond, J. S. Proteases: multifunctional enzymes in life and disease. *J Biol Chem* **283**, 30433-30437, doi:10.1074/jbc.R800035200 (2008).

2   Hartley, B. S. Proteolytic enzymes. *Annu Rev Biochem* **29**, 45-72, doi:10.1146/annurev.bi.29.070160.000401 (1960).

3   Collins, G. A. & Goldberg, A. L. The Logic of the 26S Proteasome. *Cell* **169**, 792-806, doi:10.1016/j.cell.2017.04.023 (2017).

4   Fujinaga, M., Cherney, M. M., Oyama, H., Oda, K. & James, M. N. The molecular structure and catalytic mechanism of a novel carboxyl peptidase from Scytalidium lignicolum. *Proc Natl Acad Sci U S A* **101**, 3364-3369, doi:10.1073/pnas.0400246101 (2004).

5   Voet, D., Voet, J. G. & Pratt, C. W. *Fundamentals of biochemistry : life at the molecular level*. 4th edn, (Wiley, 2013).

6   Rawson, R. B. *et al.* Complementation cloning of S2P, a gene encoding a putative metalloprotease required for intramembrane cleavage of SREBPs. *Mol Cell* **1**, 47-57 (1997).

7   Voet, D., Voet, J. G. & Pratt, C. W. *Fundamentals of biochemistry : life at the molecular level*. 3rd edn, (Wiley, 2008).

8   Erez, E., Fass, D. & Bibi, E. How intramembrane proteases bury hydrolytic reactions in the membrane. *Nature* **459**, 371-378, doi:10.1038/nature08146 (2009).

9   Ray, W. J. *et al.* Cell surface presenilin-1 participates in the gamma-secretase-like proteolysis of Notch. *J Biol Chem* **274**, 36801-36807 (1999).

10   Urban, S., Lee, J. R. & Freeman, M. Drosophila rhomboid-1 defines a family of putative intramembrane serine proteases. *Cell* **107**, 173-182 (2001).

11   Manolaridis, I. *et al.* Mechanism of farnesylated CAAX protein processing by the intramembrane protease Rce1. *Nature* **504**, 301-305, doi:10.1038/nature12754 (2013).

12   Brown, M. S., Ye, J., Rawson, R. B. & Goldstein, J. L. Regulated intramembrane proteolysis: a control mechanism conserved from bacteria to humans. *Cell* **100**, 391-398 (2000).

13   Lemberg, M. K. Intramembrane proteolysis in regulated protein trafficking. *Traffic* **12**, 1109-1118, doi:10.1111/j.1600-0854.2011.01219.x (2011).

14   Jurgens, G., Wieschaus, E., Nusslein-Volhard, C. & Kluding, H. Mutations affecting the pattern of the larval cuticle inDrosophila melanogaster : II. Zygotic loci on the third chromosome. *Wilehm Roux Arch Dev Biol* **193**, 283-295, doi:10.1007/BF00848157 (1984).

15   Bier, E., Jan, L. Y. & Jan, Y. N. rhomboid, a gene required for dorsoventral axis establishment and peripheral nervous system development in Drosophila melanogaster. *Genes Dev* **4**, 190-203 (1990).

16   Rutledge, B. J., Zhang, K., Bier, E., Jan, Y. N. & Perrimon, N. The Drosophila spitz gene encodes a putative EGF-like growth factor involved in dorsal-ventral axis formation and neurogenesis. *Genes Dev* **6**, 1503-1517 (1992).

17   Urban, S. & Wolfe, M. S. Reconstitution of intramembrane proteolysis in vitro reveals that pure rhomboid is sufficient for catalysis and specificity. *Proc Natl Acad Sci U S A* **102**, 1883-1888, doi:10.1073/pnas.0408306102 (2005).

18   Lemberg, M. K. *et al.* Mechanism of intramembrane proteolysis investigated with purified rhomboid proteases. *EMBO J* **24**, 464-472, doi:10.1038/sj.emboj.7600537 (2005).

19   Maegawa, S., Ito, K. & Akiyama, Y. Proteolytic action of GlpG, a rhomboid protease in the Escherichia coli cytoplasmic membrane. *Biochemistry* **44**, 13543-13552, doi:10.1021/bi051363k (2005).

20   Wasserman, J. D., Urban, S. & Freeman, M. A family of rhomboid-like genes: Drosophila rhomboid-1 and roughoid/rhomboid-3 cooperate to activate EGF receptor signaling. *Genes Dev* **14**, 1651-1663 (2000).

21   Ticha, A., Collis, B. & Strisovsky, K. The Rhomboid Superfamily: Structural Mechanisms and Chemical Biology Opportunities. *Trends Biochem Sci* **43**, 726-739, doi:10.1016/j.tibs.2018.06.009 (2018).

22   Lemberg, M. K. & Freeman, M. Functional and evolutionary implications of enhanced genomic analysis of rhomboid intramembrane proteases. *Genome Res* **17**, 1634-1646, doi:10.1101/gr.6425307 (2007).

23   Wang, Y., Zhang, Y. & Ha, Y. Crystal structure of a rhomboid family intramembrane protease. *Nature* **444**, 179-180, doi:10.1038/nature05255 (2006).

24   Wu, Z. *et al.* Structural analysis of a rhomboid family intramembrane protease reveals a gating mechanism for substrate entry. *Nat Struct Mol Biol* **13**, 1084-1091, doi:10.1038/nsmb1179 (2006).

25   Ben-Shem, A., Fass, D. & Bibi, E. Structural basis for intramembrane proteolysis by rhomboid serine proteases. *Proc Natl Acad Sci U S A* **104**, 462-466, doi:10.1073/pnas.0609773104 (2007).

26   Lemieux, M. J., Fischer, S. J., Cherney, M. M., Bateman, K. S. & James, M. N. The crystal structure of the rhomboid peptidase from Haemophilus influenzae provides insight into intramembrane proteolysis. *Proc Natl Acad Sci U S A* **104**, 750-754, doi:10.1073/pnas.0609981104 (2007).

27   Vinothkumar, K. R. *et al.* The structural basis for catalysis and substrate specificity of a rhomboid protease. *EMBO J* **29**, 3797-3809, doi:10.1038/emboj.2010.243 (2010).

28   Koonin, E. V. *et al.* The rhomboids: a nearly ubiquitous family of intramembrane serine proteases that probably evolved by multiple ancient horizontal gene transfers. *Genome Biol* **4**, R19 (2003).

29   Vinothkumar, K. R. Structure of rhomboid protease in a lipid environment. *J Mol Biol* **407**, 232-247, doi:10.1016/j.jmb.2011.01.029 (2011).

30   Vosyka, O. *et al.* Activity-based probes for rhomboid proteases discovered in a mass spectrometry-based assay. *Proc Natl Acad Sci U S A* **110**, 2472-2477, doi:10.1073/pnas.1215076110 (2013).

31   Zoll, S. *et al.* Substrate binding and specificity of rhomboid intramembrane protease revealed by substrate-peptide complex structures. *EMBO J* **33**, 2408-2421, doi:10.15252/embj.201489367 (2014).

32   Cho, S., Dickey, S. W. & Urban, S. Crystal Structures and Inhibition Kinetics Reveal a Two-Stage Catalytic Mechanism with Drug Design Implications for Rhomboid Proteolysis. *Mol Cell* **61**, 329-340, doi:10.1016/j.molcel.2015.12.022 (2016).

33   Bondar, A. N., del Val, C. & White, S. H. Rhomboid protease dynamics and lipid interactions. *Structure* **17**, 395-405, doi:10.1016/j.str.2008.12.017 (2009).

34   Rose, A. S. *et al.* NGL viewer: web-based molecular graphics for large complexes. *Bioinformatics* **34**, 3755-3758, doi:10.1093/bioinformatics/bty419 (2018).

35   Baker, R. P., Young, K., Feng, L., Shi, Y. & Urban, S. Enzymatic analysis of a rhomboid intramembrane protease implicates transmembrane helix 5 as the lateral substrate gate. *Proc Natl Acad Sci U S A* **104**, 8257-8262, doi:10.1073/pnas.0700814104 (2007).

36   Urban, S. & Baker, R. P. In vivo analysis reveals substrate-gating mutants of a rhomboid intramembrane protease display increased activity in living cells. *Biol Chem* **389**, 1107-1115, doi:10.1515/BC.2008.122 (2008).

37   Xue, Y. & Ha, Y. Large lateral movement of transmembrane helix S5 is not required for substrate access to the active site of rhomboid intramembrane protease. *J Biol Chem* **288**, 16645-16654, doi:10.1074/jbc.M112.438127 (2013).

38   Stevenson, L. G. *et al.* Rhomboid protease AarA mediates quorum-sensing in Providencia stuartii by activating TatA of the twin-arginine translocase. *Proc Natl Acad Sci U S A* **104**, 1003-1008, doi:10.1073/pnas.0608140104 (2007).

39   Arutyunova, E. *et al.* An internally quenched peptide as a new model substrate for rhomboid intramembrane proteases. *Biol Chem* **399**, 1389-1397, doi:10.1515/hsz-2018-0255 (2018).

40   Dusterhoft, S., Kunzel, U. & Freeman, M. Rhomboid proteases in human disease: Mechanisms and future prospects. *Biochim Biophys Acta Mol Cell Res* **1864**, 2200-2209, doi:10.1016/j.bbamcr.2017.04.016 (2017).

41   Adrain, C. *et al.* Mammalian EGF receptor activation by the rhomboid protease RHBDL2. *EMBO Rep* **12**, 421-427, doi:10.1038/embor.2011.50 (2011).

42   Fleig, L. *et al.* Ubiquitin-dependent intramembrane rhomboid protease promotes ERAD of membrane proteins. *Mol Cell* **47**, 558-569, doi:10.1016/j.molcel.2012.06.008 (2012).

43   Pascall, J. C., Luck, J. E. & Brown, K. D. Expression in mammalian cell cultures reveals interdependent, but distinct, functions for Star and Rhomboid proteins in the processing of the Drosophila transforming-growth-factor-alpha homologue Spitz. *Biochem J* **363**, 347-352 (2002).

44   Jaszai, J. & Brand, M. Cloning and expression of Ventrhoid, a novel vertebrate homologue of the Drosophila EGF pathway gene rhomboid. *Mech Dev* **113**, 73-77 (2002).

45   Spinazzi, M. & De Strooper, B. PARL: The mitochondrial rhomboid protease. *Semin Cell Dev Biol* **60**, 19-28, doi:10.1016/j.semcdb.2016.07.034 (2016).

46   Song, W. *et al.* Rhomboid domain containing 1 promotes colorectal cancer growth through activation of the EGFR signalling pathway. *Nat Commun* **6**, 8022, doi:10.1038/ncomms9022 (2015).

47   Civitarese, A. E. *et al.* Regulation of skeletal muscle oxidative capacity and insulin signaling by the mitochondrial rhomboid protease PARL. *Cell Metab* **11**, 412-426, doi:10.1016/j.cmet.2010.04.004 (2010).

48   Paschkowsky, S., Hamze, M., Oestereich, F. & Munter, L. M. Alternative Processing of the Amyloid Precursor Protein Family by Rhomboid Protease RHBDL4. *J Biol Chem* **291**, 21903-21912, doi:10.1074/jbc.M116.753582 (2016).

49   Shi, G. *et al.* Functional alteration of PARL contributes to mitochondrial dysregulation in Parkinson's disease. *Hum Mol Genet* **20**, 1966-1974, doi:10.1093/hmg/ddr077 (2011).

50   Brossier, F., Jewett, T. J., Sibley, L. D. & Urban, S. A spatially localized rhomboid protease cleaves cell surface adhesins essential for invasion by Toxoplasma. *Proc Natl Acad Sci U S A* **102**, 4146-4151, doi:10.1073/pnas.0407918102 (2005).

51   Verhelst, S. H. L. Intramembrane proteases as drug targets. *FEBS J* **284**, 1489-1502, doi:10.1111/febs.13979 (2017).

52   Yang, J. *et al.* Benzoxazin-4-ones as novel, easily accessible inhibitors for rhomboid proteases. *Bioorg Med Chem Lett* **28**, 1423-1427, doi:10.1016/j.bmcl.2017.12.056 (2018).

53   Chow, V. W., Mattson, M. P., Wong, P. C. & Gleichmann, M. An overview of APP processing enzymes and products. *Neuromolecular Med* **12**, 1-12, doi:10.1007/s12017-009-8104-z (2010).

54   Langosch, D. & Steiner, H. Substrate processing in intramembrane proteolysis by gamma-secretase - the role of protein dynamics. *Biol Chem* **398**, 441-453, doi:10.1515/hsz-2016-0269 (2017).

55   Raven, F. *et al.* Soluble Gamma-secretase Modulators Attenuate Alzheimer's beta-amyloid Pathology and Induce Conformational Changes in Presenilin 1. *EBioMedicine* **24**, 93-101, doi:10.1016/j.ebiom.2017.08.028 (2017).

56   Zhou, R. *et al.* Recognition of the amyloid precursor protein by human gamma-secretase. *Science* **363**, doi:10.1126/science.aaw0930 (2019).

57   McQuibban, G. A., Saurya, S. & Freeman, M. Mitochondrial membrane remodelling regulated by a conserved rhomboid protease. *Nature* **423**, 537-541, doi:10.1038/nature01633 (2003).

58   McQuibban, G. A., Lee, J. R., Zheng, L., Juusola, M. & Freeman, M. Normal mitochondrial dynamics requires rhomboid-7 and affects Drosophila lifespan and neuronal function. *Curr Biol* **16**, 982-989, doi:10.1016/j.cub.2006.03.062 (2006).

59   Cipolat, S. *et al.* Mitochondrial rhomboid PARL regulates cytochrome c release during apoptosis via OPA1-dependent cristae remodeling. *Cell* **126**, 163-175, doi:10.1016/j.cell.2006.06.021 (2006).

60   Pellegrini, L. *et al.* PAMP and PARL, two novel putative metalloproteases interacting with the COOH-terminus of Presenilin-1 and -2. *J Alzheimers Dis* **3**, 181-190 (2001).

61   Jeyaraju, D. V. *et al.* Phosphorylation and cleavage of presenilin-associated rhomboid-like protein (PARL) promotes changes in mitochondrial morphology. *Proc Natl Acad Sci U S A* **103**, 18562-18567, doi:10.1073/pnas.0604983103 (2006).

62   Jeyaraju, D. V., McBride, H. M., Hill, R. B. & Pellegrini, L. Structural and mechanistic basis of Parl activity and regulation. *Cell Death Differ* **18**, 1531-1539, doi:10.1038/cdd.2011.22 (2011).

63   Sik, A., Passer, B. J., Koonin, E. V. & Pellegrini, L. Self-regulated cleavage of the mitochondrial intramembrane-cleaving protease PARL yields Pbeta, a nuclear-targeted peptide. *J Biol Chem* **279**, 15323-15329, doi:10.1074/jbc.M313756200 (2004).

64   Meissner, C., Lorenz, H., Weihofen, A., Selkoe, D. J. & Lemberg, M. K. The mitochondrial intramembrane protease PARL cleaves human Pink1 to regulate Pink1 trafficking. *J Neurochem* **117**, 856-867, doi:10.1111/j.1471-4159.2011.07253.x (2011).

65   Shi, G. & McQuibban, G. A. The Mitochondrial Rhomboid Protease PARL Is Regulated by PDK2 to Integrate Mitochondrial Quality Control and Metabolism. *Cell Rep* **18**, 1458-1472, doi:10.1016/j.celrep.2017.01.029 (2017).

66   Wai, T. *et al.* The membrane scaffold SLP2 anchors a proteolytic hub in mitochondria containing PARL and the i-AAA protease YME1L. *EMBO Rep* **17**, 1844-1856, doi:10.15252/embr.201642698 (2016).

67   Deas, E. *et al.* PINK1 cleavage at position A103 by the mitochondrial protease PARL. *Hum Mol Genet* **20**, 867-879, doi:10.1093/hmg/ddq526 (2011).

68   Esser, K., Tursun, B., Ingenhoven, M., Michaelis, G. & Pratje, E. A novel two-step mechanism for removal of a mitochondrial signal sequence involves the mAAA complex and the putative rhomboid protease Pcp1. *J Mol Biol* **323**, 835-843 (2002).

69   Sesaki, H., Southard, S. M., Hobbs, A. E. & Jensen, R. E. Cells lacking Pcp1p/Ugo2p, a rhomboid-like protease required for Mgm1p processing, lose mtDNA and mitochondrial structure in a Dnm1p-dependent manner, but remain competent for mitochondrial fusion. *Biochem Biophys Res Commun* **308**, 276-283 (2003).

70   Herlan, M., Vogel, F., Bornhovd, C., Neupert, W. & Reichert, A. S. Processing of Mgm1 by the rhomboid-type protease Pcp1 is required for maintenance of mitochondrial morphology and of mitochondrial DNA. *J Biol Chem* **278**, 27781-27788, doi:10.1074/jbc.M211311200 (2003).

71   Rahman, M. & Kylsten, P. Rhomboid-7 over-expression results in Opa1-like processing and malfunctioning mitochondria. *Biochem Biophys Res Commun* **414**, 315-320, doi:10.1016/j.bbrc.2011.09.047 (2011).

72   Whitworth, A. J. *et al.* Rhomboid-7 and HtrA2/Omi act in a common pathway with the Parkinson's disease factors Pink1 and Parkin. *Dis Model Mech* **1**, 168-174; discussion 173, doi:10.1242/dmm.000109 (2008).

73   Jin, S. M. *et al.* Mitochondrial membrane potential regulates PINK1 import and proteolytic destabilization by PARL. *J Cell Biol* **191**, 933-942, doi:10.1083/jcb.201008084 (2010).

74   Sekine, S. *et al.* Rhomboid protease PARL mediates the mitochondrial membrane potential loss-induced cleavage of PGAM5. *J Biol Chem* **287**, 34635-34645, doi:10.1074/jbc.M112.357509 (2012).

75   Saita, S. *et al.* PARL mediates Smac proteolytic maturation in mitochondria to promote apoptosis. *Nat Cell Biol* **19**, 318-328, doi:10.1038/ncb3488 (2017).

76   Greene, A. W. *et al.* Mitochondrial processing peptidase regulates PINK1 processing, import and Parkin recruitment. *EMBO Rep* **13**, 378-385, doi:10.1038/embor.2012.14 (2012).

77   Yamano, K. & Youle, R. J. PINK1 is degraded through the N-end rule pathway. *Autophagy* **9**, 1758-1769, doi:10.4161/auto.24633 (2013).

78   Meissner, C., Lorenz, H., Hehn, B. & Lemberg, M. K. Intramembrane protease PARL defines a negative regulator of PINK1- and PARK2/Parkin-dependent mitophagy. *Autophagy* **11**, 1484-1498, doi:10.1080/15548627.2015.1063763 (2015).

79   Zhuang, M., Guan, S., Wang, H., Burlingame, A. L. & Wells, J. A. Substrates of IAP ubiquitin ligases identified with a designed orthogonal E3 ligase, the NEDDylator. *Mol Cell* **49**, 273-282, doi:10.1016/j.molcel.2012.10.022 (2013).

80   Walder, K. *et al.* The mitochondrial rhomboid protease PSARL is a new candidate gene for type 2 diabetes. *Diabetologia* **48**, 459-468, doi:10.1007/s00125-005-1675-9 (2005).

81   Tang, H., Liu, J., Niu, L., He, W. & Xu, Y. Variation in gene expression of presenilins-associated rhomboid-like protein and mitochondrial function in skeletal muscle of insulin-resistant rats. *Endocrine* **36**, 524-529, doi:10.1007/s12020-009-9270-3 (2009).

82   Kelley, D. E., He, J., Menshikova, E. V. & Ritov, V. B. Dysfunction of mitochondria in human skeletal muscle in type 2 diabetes. *Diabetes* **51**, 2944-2950 (2002).

83   Ritov, V. B. *et al.* Deficiency of subsarcolemmal mitochondria in obesity and type 2 diabetes. *Diabetes* **54**, 8-14 (2005).

84   Morino, K. *et al.* Reduced mitochondrial density and increased IRS-1 serine phosphorylation in muscle of insulin-resistant offspring of type 2 diabetic parents. *J Clin Invest* **115**, 3587-3593, doi:10.1172/JCI25151 (2005).

85   Petersen, K. F. *et al.* Mitochondrial dysfunction in the elderly: possible role in insulin resistance. *Science* **300**, 1140-1142, doi:10.1126/science.1082889 (2003).

86   Zhang, Y., James, M., Middleton, F. A. & Davis, R. L. Transcriptional analysis of multiple brain regions in Parkinson's disease supports the involvement of specific protein processing, energy metabolism, and signaling pathways, and suggests novel disease mechanisms. *Am J Med Genet B Neuropsychiatr Genet* **137B**, 5-16, doi:10.1002/ajmg.b.30195 (2005).

87   Spinazzi, M. *et al.* PARL deficiency in mouse causes Complex III defects, coenzyme Q depletion, and Leigh-like syndrome. *Proc Natl Acad Sci U S A* **116**, 277-286, doi:10.1073/pnas.1811938116 (2019).

88   Ishihara, N. & Mihara, K. PARL paves the way to apoptosis. *Nat Cell Biol* **19**, 263-265, doi:10.1038/ncb3504 (2017).

89   Chan, D. C. Mitochondria: dynamic organelles in disease, aging, and development. *Cell* **125**, 1241-1252, doi:10.1016/j.cell.2006.06.010 (2006).

90   Dhar, S. S., Ongwijitwat, S. & Wong-Riley, M. T. Nuclear respiratory factor 1 regulates all ten nuclear-encoded subunits of cytochrome c oxidase in neurons. *J Biol Chem* **283**, 3120-3129, doi:10.1074/jbc.M707587200 (2008).

91   Blesa, J. R. *et al.* NRF-1 is the major transcription factor regulating the expression of the human TOMM34 gene. *Biochem Cell Biol* **86**, 46-56, doi:10.1139/o07-151 (2008).

92   Eliyahu, E. *et al.* Tom20 mediates localization of mRNAs to mitochondria in a translation-dependent manner. *Mol Cell Biol* **30**, 284-294, doi:10.1128/MCB.00651-09 (2010).

93   Yakubovskaya, E. *et al.* Organization of the human mitochondrial transcription initiation complex. *Nucleic Acids Res* **42**, 4100-4112, doi:10.1093/nar/gkt1360 (2014).

94   Kanki, T. *et al.* Architectural role of mitochondrial transcription factor A in maintenance of human mitochondrial DNA. *Mol Cell Biol* **24**, 9823-9834, doi:10.1128/MCB.24.22.9823-9834.2004 (2004).

95   Chu, C. T. Tickled PINK1: mitochondrial homeostasis and autophagy in recessive Parkinsonism. *Biochim Biophys Acta* **1802**, 20-28, doi:10.1016/j.bbadis.2009.06.012 (2010).

96   Pfeffer, S., Woellhaf, M. W., Herrmann, J. M. & Forster, F. Organization of the mitochondrial translation machinery studied in situ by cryoelectron tomography. *Nat Commun* **6**, 6019, doi:10.1038/ncomms7019 (2015).

97   Kuzmenko, A. *et al.* Aim-less translation: loss of Saccharomyces cerevisiae mitochondrial translation initiation factor mIF3/Aim23 leads to unbalanced protein synthesis. *Sci Rep* **6**, 18749, doi:10.1038/srep18749 (2016).

98   Zhang, X. *et al.* MicroRNA directly enhances mitochondrial translation during muscle differentiation. *Cell* **158**, 607-619, doi:10.1016/j.cell.2014.05.047 (2014).

99   Pagliuso, A., Cossart, P. & Stavru, F. The ever-growing complexity of the mitochondrial fission machinery. *Cell Mol Life Sci* **75**, 355-374, doi:10.1007/s00018-017-2603-0 (2018).

100   Chen, H. *et al.* Mitofusins Mfn1 and Mfn2 coordinately regulate mitochondrial fusion and are essential for embryonic development. *J Cell Biol* **160**, 189-200, doi:10.1083/jcb.200211046 (2003).

101   Ferree, A. & Shirihai, O. Mitochondrial dynamics: the intersection of form and function. *Adv Exp Med Biol* **748**, 13-40, doi:10.1007/978-1-4614-3573-0_2 (2012).

102   Tatsuta, T. & Langer, T. Quality control of mitochondria: protection against neurodegeneration and ageing. *EMBO J* **27**, 306-314, doi:10.1038/sj.emboj.7601972 (2008).

103   Pellegrino, M. W., Nargund, A. M. & Haynes, C. M. Signaling the mitochondrial unfolded protein response. *Biochim Biophys Acta* **1833**, 410-416, doi:10.1016/j.bbamcr.2012.02.019 (2013).

104   Sugiura, A., McLelland, G. L., Fon, E. A. & McBride, H. M. A new pathway for mitochondrial quality control: mitochondrial-derived vesicles. *EMBO J* **33**, 2142-2156, doi:10.15252/embj.201488104 (2014).

105   Urban, S. & Freeman, M. Substrate specificity of rhomboid intramembrane proteases is governed by helix-breaking residues in the substrate transmembrane domain. *Mol Cell* **11**, 1425-1434 (2003).

106   Ulmschneider, M. B. *et al.* Transmembrane helices containing a charged arginine are thermodynamically stable. *Eur Biophys J* **46**, 627-637, doi:10.1007/s00249-017-1206-x (2017).

107   UniProt Consortium, T. UniProt: the universal protein knowledgebase. *Nucleic Acids Res* **46**, 2699, doi:10.1093/nar/gky092 (2018).

108   Pickrell, A. M. & Youle, R. J. The roles of PINK1, parkin, and mitochondrial fidelity in Parkinson's disease. *Neuron* **85**, 257-273, doi:10.1016/j.neuron.2014.12.007 (2015).

109   Okatsu, K. *et al.* PINK1 autophosphorylation upon membrane potential dissipation is essential for Parkin recruitment to damaged mitochondria. *Nat Commun* **3**, 1016, doi:10.1038/ncomms2016 (2012).

110   Okatsu, K. *et al.* A dimeric PINK1-containing complex on depolarized mitochondria stimulates Parkin recruitment. *J Biol Chem* **288**, 36372-36384, doi:10.1074/jbc.M113.509653 (2013).

111   Kazlauskaite, A. *et al.* Parkin is activated by PINK1-dependent phosphorylation of ubiquitin at Ser65. *Biochem J* **460**, 127-139, doi:10.1042/BJ20140334 (2014).

112   Kondapalli, C. *et al.* PINK1 is activated by mitochondrial membrane potential depolarization and stimulates Parkin E3 ligase activity by phosphorylating Serine 65. *Open Biol* **2**, 120080, doi:10.1098/rsob.120080 (2012).

113   Shiba-Fukushima, K. *et al.* PINK1-mediated phosphorylation of the Parkin ubiquitin-like domain primes mitochondrial translocation of Parkin and regulates mitophagy. *Sci Rep* **2**, 1002, doi:10.1038/srep01002 (2012).

114   Kane, L. A. *et al.* PINK1 phosphorylates ubiquitin to activate Parkin E3 ubiquitin ligase activity. *J Cell Biol* **205**, 143-153, doi:10.1083/jcb.201402104 (2014).

115   Chan, N. C. *et al.* Broad activation of the ubiquitin-proteasome system by Parkin is critical for mitophagy. *Hum Mol Genet* **20**, 1726-1737, doi:10.1093/hmg/ddr048 (2011).

116   Narendra, D., Walker, J. E. & Youle, R. Mitochondrial quality control mediated by PINK1 and Parkin: links to parkinsonism. *Cold Spring Harb Perspect Biol* **4**, doi:10.1101/cshperspect.a011338 (2012).

117   Ordureau, A. *et al.* Quantitative proteomics reveal a feedforward mechanism for mitochondrial PARKIN translocation and ubiquitin chain synthesis. *Mol Cell* **56**, 360-375, doi:10.1016/j.molcel.2014.09.007 (2014).

118   Sarraf, S. A. *et al.* Landscape of the PARKIN-dependent ubiquitylome in response to mitochondrial depolarization. *Nature* **496**, 372-376, doi:10.1038/nature12043 (2013).

119   Yamano, K., Fogel, A. I., Wang, C., van der Bliek, A. M. & Youle, R. J. Mitochondrial Rab GAPs govern autophagosome biogenesis during mitophagy. *Elife* **3**, e01612, doi:10.7554/eLife.01612 (2014).

120   Abeliovich, H., Zarei, M., Rigbolt, K. T., Youle, R. J. & Dengjel, J. Involvement of mitochondrial dynamics in the segregation of mitochondrial matrix proteins during stationary phase mitophagy. *Nat Commun* **4**, 2789, doi:10.1038/ncomms3789 (2013).

121   Frank, M. *et al.* Mitophagy is triggered by mild oxidative stress in a mitochondrial fission dependent manner. *Biochim Biophys Acta* **1823**, 2297-2310, doi:10.1016/j.bbamcr.2012.08.007 (2012).

122   Mao, K., Wang, K., Liu, X. & Klionsky, D. J. The scaffold protein Atg11 recruits fission machinery to drive selective mitochondria degradation by autophagy. *Dev Cell* **26**, 9-18, doi:10.1016/j.devcel.2013.05.024 (2013).

123   Buhlman, L. *et al.* Functional interplay between Parkin and Drp1 in mitochondrial fission and clearance. *Biochim Biophys Acta* **1843**, 2012-2026, doi:10.1016/j.bbamcr.2014.05.012 (2014).

124   Tanaka, A. *et al.* Proteasome and p97 mediate mitophagy and degradation of mitofusins induced by Parkin. *J Cell Biol* **191**, 1367-1380, doi:10.1083/jcb.201007013 (2010).

125   Twig, G. *et al.* Fission and selective fusion govern mitochondrial segregation and elimination by autophagy. *EMBO J* **27**, 433-446, doi:10.1038/sj.emboj.7601963 (2008).

126   Deng, H., Dodson, M. W., Huang, H. & Guo, M. The Parkinson's disease genes pink1 and parkin promote mitochondrial fission and/or inhibit fusion in Drosophila. *Proc Natl Acad Sci U S A* **105**, 14503-14508, doi:10.1073/pnas.0803998105 (2008).

127   Poole, A. C. *et al.* The PINK1/Parkin pathway regulates mitochondrial morphology. *Proc Natl Acad Sci U S A* **105**, 1638-1643, doi:10.1073/pnas.0709336105 (2008).

128   Yang, Y. *et al.* Pink1 regulates mitochondrial dynamics through interaction with the fission/fusion machinery. *Proc Natl Acad Sci U S A* **105**, 7070-7075, doi:10.1073/pnas.0711845105 (2008).

129   Liu, S. *et al.* Parkinson's disease-associated kinase PINK1 regulates Miro protein level and axonal transport of mitochondria. *PLoS Genet* **8**, e1002537, doi:10.1371/journal.pgen.1002537 (2012).

130   Morais, V. A. *et al.* PINK1 loss-of-function mutations affect mitochondrial complex I activity via NdufA10 ubiquinone uncoupling. *Science* **344**, 203-207, doi:10.1126/science.1249161 (2014).

131   de Rijk, M. C. *et al.* Prevalence of Parkinson's disease in the elderly: the Rotterdam Study. *Neurology* **45**, 2143-2146 (1995).

132   von Campenhausen, S. *et al.* Prevalence and incidence of Parkinson's disease in Europe. *Eur Neuropsychopharmacol* **15**, 473-490, doi:10.1016/j.euroneuro.2005.04.007 (2005).

133   de Lau, L. M. & Breteler, M. M. Epidemiology of Parkinson's disease. *Lancet Neurol* **5**, 525-535, doi:10.1016/S1474-4422(06)70471-9 (2006).

134   Lang, A. E. & Lozano, A. M. Parkinson's disease. First of two parts. *N Engl J Med* **339**, 1044-1053, doi:10.1056/NEJM199810083391506 (1998).

135   Lang, A. E. & Lozano, A. M. Parkinson's disease. Second of two parts. *N Engl J Med* **339**, 1130-1143, doi:10.1056/NEJM199810153391607 (1998).

136   Garcia-Ruiz, P. J., Chaudhuri, K. R. & Martinez-Martin, P. Non-motor symptoms of Parkinson's disease A review...from the past. *J Neurol Sci* **338**, 30-33, doi:10.1016/j.jns.2014.01.002 (2014).

137   Belin, A. C. & Westerlund, M. Parkinson's disease: a genetic perspective. *FEBS J* **275**, 1377-1383, doi:10.1111/j.1742-4658.2008.06301.x (2008).

138   Houlden, H. & Singleton, A. B. The genetics and neuropathology of Parkinson's disease. *Acta Neuropathol* **124**, 325-338, doi:10.1007/s00401-012-1013-5 (2012).

139   Langston, J. W., Ballard, P., Tetrud, J. W. & Irwin, I. Chronic Parkinsonism in humans due to a product of meperidine-analog synthesis. *Science* **219**, 979-980 (1983).

140   Mizuno, Y. *et al.* Deficiencies in complex I subunits of the respiratory chain in Parkinson's disease. *Biochem Biophys Res Commun* **163**, 1450-1455 (1989).

141   Bove, J. & Perier, C. Neurotoxin-based models of Parkinson's disease. *Neuroscience* **211**, 51-76, doi:10.1016/j.neuroscience.2011.10.057 (2012).

142   Polymeropoulos, M. H. *et al.* Mutation in the alpha-synuclein gene identified in families with Parkinson's disease. *Science* **276**, 2045-2047 (1997).

143   Kitada, T. *et al.* Mutations in the parkin gene cause autosomal recessive juvenile parkinsonism. *Nature* **392**, 605-608, doi:10.1038/33416 (1998).

144   Sulzer, D. Multiple hit hypotheses for dopamine neuron loss in Parkinson's disease. *Trends Neurosci* **30**, 244-250, doi:10.1016/j.tins.2007.03.009 (2007).

145   Haddad, D. & Nakamura, K. Understanding the susceptibility of dopamine neurons to mitochondrial stressors in Parkinson's disease. *FEBS Lett* **589**, 3702-3713, doi:10.1016/j.febslet.2015.10.021 (2015).

146   Kouli, A., Torsney, K. M. & Kuan, W. L. in *Parkinson's Disease: Pathogenesis and Clinical Aspects*   (eds T. B. Stoker & J. C. Greenland) (2018).

147   Valente, E. M. *et al.* Localization of a novel locus for autosomal recessive early-onset parkinsonism, PARK6, on human chromosome 1p35-p36. *Am J Hum Genet* **68**, 895-900 (2001).

148   Matsumine, H. *et al.* Localization of a gene for an autosomal recessive form of juvenile Parkinsonism to chromosome 6q25.2-27. *Am J Hum Genet* **60**, 588-596 (1997).

149   Lin, W. & Kang, U. J. Characterization of PINK1 processing, stability, and subcellular localization. *J Neurochem* **106**, 464-474, doi:10.1111/j.1471-4159.2008.05398.x (2008).

150   Goldberg, M. S. *et al.* Parkin-deficient mice exhibit nigrostriatal deficits but not loss of dopaminergic neurons. *J Biol Chem* **278**, 43628-43635, doi:10.1074/jbc.M308947200 (2003).

151   Itier, J. M. *et al.* Parkin gene inactivation alters behaviour and dopamine neurotransmission in the mouse. *Hum Mol Genet* **12**, 2277-2291, doi:10.1093/hmg/ddg239 (2003).

152   Kitada, T. *et al.* Impaired dopamine release and synaptic plasticity in the striatum of PINK1-deficient mice. *Proc Natl Acad Sci U S A* **104**, 11441-11446, doi:10.1073/pnas.0702717104 (2007).

153   Palacino, J. J. *et al.* Mitochondrial dysfunction and oxidative damage in parkin-deficient mice. *J Biol Chem* **279**, 18614-18622, doi:10.1074/jbc.M401135200 (2004).

154   Periquet, M., Corti, O., Jacquier, S. & Brice, A. Proteomic analysis of parkin knockout mice: alterations in energy metabolism, protein handling and synaptic function. *J Neurochem* **95**, 1259-1276, doi:10.1111/j.1471-4159.2005.03442.x (2005).

155   Gandhi, S. *et al.* PINK1-associated Parkinson's disease is caused by neuronal vulnerability to calcium-induced cell death. *Mol Cell* **33**, 627-638, doi:10.1016/j.molcel.2009.02.013 (2009).

156   Gautier, C. A. *et al.* Regulation of mitochondrial permeability transition pore by PINK1. *Mol Neurodegener* **7**, 22, doi:10.1186/1750-1326-7-22 (2012).

157   Heeman, B. *et al.* Depletion of PINK1 affects mitochondrial metabolism, calcium homeostasis and energy maintenance. *J Cell Sci* **124**, 1115-1125, doi:10.1242/jcs.078303 (2011).

158   Greene, J. C. *et al.* Mitochondrial pathology and apoptotic muscle degeneration in Drosophila parkin mutants. *Proc Natl Acad Sci U S A* **100**, 4078-4083, doi:10.1073/pnas.0737556100 (2003).

159   Clark, I. E. *et al.* Drosophila pink1 is required for mitochondrial function and interacts genetically with parkin. *Nature* **441**, 1162-1166, doi:10.1038/nature04779 (2006).

160   Park, J. *et al.* Mitochondrial dysfunction in Drosophila PINK1 mutants is complemented by parkin. *Nature* **441**, 1157-1161, doi:10.1038/nature04788 (2006).

161   Yang, Y. *et al.* Mitochondrial pathology and muscle and dopaminergic neuron degeneration caused by inactivation of Drosophila Pink1 is rescued by Parkin. *Proc Natl Acad Sci U S A* **103**, 10793-10798, doi:10.1073/pnas.0602493103 (2006).

162   Lu, W. *et al.* Genetic deficiency of the mitochondrial protein PGAM5 causes a Parkinson's-like movement disorder. *Nat Commun* **5**, 4930, doi:10.1038/ncomms5930 (2014).

163   Truban, D., Hou, X., Caulfield, T. R., Fiesel, F. C. & Springer, W. PINK1, Parkin, and Mitochondrial Quality Control: What can we Learn about Parkinson's Disease Pathobiology? *J Parkinsons Dis* **7**, 13-29, doi:10.3233/JPD-160989 (2017).

164   Brooks, C. L., Morrison, M. & Joanne Lemieux, M. Rapid expression screening of eukaryotic membrane proteins in Pichia pastoris. *Protein Sci* **22**, 425-433, doi:10.1002/pro.2223 (2013).

165   Oberg, F., Sjohamn, J., Conner, M. T., Bill, R. M. & Hedfalk, K. Improving recombinant eukaryotic membrane protein yields in Pichia pastoris: the importance of codon optimization and clone selection. *Mol Membr Biol* **28**, 398-411, doi:10.3109/09687688.2011.602219 (2011).

166   Mizutani, K., Yoshioka, S., Mizutani, Y., Iwata, S. & Mikami, B. High-throughput construction of expression system using yeast Pichia pastoris, and its application to membrane proteins. *Protein Expr Purif* **77**, 1-8, doi:10.1016/j.pep.2010.12.009 (2011).

167   Wagner, S., Bader, M. L., Drew, D. & de Gier, J. W. Rationalizing membrane protein overexpression. *Trends Biotechnol* **24**, 364-371, doi:10.1016/j.tibtech.2006.06.008 (2006).

168   Macauley-Patrick, S., Fazenda, M. L., McNeil, B. & Harvey, L. M. Heterologous protein production using the Pichia pastoris expression system. *Yeast* **22**, 249-270, doi:10.1002/yea.1208 (2005).

169   Li, P. *et al.* Expression of recombinant proteins in Pichia pastoris. *Appl Biochem Biotechnol* **142**, 105-124 (2007).

170   Oldham, M. L., Grigorieff, N. & Chen, J. Structure of the transporter associated with antigen processing trapped by herpes simplex virus. *Elife* **5**, doi:10.7554/eLife.21829 (2016).

171   Pau, V., Zhou, Y., Ramu, Y., Xu, Y. & Lu, Z. Crystal structure of an inactivated mutant mammalian voltage-gated K(+) channel. *Nat Struct Mol Biol* **24**, 857-865, doi:10.1038/nsmb.3457 (2017).

172   Diver, M. M., Pedi, L., Koide, A., Koide, S. & Long, S. B. Atomic structure of the eukaryotic intramembrane RAS methyltransferase ICMT. *Nature* **553**, 526-529, doi:10.1038/nature25439 (2018).

173   Cereghino, J. L. & Cregg, J. M. Heterologous protein expression in the methylotrophic yeast Pichia pastoris. *FEMS Microbiol Rev* **24**, 45-66, doi:10.1111/j.1574-6976.2000.tb00532.x (2000).

174   Ellis, S. B. *et al.* Isolation of alcohol oxidase and two other methanol regulatable genes from the yeast Pichia pastoris. *Mol Cell Biol* **5**, 1111-1121 (1985).

175   Gellissen, G. Heterologous protein production in methylotrophic yeasts. *Appl Microbiol Biotechnol* **54**, 741-750 (2000).

176   Panwar, P. & Lemieux, M. J. Expression and Purification of Haemophilus influenzae Rhomboid Intramembrane Protease GlpG for Structural Studies. *Curr Protoc Protein Sci* **76**, 29 29 21-25, doi:10.1002/0471140864.ps2909s76 (2014).

177   Arutyunova, E. *et al.* Allosteric regulation of rhomboid intramembrane proteolysis. *EMBO J* **33**, 1869-1881, doi:10.15252/embj.201488149 (2014).

178   Dickey, S. W., Baker, R. P., Cho, S. & Urban, S. Proteolysis inside the membrane is a rate-governed reaction not driven by substrate affinity. *Cell* **155**, 1270-1281, doi:10.1016/j.cell.2013.10.053 (2013).

179   Pierrat, O. A. *et al.* Monocyclic beta-lactams are selective, mechanism-based inhibitors of rhomboid intramembrane proteases. *ACS Chem Biol* **6**, 325-335, doi:10.1021/cb100314y (2011).

180   Zauner, T., Berger-Hoffmann, R., Muller, K., Hoffmann, R. & Zuchner, T. Highly adaptable and sensitive protease assay based on fluorescence resonance energy transfer. *Anal Chem* **83**, 7356-7363, doi:10.1021/ac201274f (2011).

181   Liu, Y. & Liao, J. Quantitative FRET (Forster Resonance Energy Transfer) analysis for SENP1 protease kinetics determination. *J Vis Exp*, e4430, doi:10.3791/4430 (2013).

182   Song, Y., Madahar, V. & Liao, J. Development of FRET assay into quantitative and high-throughput screening technology platforms for protein-protein interactions. *Ann Biomed Eng* **39**, 1224-1234, doi:10.1007/s10439-010-0225-x (2011).

183   Strisovsky, K., Sharpe, H. J. & Freeman, M. Sequence-specific intramembrane proteolysis: identification of a recognition motif in rhomboid substrates. *Mol Cell* **36**, 1048-1059, doi:10.1016/j.molcel.2009.11.006 (2009).

184   O'Donoghue, A. J. *et al.* Global identification of peptidase specificity by multiplex substrate profiling. *Nat Methods* **9**, 1095-1100, doi:10.1038/nmeth.2182 (2012).

185   Lapek, J. D., Jr. *et al.* Quantitative Multiplex Substrate Profiling of Peptidases by Mass Spectrometry. *Mol Cell Proteomics*, doi:10.1074/mcp.TIR118.001099 (2019).

186   Calvo, S. E., Clauser, K. R. & Mootha, V. K. MitoCarta2.0: an updated inventory of mammalian mitochondrial proteins. *Nucleic Acids Res* **44**, D1251-1257, doi:10.1093/nar/gkv1003 (2016).

187   Guillery, O. *et al.* Metalloprotease-mediated OPA1 processing is modulated by the mitochondrial membrane potential. *Biol Cell* **100**, 315-325, doi:10.1042/BC20070110 (2008).

188   Chao, J. R. *et al.* Hax1-mediated processing of HtrA2 by Parl allows survival of lymphocytes and neurons. *Nature* **452**, 98-102, doi:10.1038/nature06604 (2008).

189   Jeyaraju, D. V., Cisbani, G., De Brito, O. M., Koonin, E. V. & Pellegrini, L. Hax1 lacks BH modules and is peripherally associated to heavy membranes: implications for Omi/HtrA2 and PARL activity in the regulation of mitochondrial stress and apoptosis. *Cell Death Differ* **16**, 1622-1629, doi:10.1038/cdd.2009.110 (2009).

190   Julien, O. & Wells, J. A. Caspases and their substrates. *Cell Death Differ* **24**, 1380-1389, doi:10.1038/cdd.2017.44 (2017).

191   Arutyunova, E., Strisovsky, K. & Lemieux, M. J. Activity Assays for Rhomboid Proteases. *Methods Enzymol* **584**, 395-437, doi:10.1016/bs.mie.2016.11.002 (2017).

192   Ticha, A. *et al.* Sensitive Versatile Fluorogenic Transmembrane Peptide Substrates for Rhomboid Intramembrane Proteases. *J Biol Chem* **292**, 2703-2713, doi:10.1074/jbc.M116.762849 (2017).

193   Menard, R. & Storer, A. C. Oxyanion hole interactions in serine and cysteine proteases. *Biol Chem Hoppe Seyler* **373**, 393-400 (1992).

194   Kamp, F. *et al.* Intramembrane proteolysis of beta-amyloid precursor protein by gamma-secretase is an unusually slow process. *Biophys J* **108**, 1229-1237, doi:10.1016/j.bpj.2014.12.045 (2015).

195   Schafer, A. *et al.* Intramembrane proteolysis of Mgm1 by the mitochondrial rhomboid protease is highly promiscuous regarding the sequence of the cleaved hydrophobic segment. *J Mol Biol* **401**, 182-193, doi:10.1016/j.jmb.2010.06.014 (2010).

196   Beel, A. J. & Sanders, C. R. Substrate specificity of gamma-secretase and other intramembrane proteases. *Cell Mol Life Sci* **65**, 1311-1334, doi:10.1007/s00018-008-7462-2 (2008).

197   Naing, S. H. *et al.* Both positional and chemical variables control in vitro proteolytic cleavage of a presenilin ortholog. *J Biol Chem* **293**, 4653-4663, doi:10.1074/jbc.RA117.001436 (2018).

198   Lee, A. G. How lipids affect the activities of integral membrane proteins. *Biochim Biophys Acta* **1666**, 62-87, doi:10.1016/j.bbamem.2004.05.012 (2004).

199   Zhou, Y., Moin, S. M., Urban, S. & Zhang, Y. An internal water-retention site in the rhomboid intramembrane protease GlpG ensures catalytic efficiency. *Structure* **20**, 1255-1263, doi:10.1016/j.str.2012.04.022 (2012).

200   Urban, S. & Moin, S. M. A subset of membrane-altering agents and gamma-secretase modulators provoke nonsubstrate cleavage by rhomboid proteases. *Cell Rep* **8**, 1241-1247, doi:10.1016/j.celrep.2014.07.039 (2014).

201   Chan, E. Y. & McQuibban, G. A. Phosphatidylserine decarboxylase 1 (Psd1) promotes mitochondrial fusion by regulating the biophysical properties of the mitochondrial membrane and alternative topogenesis of mitochondrial genome maintenance protein 1 (Mgm1). *J Biol Chem* **287**, 40131-40139, doi:10.1074/jbc.M112.399428 (2012).

202   Sesaki, H. *et al.* Ups1p, a conserved intermembrane space protein, regulates mitochondrial shape and alternative topogenesis of Mgm1p. *J Cell Biol* **173**, 651-658, doi:10.1083/jcb.200603092 (2006).

203   Tamura, Y., Endo, T., Iijima, M. & Sesaki, H. Ups1p and Ups2p antagonistically regulate cardiolipin metabolism in mitochondria. *J Cell Biol* **185**, 1029-1045, doi:10.1083/jcb.200812018 (2009).

204   Osman, C. *et al.* The genetic interactome of prohibitins: coordinated control of cardiolipin and phosphatidylethanolamine by conserved regulators in mitochondria. *J Cell Biol* **184**, 583-596, doi:10.1083/jcb.200810189 (2009).

205   van Meer, G., Voelker, D. R. & Feigenson, G. W. Membrane lipids: where they are and how they behave. *Nat Rev Mol Cell Biol* **9**, 112-124, doi:10.1038/nrm2330 (2008).

206   Dudek, J. Role of Cardiolipin in Mitochondrial Signaling Pathways. *Front Cell Dev Biol* **5**, 90, doi:10.3389/fcell.2017.00090 (2017).

207   Kawai, F. *et al.* Cardiolipin domains in Bacillus subtilis marburg membranes. *J Bacteriol* **186**, 1475-1483 (2004).

208   Nishibori, A., Kusaka, J., Hara, H., Umeda, M. & Matsumoto, K. Phosphatidylethanolamine domains and localization of phospholipid synthases in Bacillus subtilis membranes. *J Bacteriol* **187**, 2163-2174, doi:10.1128/JB.187.6.2163-2174.2005 (2005).

209   Foo, A. C., Harvey, B. G., Metz, J. J. & Goto, N. K. Influence of hydrophobic mismatch on the catalytic activity of Escherichia coli GlpG rhomboid protease. *Protein Sci* **24**, 464-473, doi:10.1002/pro.2585 (2015).

210   Gohil, V. M., Gvozdenovic-Jeremic, J., Schlame, M. & Greenberg, M. L. Binding of 10-N-nonyl acridine orange to cardiolipin-deficient yeast cells: implications for assay of cardiolipin. *Anal Biochem* **343**, 350-352, doi:10.1016/j.ab.2005.04.039 (2005).

211   Wong, E. D. *et al.* The dynamin-related GTPase, Mgm1p, is an intermembrane space protein required for maintenance of fusion competent mitochondria. *J Cell Biol* **151**, 341-352 (2000).

212   Musatov, A. & Sedlak, E. Role of cardiolipin in stability of integral membrane proteins. *Biochimie* **142**, 102-111, doi:10.1016/j.biochi.2017.08.013 (2017).

213   Pope, S., Land, J. M. & Heales, S. J. Oxidative stress and mitochondrial dysfunction in neurodegeneration; cardiolipin a critical target? *Biochim Biophys Acta* **1777**, 794-799, doi:10.1016/j.bbabio.2008.03.011 (2008).

214   Oliver, P. M. *et al.* Localization of anionic phospholipids in Escherichia coli cells. *J Bacteriol* **196**, 3386-3398, doi:10.1128/JB.01877-14 (2014).

215   Planas-Iglesias, J. *et al.* Cardiolipin Interactions with Proteins. *Biophys J* **109**, 1282-1294, doi:10.1016/j.bpj.2015.07.034 (2015).

216   Vos, M. *et al.* Cardiolipin promotes electron transport between ubiquinone and complex I to rescue PINK1 deficiency. *J Cell Biol* **216**, 695-708, doi:10.1083/jcb.201511044 (2017).

217   Zhang, Y. *et al.* Lysine desuccinylase SIRT5 binds to cardiolipin and regulates the electron transport chain. *J Biol Chem* **292**, 10239-10249, doi:10.1074/jbc.M117.785022 (2017).

218   Lee, H. J., Mayette, J., Rapoport, S. I. & Bazinet, R. P. Selective remodeling of cardiolipin fatty acids in the aged rat heart. *Lipids Health Dis* **5**, 2, doi:10.1186/1476-511X-5-2 (2006).

219   Lewis, R. N. & McElhaney, R. N. The physicochemical properties of cardiolipin bilayers and cardiolipin-containing lipid membranes. *Biochim Biophys Acta* **1788**, 2069-2079, doi:10.1016/j.bbamem.2009.03.014 (2009).

220   Boyd, K. J., Alder, N. N. & May, E. R. Buckling Under Pressure: Curvature-Based Lipid Segregation and Stability Modulation in Cardiolipin-Containing Bilayers. *Langmuir* **33**, 6937-6946, doi:10.1021/acs.langmuir.7b01185 (2017).

221   Ren, M., Phoon, C. K. & Schlame, M. Metabolism and function of mitochondrial cardiolipin. *Prog Lipid Res* **55**, 1-16, doi:10.1016/j.plipres.2014.04.001 (2014).

222   Fry, M. & Green, D. E. Cardiolipin requirement for electron transfer in complex I and III of the mitochondrial respiratory chain. *J Biol Chem* **256**, 1874-1880 (1981).

223   Fry, M. & Green, D. E. Cardiolipin requirement by cytochrome oxidase and the catalytic role of phospholipid. *Biochem Biophys Res Commun* **93**, 1238-1246 (1980).

224   Noel, H. & Pande, S. V. An essential requirement of cardiolipin for mitochondrial carnitine acylcarnitine translocase activity. Lipid requirement of carnitine acylcarnitine translocase. *Eur J Biochem* **155**, 99-102 (1986).

225   Althoff, T., Mills, D. J., Popot, J. L. & Kuhlbrandt, W. Arrangement of electron transport chain components in bovine mitochondrial supercomplex I1III2IV1. *EMBO J* **30**, 4652-4664, doi:10.1038/emboj.2011.324 (2011).

226   Ruggiero, F. M., Cafagna, F., Petruzzella, V., Gadaleta, M. N. & Quagliariello, E. Lipid composition in synaptic and nonsynaptic mitochondria from rat brains and effect of aging. *J Neurochem* **59**, 487-491 (1992).

227   Klein, C. & Westenberger, A. Genetics of Parkinson's disease. *Cold Spring Harb Perspect Med* **2**, a008888, doi:10.1101/cshperspect.a008888 (2012).

228   Valente, E. M. *et al.* Hereditary early-onset Parkinson's disease caused by mutations in PINK1. *Science* **304**, 1158-1160, doi:10.1126/science.1096284 (2004).

229   Marongiu, R. *et al.* PINK1 heterozygous rare variants: prevalence, significance and phenotypic spectrum. *Hum Mutat* **29**, 565, doi:10.1002/humu.20719 (2008).

230   Butterfield, S. M., Patel, P. R. & Waters, M. L. Contribution of aromatic interactions to alpha-helix stability. *J Am Chem Soc* **124**, 9751-9755 (2002).

231   de Groot, N. S., Castillo, V., Grana-Montes, R. & Ventura, S. AGGRESCAN: method, application, and perspectives for drug design. *Methods Mol Biol* **819**, 199-220, doi:10.1007/978-1-61779-465-0_14 (2012).